DEFECT EVOLUTION IN HIGH-TEMPERATURE IRRADIATED NUCLEAR GRAPHITE

by

Steve Johns

A dissertation

submitted in partial fulfillment

of the requirements for the degree of

Doctor of Philosophy in Materials Science and Engineering

Boise State University

December 2020

BOISE STATE UNIVERSITY GRADUATE COLLEGE

DEFENSE COMMITTEE AND FINAL READING APPROVALS

of the dissertation submitted by

Steve Johns

Dissertation Title: Defect Evolution in High-temperature Irradiated Nuclear Graphite

Date of Final Oral Examination: 23 October 2020

The following individuals read and discussed the dissertation submitted by student Steve Johns, and they evaluated his presentation and response to questions during the final oral examination. They found that the student passed the final oral examination.

Rick Ubic, Ph.D.	Chair, Supervisory Committee
Karthik Chinnathambi, Ph.D.	Co-Chair, Supervisory Committee
William E. Windes, Ph.D.	Member, Supervisory Committee
Peter Mullner, Ph.D.	Member, Supervisory Committee

The final reading approval of the dissertation was granted by Rick Ubic, Ph.D., Chair of the Supervisory Committee. The dissertation was approved by the Graduate College.

DEDICATION

This work is dedicated to my children, Lexi and Nate, who have been a constant source of motivation. Thank you both for your unconditional love, support and understanding when I was distant or distracted working on this project. I love you both to the moon and back.

ACKNOWLEDGMENTS

First, I would like to express my sincere gratitude to my advisors Dr. Rick Ubic and Dr. Karthik Chinnathambi. Through countless hours of invaluable scientific discussion, continual training on transmission electron microscopy, detailed proof-readings of publications, presentations, and proposals, they both were vital in my success. It has been a privilege working for both Dr. Rick Ubic and Dr. Karthik Chinnathambi. I am indebted to them both for the time and support they invested in me as a researcher and an individual throughout my academic endeavors.

I would also like to acknowledge my committee members, Dr. William E. Windes and Dr. Peter Mullner, for their willingness to set aside time in their busy schedules to provide intellectual support and encouragement throughout this project. In particular, I would like to thank Dr. William E. Windes for facilitating collaboration with Idaho National Laboratory, without which, this work would not be possible.

I would like to acknowledge this dissertation work was supported by the U. S. Department of Energy's EPSCoR-State/National Laboratory Partnership Program (Award # DE-SC0016427). TEM studies were carried out at the Boise State Center for Materials Characterization (BSCMC). Aberration-corrected TEM work was conducted at the Molecular Foundry and supported by the Office of Science, Office of Basic Energy Sciences, of the U.S. Department of Energy (Contract # DE-AC02-05CH11231).

I would like to extend my thank you to a few specific individuals: Dr. Joshua J. Kane and Dr. Lingfeng He at Idaho National laboratory for their research collaborations;

Dr. Karen Bustillo at the Nation Center for Electron Microscopy for her expert guidance in electron microscopy; Dr. Brian Jacques and Allyssa Bateman for helping with the safe handling of neutron-irradiated specimens; Arvin Cunningham for helping fabricate equipment used for specimen preparation; Dr. Michael Hurley and Dr. Nick Bulloss who were instrumental in supporting my early interests in electron microscopy. There are countless others who in some way, shape or form contributed to this dissertation, I thank you all.

ABSTRACT

Graphite has historically been used as a moderator material in nuclear reactor designs dating back to the first man-made nuclear reactor to achieve criticality (Chicago Pile 1) in 1942. Additionally, graphite is a candidate material for use in the future envisioned next-generation nuclear reactors (Gen IV); specifically, the molten-salt-cooled (MSR) and very-high-temperature reactor (VHTR) concepts. Gen IV reactor concepts will introduce material challenges as temperature regimes and reactor lifetimes are anticipated to far exceed those of earlier reactors. Irradiation-induced defect evolution is a fundamental response in nuclear graphite subjected to irradiation. These defects directly influence the many property changes of nuclear graphite subjected to displacing radiation; however, a comprehensive explanation for irradiation-induced dimensional change remains elusive. The macroscopic response of graphite subjected to displacing irradiation is often modeled semi-empirically based on irradiation data of specific graphite grades (some of which are obsolete). The lack of an analytical description of the response of nuclear graphite subjected to irradiation is due in part to the complex microstructure of synthetic semi-isotropic graphites.

Chapter One provides a general overview of the application, processing, and irradiation-induced property changes of nuclear graphite. The key properties affected by displacing irradiation include, but are not limited to, coefficient of thermal expansion (CTE), irradiation creep, and irradiation-induced dimensional change. Additionally, historical models of radiation damage in nuclear graphite, including their inadequacies in

accurately describing property changes, are discussed. It should be noted that a comprehensive explanation for all irradiation-induced property change is beyond the scope of this work, which is focused on the evolution of novel atomic-level defects in high-temperature irradiated nuclear graphite and the implications of these defects for the current understanding of irradiation-induced dimensional change.

Chapter Two is focused on the development of a novel oxidation-based transmission electron microscopy (TEM) sample-preparation technique for nuclear-grade graphite. Conventionally, TEM specimens are prepared via ion-milling or a focused ion beam (FIB); however, these techniques require the use of displacing radiation and may result in localized areas of irradiation damage. As a result, distinguishing defect structures created as artifacts during sample preparation from those created by electron- or neutron-irradiation can be challenging. Bulk nuclear graphite grades IG-110, NBG-18, and highly oriented pyrolytic graphite (HOPG) were oxidized using a new jet-polishing-like setup where oxygen is used as an etchant. This technique is shown to produce self-supporting electron-transparent TEM specimens free of irradiation-induced artifacts; thus, these specimens can be used as a baseline for in situ irradiation experiments as they have no irradiation-induced damage.

Chapter Three examines the dynamic evolution of defect structures in nuclear graphite IG-110 subjected to electron-irradiation. As use of fast neutrons for irradiation experiments is dangerous, expensive, and time consuming, electron-irradiation is arguably a useful surrogate; however, comparisons between the two irradiating particles is also discussed. In situ video recordings of specimens undergoing simultaneous heating and electron-irradiation were used to analyze the dynamic atomic-level defect evolution

in real time. Novel fullerene-like defect structures are shown to evolve as a direct result of high-temperature electron-irradiation and cause significant dimensional change to crystallites.

Neutron-irradiated nuclear graphite IG-110 was supplied by Idaho National Laboratory as part of the Advanced Graphite Creep capsule experiments (AGC-3). Chapter Four reports the preliminary characterization of IG-110 neutron-irradiated at 817°C to a dose of 3.56 displacements per atom (dpa). Shown is experimental evidence of a 'ruck and tuck' defect occurring in high-temperature neutron-irradiated nuclear graphite. The 'ruck and tuck' defect arises due to irradiation-induced defects. The interaction of these defects results in the buckling of atomic planes and the formation of a structure composed of two partial carbon nanotubes. The "buckle, ruck and tuck" model was first theoretically predicted via computational modeling in 2011 as a plausible defect structure/mechanism occurring in high-temperature neutron-irradiated graphite by Prof. Malcolm Heggie et al. Chapter Four shows the first direct experimental results to support the "buckle, ruck and tuck" model.

Chapter Five further characterizes nuclear graphite IG-110 neutron-irradiated at high temperature (≥800 °C) at doses of 1.73 and 3.56 dpa. Results show further evidence to support the "buckle, ruck and tuck" model and additionally show the presence of larger concentric shelled fullerene-like defects. Fullerene-like defects were found to occur in disordered regions of the microstructure including within nanocracks (Mrozowski cracks). These results agree with high-temperature electron-irradiation studies which showed the formation of fullerene-like defects in-situ and give additional validity to the use of high-flux electron-irradiation as a useful approximation to neutron-irradiation.

Furthermore, Chapter Five gives valuable insight to unresolved quantitative anomalies of historical models of graphite expansion and may improve the understanding of current empirical and theoretical models of irradiation-induced property changes in nuclear graphite.

TABLE OF CONTENTS

LIST OF FIGURES

LIST OF ABBREVIATIONS

AGC	Advanced Graphite Creep Capsule
AGR	Advanced Gas-cooled Reactor
CTE	Coefficient of Thermal Expansion
DFT	Density Functional Theory
DPA	Displacements Per Atom
EELS	Electron Energy Loss Spectroscopy
ELNES	Energy Loss Near Edge Structure
EXELFS	Extended Energy Loss Fine Structure
FFT	Fast Fourier Transform
FIB	Focused Ion Beam
Gen IV	Fourth Generation Nuclear Reactor
HOPG	Highly Oriented Pyrolytic Graphite
HRTEM	High Resolution Transmission Electron Microscopy
MD	Molecular Dynamics
MSR	Molten Salt-cooled Reactor
TEM	Transmission Electron Microscopy
VHTR	Very-High-Temperature Reactor
QI	Quinoline Insoluble Particle

CHAPTER ONE: INTRODUCTION

1.1 Application of Graphite in Nuclear Reactors

Commercial nuclear reactors operate by utilizing the energy produced from controlled and sustained fission reactions. In the case of uranium-based fuels which utilize the isotope ^{235}U, the fission reaction can occur in as many as 30 different ways, which leads to the possibility of 60 different fission products [1]. In general, a fission reaction may be expressed as,

$$^{235}\mathrm{U} + \text{themal neutron} \rightarrow {}^{92}\mathrm{Kr} + {}^{142}\mathrm{Br} + 2\ \text{fast nuetrons} + \text{energy} \qquad (1.1)$$

where on average the reaction releases 2 fast neutrons [1]. Fast neutrons produced by fission reactions typically have energies in the range 1-10 MeV. To sustain a fission chain reaction in the reactor, these fast neutrons must dissipate most of their energy before they can react further with more ^{235}U atoms. Thermalized neutrons typically have energies below 0.1eV. The process of thermalization of fast neutrons is achieved by interaction with a moderator material. Moderating materials are often light elemental species such as H_2O, D_2O, and carbon (graphite).

The first man-made nuclear reactor to achieve criticality, Chicago Pile 1, was a graphite-moderated reactor. Since that time, graphite has been used as a moderator material in more than 100 reactors, around 30 of which remain in operation [2]. These include many reactor concepts including the advanced gas-cooled reactors (AGR) of the United Kingdom and the water-cooled RMBK reactors designed by the Soviet Union.

Graphite has remained a candidate moderating and structural material for reactor designs as it is relatively inexpensive (compared to other moderator materials such as D_20), easily machined into complex geometries, and has suitable mechanical properties for structural applications in nuclear reactors. Figure 1.1 shows a graphite prismatic fuel and reflector block typical for high-temperature gas-cooled reactor designs [3].

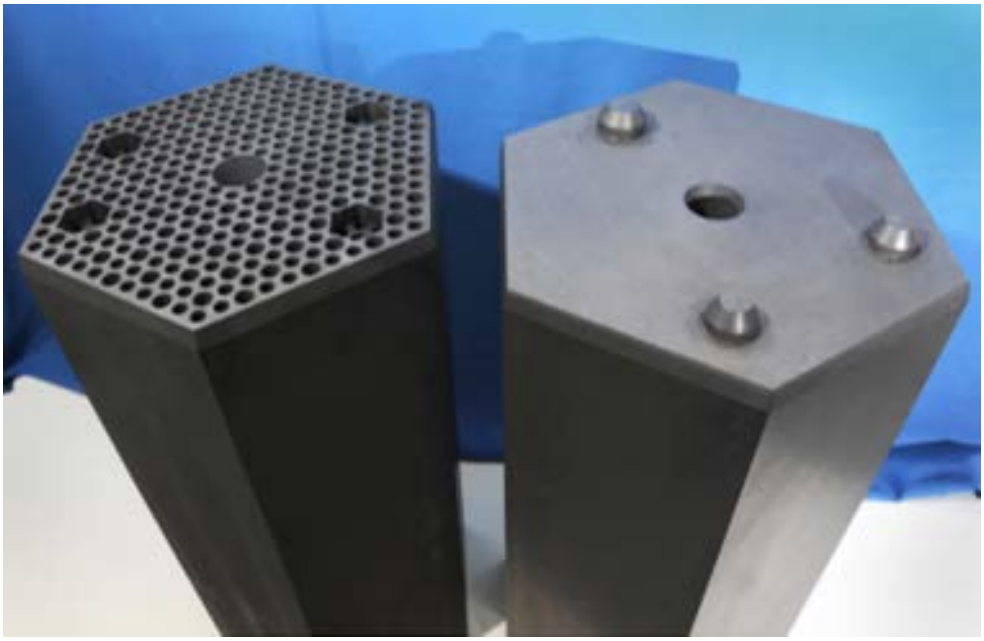

Figure 1.1 Typical prismatic fuel block (left) and a reflector block (right) common to both prismatic and pebble-bed reactor designs. Adapted from Windes et al. [3].

The envisioned next-generation nuclear reactor concepts (Gen IV) will also incorporate graphite as a moderator material, specifically the molten salt reactors (MSRs) and very-high-temperature reactors (VHTRs) [4]. Gen IV reactors are envisioned to operate at temperatures up to 1250°C and have lifetimes far exceeding those of previous-generation reactors; however, an adequate database for the response of nuclear graphite undergoing high-temperature high-dose irradiation remains to be fully established. Furthermore, much of the established data on the irradiation response of nuclear graphite

are based on historical grades of graphite which no longer exist. As the processing techniques will vary amongst each grade of nuclear graphite, their inherent virgin properties and irradiation responses can differ significantly [2]. Thus, characterization and irradiation programs for nuclear graphite must be completed for each prospective grade. The cost and scope of these programs may be significantly reduced by further understanding the relationship between irradiation-induced microstructure change and properties.

1.2 Manufacturing of Nuclear Graphite

Nuclear grade graphite is a specially developed synthetic polycrystalline graphite manufactured from a filler coke (generally petroleum or coal-tar based) and a pitch binder. Manufacturing and processing of nuclear grade graphite is conducted in a manner to produce a near-isotropic material. Figure 1.2 shows a generalized flow chart for the processing steps in the manufacture of nuclear graphite. Raw petroleum or pitch coke is calcined in an oxygen-deficient atmosphere at temperatures of approximately 1300°C, at which volatile substances are driven off. Calcined coke is then ground to a desired particle size, blended, and mixed with a pitch binder. The resulting material is then either extruded, molded or isostatically pressed into what is termed a green artifact. Carbonization of the green artifact is then conducted at temperatures above 2500°C and the resulting baked artifact is typically impregnated with a petroleum pitch and re-baked to densify the part. The process of impregnating and re-carbonization may occur several times to attain the required density [5].

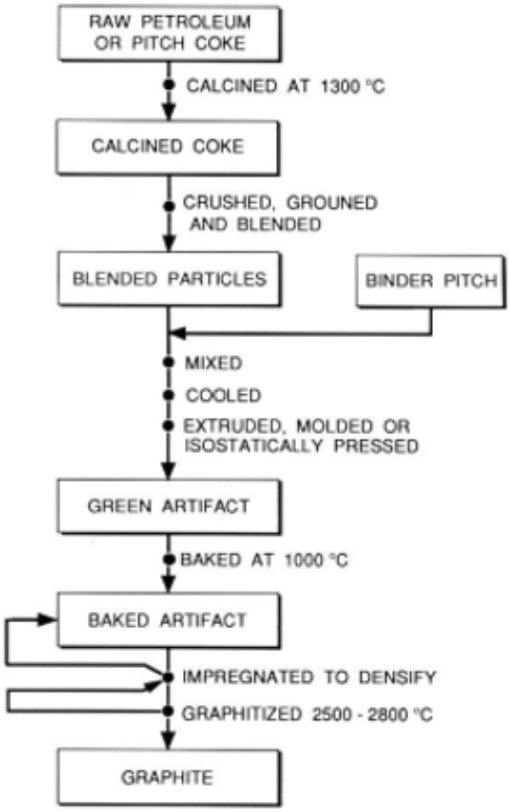

Figure 1.2 Generalized flow chart showing the processing steps for nuclear grade graphite. Adapted from Windes et al. [3].

1.3 Microstructures of Nuclear Graphites

On the atomic scale, graphite's basal planes stack in an ABA… sequence to form a primitive hexagonal unit cell with space group $P6_3/mmc$ with lattice constants $a = b =$ 0.246 nm, $c = 0.669$ nm and a basal plane interatomic spacing of 0.335 nm ($d_{002} = c/2$) (Figure 1.3). Single-crystal graphite is anisotropic with strong in-plane sp^2 covalent bonding within the *ab* plane and weak Van der Waals bonding parallel to the *c* axis. Polycrystalline nuclear graphites have a complex microstructure composed of filler, binder, quinoline insoluble (QI) particles, micropores, a turbostratic graphite phase, and nanocracks (Mrozowski cracks) [6,7]. Mrozowski cracks are lenticular cracks, a few nanometers to several hundred nanometers in length, which form between basal planes

due to the weak Van der Waals bonding and volumetric shrinkage during cooling from graphitization temperatures [8].

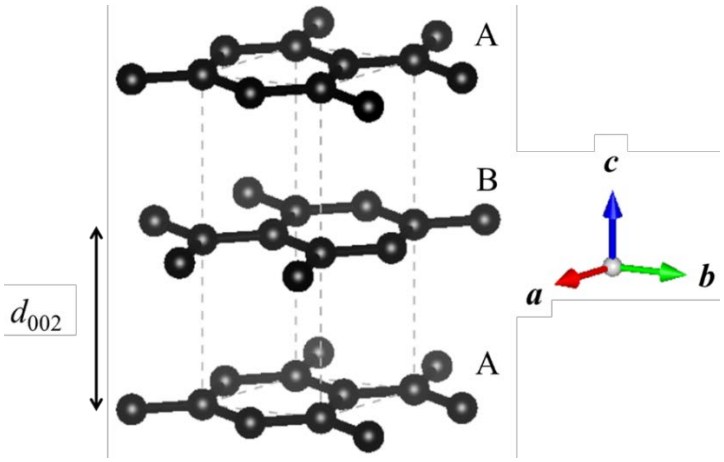

Figure 1.3 Crystallographic structure of hexagonal graphite with an ABA stacking sequence of basal planes and the interatomic distance d_{002} = 0.335 nm indicated.

As a result, Mrozowski cracks have lengths within the *ab* plane and widths parallel to the *c* axis of crystallites. Figure 1.4 (a) and (b) show bright-field TEM micrographs representative of the microstructure of nuclear graphite. Figure 1.4 (a) shows a filler particle containing Mrozowski cracks. Inside the Mrozowski cracks there is contrast consistent with a disordered carbon phase, as previously observed by others [9]; however, this conclusion has been disputed and there remains no consensus [10]. Within the binder phase, as shown in Figure 1.4 (b), additional microstructural features such as quinoline insoluble (QI) particles may be found. QI particles are poorly graphitized rosette-like structures that form due to aromatic molecules present within the binder material during manufacturing. Depending on the processing technique, the distribution and size of these microstructural features varies significantly between grades of nuclear graphite [4,5]. As a result, the mechanical properties and response to irradiation can also vary between grades of nuclear graphite.

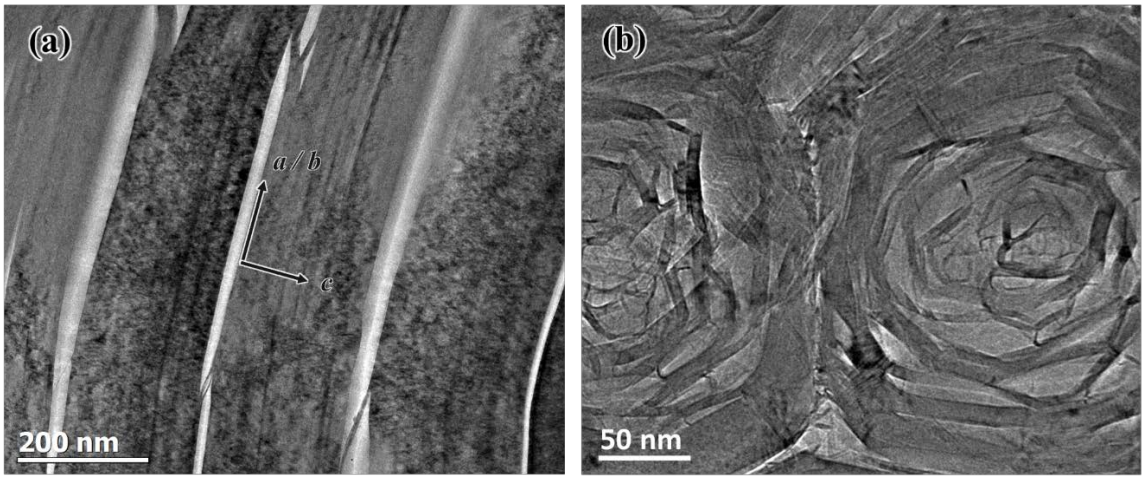

Figure 1.4 (a) Bright-field TEM micrograph showing Mrozowski cracks and their orientation relative to crystallite directions. (b) TEM micrograph of QI particles often found in the binder phase of nuclear graphite.

1.4 Irradiation Induced Property Change

While in reactors, irradiation damage is accumulated in graphite over time from a fluence of fast neutrons. Irradiation-induced defect evolution is a fundamental response in nuclear graphite subjected to irradiation. These defects directly influence the many property changes of nuclear graphite subjected to displacing radiation. The three most important properties which change due to irradiation damage are the specific volume (dimensional change), coefficient of thermal expansion (CTE), and creep behavior [2,11]. Understanding these property changes is essential to reactor design, safety, maintenance and the operational lifetime of graphite-moderated reactors.

1.4.1 Dimensional Change

During neutron-irradiation, nuclear graphite will undergo significant dimensional change. Irradiation-induced dimensional change is arguably the most important parameter when considering the in-service lifetime of graphite components. At the onset of irradiation, a high rate of dimensional shrinkage occurs. As irradiation continues, the rate of shrinkage decreases until there is a reversal and the graphite then begins to expand

(turnaround point). With prolonged irradiation, nuclear graphite continues to expand reaching the component's pre-irradiated dimensions (crossover). The phenomena of turnaround and crossover are strong functions of irradiating temperature. At high temperatures, turnaround and crossover occur at significantly lower doses compared to lower-temperature irradiations. Figure 1.7 shows empirically based curves for dimensional change in nuclear graphite IG-110 as a function of neutron fluence at various temperatures.

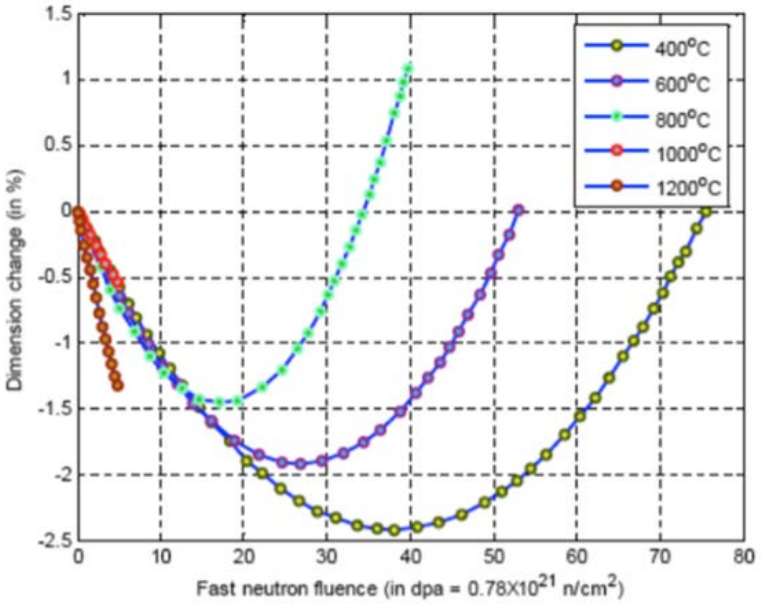

Figure 1.5 Empirical curves of dimensional change for IG-110 as a function of neutron fluence at various temperatures. Adapted from Ref. [12].

The current theory for dimensional change holds that the irradiation-induced *c*-axis expansion of crystallites is initially accommodated by porosity and Mrozowski cracks, and contraction occurs along the *ab* plane (reasoned to be driven by vacancy species) resulting in a net shrinkage. After the accommodating porosity densifies (turnaround), irradiation-induced crystallite expansion causes internal stresses resulting in new crack formation and runaway dimensional change [13,14]; however, a consensus on

atomic defect structures responsible for crystallite expansion has not been established to date [15,16]. If considering a single defect mechanism throughout the irradiation temperatures, it remains unclear how such large dimensional changes occur during high-temperature irradiation even when the graphite has undergone a relatively small irradiation dose.

1.4.2 Coefficient of Thermal Expansion

The thermal expansion of graphite is particularly important when considering dimensional tolerances between the graphite fuel/reflector blocks and additionally other reactor core components (fuel rods/channels, control rods, etc…) during normal operation and abnormal events. The unirradiated CTE change in polycrystalline graphite is reasonably well established by many semi-empirical relationships [2,17–19]. Figure 1.5 (a) and (b) show the temperature dependence on CTE for graphite crystal expansion along the *a* axis and *c* axis in which all models show good agreement, especially at low temperatures. A key parameter included in models of CTE change is a structural term which accounts for crystallite orientation and the role that accommodating porosity (Mrozowski cracks) has on crystallite expansion; however, this term is generally assumed independent of temperature [17,20].

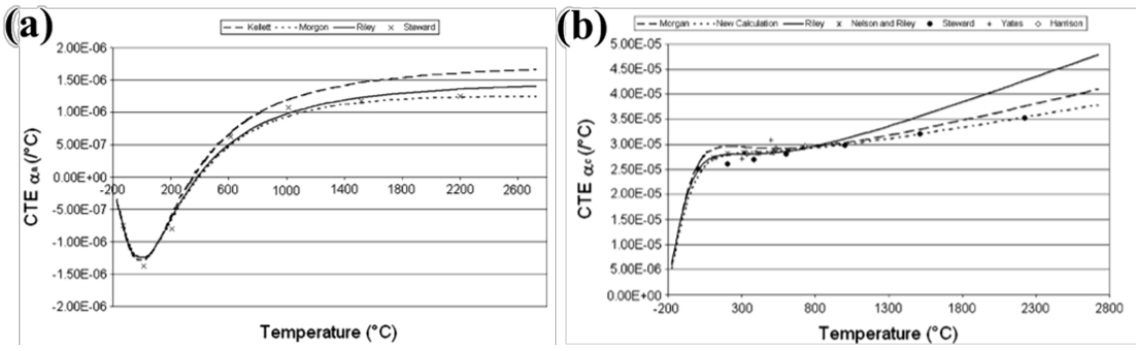

Figure 1.6 Temperature dependence of CTE for graphite along the *a*-axis (a) and along the *c*-axis (b). Adapted from Ref. [17].

Figure 1.6 shows the bulk CTE change in nuclear graphite IG-110 as a function of dose at various temperatures. The curves shown in Figure 1.6 are empirically based using irradiation data for IG-110 [12]. Initially there is an increase in CTE until reaching a maximum followed by a rapid decrease, after which it continues to decreases linearly more slowly [21,22]. The initial rise in CTE is believed to occur due to the closure of Mrozowski cracks; however, mechanisms to account for the reduction in CTE are not well understood. Furthermore, this reduction does not occur in some grades of nuclear graphite [21,23]. The present understanding reasons that the reduction in CTE occurs as a result of new porosity created from irradiation-induced damage [24]; however, this conclusion does not agree with the current theory for dimensional change and is discussed further in Chapter Five [13].

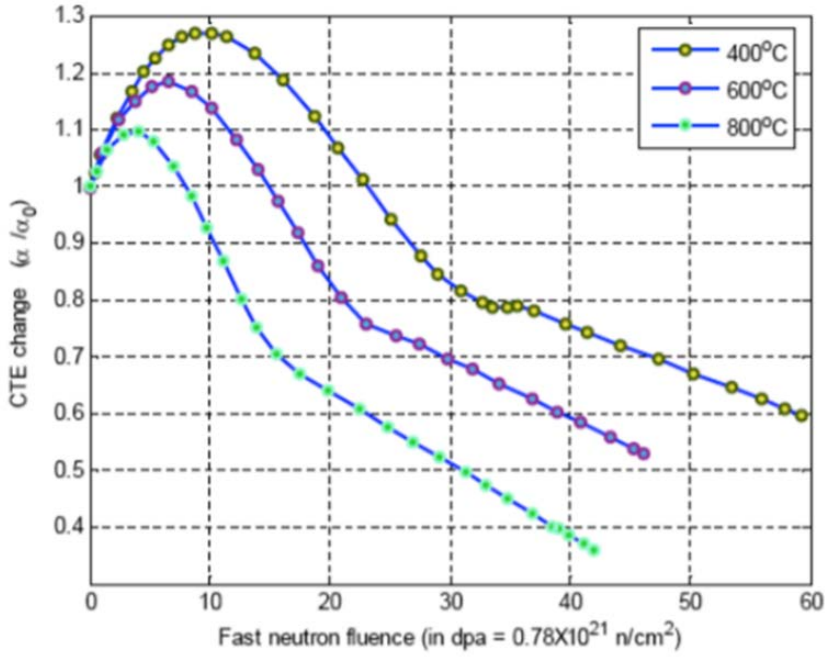

Figure 1.7 Empirical curves of CTE change for IG-110 as a function of neutron fluence at various temperatures. Adapted from Ref. [12].

1.4.3 Irradiation Creep

Irradiation creep is defined as the difference in dimensional change between an unloaded specimen and a loaded specimen subjected to the same irradiation conditions. In general, compressive loads result in an increase in dimensional change and tensile stresses result in a decrease in dimensional change (Figure 1.8) [2].

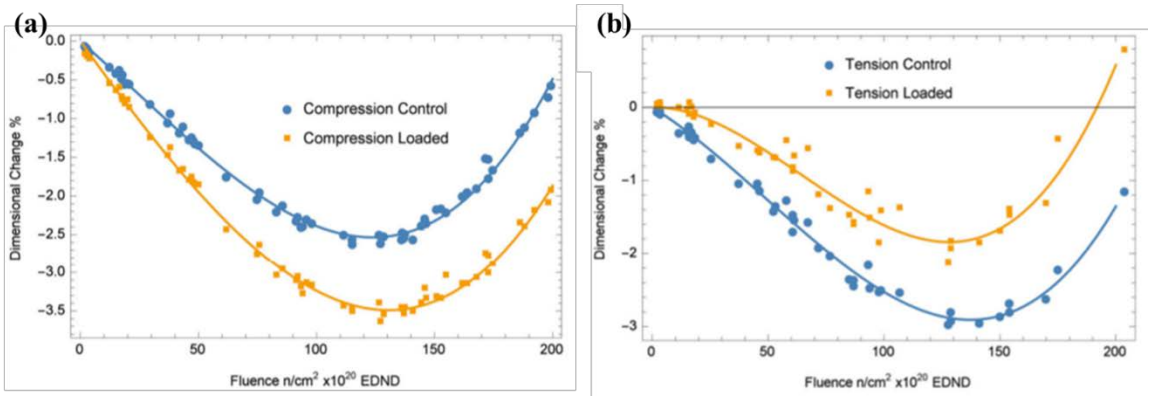

Figure 1.8 Irradiation creep in loaded and unloaded nuclear graphite ATR-2E. Adapted from Ref. [2].

Irradiation creep in nuclear graphite is not considered detrimental, as it significantly reduces the amount of stress during irradiation. Without the presence of irradiation creep, stresses caused by both thermal and irradiation-induced effects would result in failure of graphite components within a few years of operation [25].

Theoretical models of irradiation creep as a function of applied stress are built on foundational theories of dislocation movement/migration. The pinning and un-pinning of dislocations is one such theory that explains the observed increase in modulus [26]. This theory also implies a dislocation movement of glide (a.k.a slide) [27]; however, others suggest that a glide mechanism would result in a stress dependence of a power of two, whereas most experimental data shows a linear dependence and may indicate a climb

mechanism for dislocations [28]; although significant microstructural evidence of either mechanisms has yet to be thoroughly established.

1.5 Radiation Damage in Graphite

The aforementioned property changes in nuclear graphite are fundamentally a result of radiation damage to the crystalline structure of graphite; however, in all cases, an analytical description relating atomic defect structures to property change has yet to emerge. This is partially due to the complex microstructure of nuclear graphite and the difficulties in monitoring the dynamic nature of irradiation-induced defects.

1.5.1 Historical Model of Radiation Damage

The historical model for radiation damage in nuclear graphite holds that interstitially displaced carbon atoms will result in contraction along the *a/b* axes (due to vacancy species) and expansion along the *c* axis due to interstitial species. This point-defect model also assumes interstitially displaced carbon atoms will coalesce resulting in the formation of additional basal planes and vacancy loops. Much of this reasoning is deduced from early studies on neutron-irradiated natural graphite [9]. Early studies did show evidence of vacancy and interstitial loops occurring in high-temperature irradiated natural graphite (Figure 1.9); however, experimental observations of such defect structures were aided by high-temperature annealing in excess of 1600°C [9]. Similar studies were conducted on electron-irradiation natural graphite; however, results showed high-temperature electron-irradiation resulted in the formation of dislocation loops only *after* annealing quenched-in irradiation damage at a temperature of 1200°C [29]. These results are arguably ambiguous and may not represent the actual defect evolution of nuclear graphite during normal operation of nuclear reactors.

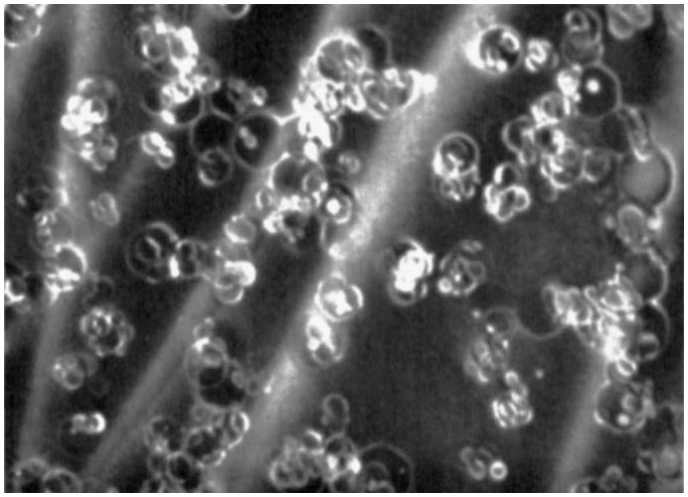

Figure 1.9 TEM micrograph showing dislocation loops in neutron-irradiated natural graphite. Adapted from Ref. [9]. Note: no scale bar provided in original publication, dislocation loops are approximately 20-40 nm.

1.5.1.1 Inadequacies of the Historical Model

The historical basal plane formation model inadequately explains many property changes of irradiated nuclear graphite. As mentioned in section 1.4.2, it is unclear how low-dose high-temperature irradiation can produce a sufficient number of vacancies or interstitials to result in *a*/*b* contraction or *c* expansion as the observed behavior clearly demonstrates (Figure 1.7). Indeed, the actual amount of irradiation-induced dimensional change expected from the historical model is less than half of the actual measured dimensional change [15,29,30]. Furthermore, the well agreed-upon ground-state spiro-interstitial [15,30,31] has an activation energy for migration of 1.2 eV. Experimental evidence via differential scanning calorimetry (DSC) shows Wigner energy release at cryogenic-irradiation temperatures which cannot overcome the 1.2 eV activation energy for the migration of the ground state spiro-interstitials, and thus their movement cannot be explained by the historical model [30,32,33].

1.5.2 Experimentally Derived Models

More recent studies on graphite undergoing irradiation damage (neutron, electron, or ion) provide little to no evidence for the formation of dislocation loops [16,34–37]. Kioke's room-temperature electron-irradiation studies showed an extraordinary 300% *c*-axis expansion in highly oriented pyrolytic graphite (HOPG), and it was proposed that such expansion was due to fragmentation of basal planes by small clusters of interstitial atoms [37]. Karthik et. al. [36] conducted room-temperature electron-irradiation on nuclear graphite NBG-18 and showed a noise-filtered video recording of dynamic defect evolution in real time. Those results suggested additional basal-plane formation by dynamic disassociation of dislocation loops via a dislocation climb mechanism [36]. It should be noted that a dislocation climb mechanism supports current theories for a linear stress dependence of irradiation induced creep [28]. On the other hand, studies on HOPG undergoing room-temperature ion-irradiation showed displacement of basal planes by the formation of networks of kink bands which were purportedly driven by the agglomeration of point defects and basal plane contraction [16]. As such, there remains no clear consensus on the atomic mechanisms resulting in property changes in nuclear graphite.

While there is a considerable amount of experimental research reported on room-temperature irradiation, that conducted at elevated temperatures (comparable to conditions in nuclear reactors) remains scant [34,38,39]; however, there are many studies on disordered carbonaceous species undergoing high-temperature irradiation [40–43]. Almost all graphitic precursors show a transformation to fullerene phases upon sufficient irradiation [40–43]. As nuclear graphites do contain localized regions of disordered

carbon one may expect such transformations to occur during high-temperature irradiation.

1.5.3 Alternative Models via Computational Modeling

Given the complex and dynamic nature of radiation damage in nuclear graphite, computational modeling, such as density functional theory (DFT) and molecular dynamics (MD), provides an alternative means to predict the behavior of graphite subjected to displacing irradiation. It is well documented in literature that domains of non-six-member rings (basal plane dislocations) will result in the buckling and out-of-plane distortion of basal planes [30,44–49]. Perhaps most notable is the 'buckle, ruck and tuck' model proposed by Heggie et al. [30] which provided an alternative mechanism to account for large amounts of irradiation-induced dimensional change. According to this model, pinning defects mostly disappear during high-temperature irradiation, allowing for migration and rearrangement of basal-plane dislocations. As a consequence, such defect evolution was predicted to result in the buckling of atomic planes and the formation of a structure composed of two partial carbon nanotubes, otherwise known as a 'ruck and tuck' defect (Figure 1.10). Chapter Four provides the first direct experimental evidence of a 'ruck and tuck' defect occurring in high-temperature neutron-irradiated nuclear graphite.

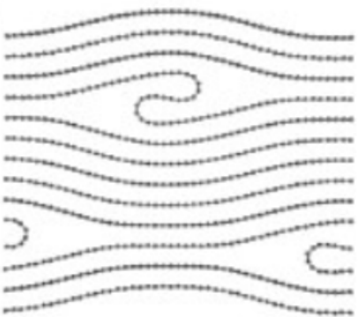

Figure 1.10 Theoretically proposed ruck and tuck defect. Adapted from Ref. [30].

1.6 Approach to Characterization of High-temperature Irradiation Damage

Irradiation-induced property changes of nuclear graphite are governed by the evolution of defect species driven by neutron damage; however, there remains no clear consensus on the nature of such defects, specifically during high-temperature irradiation. This dissertation focuses on the characterization of high-temperature irradiation-induced defect evolution in nuclear graphite via TEM. Conventional TEM sample-preparation techniques require the use of displacing irradiation and may result in localized areas of irradiation damage. Novel oxidative TEM specimen preparation, which does not require displacing irradiation, was developed to produce baseline specimens (refer to Chapter Two). As use of fast neutrons for irradiation experiments is dangerous, expensive, and time consuming, electron-irradiation is arguably a useful surrogate. In situ video recordings of specimens undergoing electron-irradiation and heating were used to analyze the dynamic atomic-level defect evolution in real time. Novel fullerene-like defect structures are shown to evolve as a direct result of high-temperature electron-irradiation and cause significant dimensional change (refer to Chapters Three and Five). In situ electron-irradiation results were compared to those caused by actual neutron-irradiation at comparable doses and temperatures via ex situ characterization (refer to Chapters Four and Five).

1.7 References

[1] K. Linga, I. Charit, An Introduction to Nuclear Materials, Wiley_VCH, 2013.

[2] B.J. Marsden, M. Haverty, W. Bodel, G.N. Hall, A.N. Jones, P.M. Mummery, M. Treifi, Dimensional change, irradiation creep and thermal/mechanical property changes in nuclear graphite, 61 (2016) 155–182. doi:10.1080/09506608.2015.1136460.

[3] W. Windes, G. Strydom, R. Smith, J. Kane, Role of Nuclear Grade Graphite in Controlling Oxidation in Modular HTGRs, (2014). doi:INL/EXT-14-31720.

[4] B.J. Marsden, A.N. Jones, G.N. Hall, M. Treifi, P.M. Mummery, Graphite as a core material for Generation IV nuclear reactors, in: P. Yvon (Ed.), Struct. Mater. Gener. IV Nucl. React., Woodhead Publishing, 2017: pp. 495–532.

[5] W. Windes, T. Burchell, R. Bratton, Graphite Technology Development Plan, (2007).

[6] K.Y. Wen, T.J. Marrow, B.J. Marsden, The microstructure of nuclear graphite binders, Carbon N. Y. 46 (2008) 62–71. doi:10.1016/j.carbon.2007.10.025.

[7] C. Karthik, J. Kane, D.P. Butt, W.E. Windes, R. Ubic, Microstructural Characterization of Next Generation Nuclear Graphites, Microsc. Microanal. 18 (2012) 272–278. doi:10.1017/S1431927611012360.

[8] S. Mrozowski, Mechanical strength, thermal expansion and structure of cokes and carbons, Proc. 1st 2nd Conf. Carbon. (1954) 31. doi:papers://D9F9AA35-5CC8-482E-89C5-625C9FC6984D/Paper/p2585.

[9] P.A. Thrower, Interstitial and vacancy loops in graphite irradiated at high temperatures, Br. J. Appl. Phys. 15 (1964) 1153–1159. doi:10.1088/0508-3443/15/10/302.

[10] D. Liu, D. Cherns, Nano-cracks in a synthetic graphite composite for nuclear applications, Philos. Mag. 98 (2018) 1272–1283. doi:10.1080/14786435.2018.1433886.

[11] W.E. Windes, Graphite Technology Development Plan, 2010.

[12] S. Mohanty, S. Majumdar, M. Srinivasan, U.S.N.R. Commission, HTGR Graphite Core Component Stress Analysis Research Program – Task 1 Technical Letter Report, 2011.

[13] G.B. Neighbour, Modelling of dimensional changes in irradiated nuclear graphites, J. Phys. D. Appl. Phys. 33 (2000) 2966–2972. doi:10.1088/0022-3727/33/22/315.

[14] D.K.L. Tsang, B.J. Marsden, Effects of dimensional change strain in nuclear graphite component stress analysis, Nucl. Eng. Des. 237 (2007) 897–904. doi:10.1016/j.nucengdes.2006.01.015.

[15] R.H. Telling, M.I. Heggie, Radiation defects in graphite, 2007. doi:10.1080/14786430701210023.

[16] J.A. Hinks, S.J. Haigh, G. Greaves, F. Sweeney, C.T. Pan, R.J. Young, S.E. Donnelly, Dynamic microstructural evolution of graphite under displacing irradiation, Carbon N. Y. 68 (2014) 273–284. doi:10.1016/j.carbon.2013.11.002.

[17] D.K.L. Tsang, B.J. Marsden, S.L. Fok, G. Hall, Graphite thermal expansion relationship for different temperature ranges, Carbon N. Y. 43 (2005) 2902–2906. doi:10.1016/j.carbon.2005.06.009.

[18] E.A. Kellett, B.P. Richards, The thermal expansion of graphite within the layer planes, J. Nucl. Mater. 12 (1964) 184–192. doi:10.1016/0022-3115(64)90139-4.

[19] W.C. Morgan, THERMAL EXPANSION COEFFICIENTS OF GRAPHITE CRYSTALS., Richland, WA (United States), 1971. doi:10.2172/4713298.

[20] J.H.W. Simmons, Radiation Damage in Graphite, 1st Editio, Pergamon, 1965.

[21] B.J. Marsden, G.N. Hall, O. Wouters, J.A. Vreeling, J. van der Laan, Dimensional and material property changes to irradiated Gilsocarbon graphite irradiated between 650 and 750 °C, J. Nucl. Mater. 381 (2008) 62–67. doi:10.1016/j.jnucmat.2008.07.018.

[22] X. Fang, H. Wang, S. Yu, C. Li, The various creep models for irradiation behavior of nuclear graphite, Nucl. Eng. Des. 242 (2012) 19–25. doi:10.1016/j.nucengdes.2011.09.024.

[23] J.E. Brocklehurst, B.T. Kelly, Analysis of the dimensional changes and structural changes in polycrsytalline graphite under fast neutron irradiation, Carbon N. Y. 31 (1993) 155–178.

[24] G. Haag, Properties of ATR-2E Graphite and Property Changes due to Fast Neutron Irradiation, 2005. doi:0944-2952.

[25] D.K.L. Tsang, B.J. Marsden, Constitutive material model for the prediction of stresses in irradiated anisotropic graphite components, J. Nucl. Mater. 381 (2008) 129–136. doi:10.1016/j.jnucmat.2008.07.025.

[26] A.. Perks, J.H.. Simmons, Radiation-induced creep in graphite, Carbon N. Y. 1 (1964) 441–449. doi:10.1016/0008-6223(64)90005-3.

[27] B.T. Kelly, A.J.E. Foreman, The theory of irradiation creep in reactor graphite—The dislocation pinning-unpinning model, Carbon N. Y. 12 (1974) 151–158. doi:10.1016/0008-6223(74)90021-9.

[28] A.A. Campbell, Historical experiment to measure irradiation-induced creep of graphite, Carbon N. Y. 139 (2018) 279–288. doi:10.1016/j.carbon.2018.06.055.

[29] S. Amelinckx, P. Delavignette, Dislocation loops due to quenched-in point defects in graphite, Phys. Rev. B. (1960) 50.

[30] M.I. Heggie, I. Suarez-Martinez, C. Davidson, G. Haffenden, Buckle, ruck and tuck: A proposed new model for the response of graphite to neutron irradiation, J. Nucl. Mater. 413 (2011) 150–155. doi:10.1016/j.jnucmat.2011.04.015.

[31] L. Li, S. Reich, J. Robertson, Defect energies of graphite: Density-functional calculations, Phys. Rev. B. 72 (2005) 184109. doi:10.1103/PhysRevB.72.184109.

[32] L. Bochirol, E. Bonjour, Irradiation of graphite at low temperature by neutrons and electrons. Measurement of stored energy and of variation in electrical resisitivity, Carbon N. Y. 6 (1966) 661–669. doi:10.1016/0008-6223(68)90010-9.

[33] C.P. Ewels, R.H. Telling, A.A. El-Barbary, M.I. Heggie, P.R. Briddon, Metastable Frenkel Pair Defect in Graphite: Source of Wigner Energy?, Phys. Rev. Lett. 91 (2003) 1–4. doi:10.1103/PhysRevLett.91.025505.

[34] S. Muto, T. Tanabe, Fragmentation of graphite crystals by electron irradiation at elevated temperatures, J. Electron Microsc. (Tokyo). 48 (1999) 519–523. doi:10.1093/oxfordjournals.jmicro.a023710.

[35] C. Karthik, J. Kane, D.P. Butt, W.E. Windes, R. Ubic, Neutron irradiation induced microstructural changes in NBG-18 and IG-110 nuclear graphites, Carbon N. Y. 86 (2015) 124–131. doi:10.1016/j.carbon.2015.01.036.

[36] C. Karthik, J. Kane, D.P. Butt, W.E. Windes, R. Ubic, In situ transmission electron microscopy of electron-beam induced damage process in nuclear grade graphite, J. Nucl. Mater. 412 (2011) 321–326. doi:10.1016/j.jnucmat.2011.03.024.

[37] J. Koike, D.F. Pedraza, Dimensional changes in highly oriented pyrolytic graphite due to electron-irradiation, J. Mater. Res. 9 (1994) 1899–1907. doi:10.1557/JMR.1994.1899.

[38] H.M. Freeman, A.J. Scott, R.M.D. Brydson, Thermal annealing of nuclear graphite during in-situ electron irradiation, Carbon N. Y. 115 (2017) 659–664. doi:10.1016/j.carbon.2017.01.057.

[39] S. Muto, T. Tanabe, Damage process in electron-irradiated graphite studied by transmission electron microscopy. I. high-resolution observation of highly graphitized carbon fibre, Philos. Mag. A Phys. Condens. Matter, Struct. Defects Mech. Prop. 76 (1997) 679–690. doi:10.1080/01418619708214029.

[40] F. Banhart, Irradiation effects in carbon nanostructures, Reports Prog. Phys. 62 (1999) 1181–1221. doi:10.1088/0034-4885/62/8/201.

[41] D. Ugarte, Curling and closure of graphitic networks under electron-beam irradiation, Nature. 359 (1992) 707–709. doi:10.1038/359707a0.

[42] A. V. Krasheninnikov, K. Nordlund, Ion and electron irradiation-induced effects in nanostructured materials, J. Appl. Phys. 107 (2010). doi:10.1063/1.3318261.

[43] A.P. Burden, J.L. Hutchison, Real-time observation of fullerene generation in a modified electron microscope, J. Cryst. Growth. 158 (1996) 185–188. doi:10.1016/0022-0248(95)00547-1.

[44] F. Banhart, J. Kotakoski, A. V Krasheninnikov, Structural Defects in Graphene, ACS Nano. 5 (2011) 26–41. doi:10.1021/nn102598m.

[45] M.T. Lusk, L.D. Carr, Nanoengineering defect structures on graphene, Phys. Rev. Lett. 100 (2008) 1–4. doi:10.1103/PhysRevLett.100.175503.

[46] D.H. Robertson, D.W. Brenner, C.T. White, On the way to fullerenes: Molecular dynamics study of the curling and closure of graphitic ribbons, J. Phys. Chem. 96 (1992) 6133–6135. doi:10.1021/j100194a011.

[47] S.T. Skowron, I. V. Lebedeva, A.M. Popov, E. Bichoutskaia, Approaches to modelling irradiation-induced processes in transmission electron microscopy, Nanoscale. 5 (2013) 6677–6692. doi:10.1039/c3nr02130k.

[48] J. Gruber, A.C. Lang, J. Griggs, M.L. Taheri, G.J. Tucker, M.W. Barsoum, Evidence for Bulk Ripplocations in Layered Solids, Sci. Rep. 6 (2016). doi:10.1038/srep33451.

[49] M.W. Barsoum, G.J. Tucker, Deformation of layered solids: Ripplocations no basal dislocations, Scr. Mater. 139 (2017) 166–172. doi:10.1016/j.scriptamat.2017.04.002.

CHAPTER TWO: A NEW OXIDATION BASED TECHNIQUE FOR ARTIFACT FREE TEM SPECIMEN PREPARATION OF NUCLEAR GRAPHITE*

This chapter is published by Elsevier in *Journal of Nuclear Materials* and should be referenced appropriately.

Reference:

S. Johns, W. Shin, J.J. Kane, W.E. Windes, R. Ubic, C. Karthik, A new oxidation based technique for artifact free TEM specimen preparation of nuclear graphite, J. Nucl. Mater. 505 (2018) 62–68.

*This chapter includes modifications the originally published version.

A NEW OXIDATION BASED TECHNIQUE FOR ARTIFACT FREE TEM SPECIMEN PREPARATION OF NUCLEAR GRAPHITE

Steve Johns[1]

Wontak Shin[1]

Joshua J. Kane[2]

William E. Windes[2]

Rick Ubic[1]

Chinnathambi Karthik[1]

Accepted for publication in:

Journal of Nuclear Materials

March, 2018

[1] *Micron School of Materials Science and Engineering, Boise State University, Boise, ID 83725, USA*

[2] *Idaho National Laboratory, 2525 Fremont Ave, Idaho Falls, ID 83402, USA*

Abstract

Graphite is a key component in designs of current and future nuclear reactors whose in-service lifetimes are dependent upon the mechanical performance of the graphite. Irradiation damage from fast neutrons creates lattice defects which have a dynamic effect on the microstructure and mechanical properties of graphite. TEM can offer real-time monitoring of the dynamic atomic-level response of graphite subjected to irradiation; however, conventional TEM specimen-preparation techniques, such as argon ion milling itself, damage the graphite specimen and introduce lattice defects. It is impossible to distinguish these defects from the ones created by electron or neutron irradiation. To ensure that TEM specimens are artifact-free, a new oxidation-based technique has been developed. Bulk nuclear grades of graphite (IG-110 and NBG-18) and highly oriented pyrolytic graphite (HOPG) were initially mechanically thinned to ~60μm. Discs 3mm in diameter were then oxidized at temperatures between 575°C and 625°C in oxidizing gasses using a new jet-polisher-like set-up in order to achieve optimal oxidation conditions to create self-supporting electron-transparent TEM specimens. The quality of these oxidized specimens were established using optical and electron microscopy. Samples oxidized at 575°C exhibited large areas of electron transparency and the corresponding lattice imaging showed no apparent damage to the graphite lattice.

2.1 Introduction

Graphite has been used as a moderator in molten-salt reactor (MSR) designs and CO_2-cooled reactor concepts like the advanced gas-cooled reactor (AGR), and it is a leading candidate core material for the extreme operating temperatures envisioned for Generation IV He-cooled reactor concepts like the very high temperature reactor (VHTR)

[1]. Graphite is exposed to harsh environments while in the reactor, leading to significant structural changes. Specifically, irradiation damage from fast neutrons create lattice defects which cause internal stresses and changes in mechanical properties. Internal stresses are relieved under irradiation via plastic deformation [2]; however, the mechanisms behind irradiation-induced creep and defect evolution in graphite are not well understood, which results in uncertainty in predicting the response of graphite components in reactors. For this reason, a complete understanding of irradiation-induced structural changes in nuclear graphite is critical to the determination of component in-service lifetimes.

When subjected to irradiation, complex dimensional changes occur in polycrystalline graphites, whereas graphite with a monocrystalline structure such as HOPG undergoes expansion in a direction normal to the basal planes accompanied by contraction within the basal planes [3]. The current understanding for the observed expansion along the c-axis is that displacement of carbon atoms occurs during irradiation which results in nucleation and clustering of interstitial loops between the basal planes. Formation of new basal planes results from rearrangement of these interstitial clusters, giving rise to expansion along the c-axis, and contraction within the basal plane [4-7]; however, this theory has been contradicted by Tanabe et al. [8,9] whose analysis of carbon fibers with room temperature transmission electron microscopy showed no evidence of interstitial basal plane formation, as such their existence at room temperature remains contentious. Another model exists which explains irradiation-induced dimensional change and amorphization of the graphite lattice at low temperature, which is explained by the accumulation of partial dislocations[10]; however, no clear consensus

as to the nature of such dislocations exists. The lack of a clear understanding of irradiation-induced microstructural changes can be attributed to the difficulty in acquiring experimental observations in real time of the dynamic natured microstructural changes along with the complex microstructure of nuclear graphite. In-situ transmission electron TEM studies (using electrons as a substitute for neutrons) has been shown as a means to overcome difficulties monitoring the atomic level response of nuclear graphites to irradiation [7,11-17]. One of the drawbacks of TEM studies in general is that the samples need to be thinned down to electron transparency. Conventional TEM specimen-preparation techniques such as ion milling and focused ion-beam (FIB) thinning result in ion-beam-induced irradiation damage to the graphite lattice. Distinguish these defects from ones created by neutron and electron irradiation can be difficult, making the study of the atomic level response of the graphite lattice to irradiation ambigous. For accurate microstructural and irradiation-induced defect analysis, it is imperative that specimens are free of any artifacts introduced during specimen preparation.

To avoid any such damage to the graphite lattice, a new TEM specimen-preparation technique via oxidation has been developed and optimized. Graphite may be readily oxidized at temperatures above 450°C, in which displacement of carbon atoms via desorption of reaction products occurs. Utilizing the thermal oxidation of graphite, combined with the use of a jet-polishing-like set-up, an optimal experimental procedure has been developed to produce quality electron-transparent TEM specimens without any damage to the lattice.

2.2 Experimental

IG-110, NBG-18 and HOPG grades of graphite were used in this work. IG-110, manufactured by Toyo Tanso Co., Kagawa, Japan, is a petroleum-coke-based, fine-grained, iso-molded nuclear graphite. NBG-18, manufactured by SGL Group, Wiesbade, Germany, is a pitch-coke-based, medium-grained, vibration-molded nuclear graphite. Both grades of NBG-18 and IG-110 have a complex microstructure composed of filler, binder, QI particles, micropores, Mrozowski cracks, and turbostatic graphite phase [18,19]. Grade 1 HOPG graphite was supplied by SPI supplies as 3 mm discs approximately 40 μm thick. In addition, HOPG has been used as an approximation of single crystal graphite due to the highly oriented nature of the crystallites [3]. Bulk samples of NBG-18 and IG-110 were cut using a low-speed diamond wafering blade into approximately 0.5 mm thick slabs. Samples were further mechanically thinned to approximately 60 μm via grinding and polishing, then 3mm specimens were cut using a Gatan TEM specimen disc punch or a rotary disc cutter (Model 360, Southbay, San Clemente, CA). Final thinning of specimens to electron transparency was achieved by controlled oxidation experiments in which the center of the 3 mm specimen discs were selectively oxidized, resulting in self-supporting TEM specimens.

Specimens of HOPG were dimple-ground with 1 μm diamond paste until perforated, with final thinning via oxidation. This alternative sample preparation was adopted due to the crystallographic structure of HOPG. For HOPG samples, basal planes are parallel to the surface of the specimen exposed for oxidation. As such, to expose active sites for oxidation to readily occur without the need of excessive oxidation times, basal plane edges were exposed via dimple grinding. Oxidation of exposed basal plane

edges was conducted such that mechanically induced damage equal to at least three times the abrasive size used was removed.

When graphite is subjected to oxidation at high temperatures, molecular oxygen is chemisorbed on active sites within the graphite lattice. These sites are often referred to as arm chair or zig zag sites, both of which are located on basal plane edges (Figure 2.1). It is highly thermodynamically unfavorable for oxidation to occur on an interior lattice point [20-23]. Due to oxidation occurring primarily on these active sites, nuclear grades NBG-18 and IG-110 show preferential oxidation in the binder or matrix phase, followed by the filler regions then QI particles [24]. As such, sample preparation via oxidation may produce specimens with large areas of filler and QI particles present, so for the purpose of this study, high-resolution TEM (HRTEM) of single graphite crystallites was conducted in either the binder or filler regions of artificial nuclear graphites.

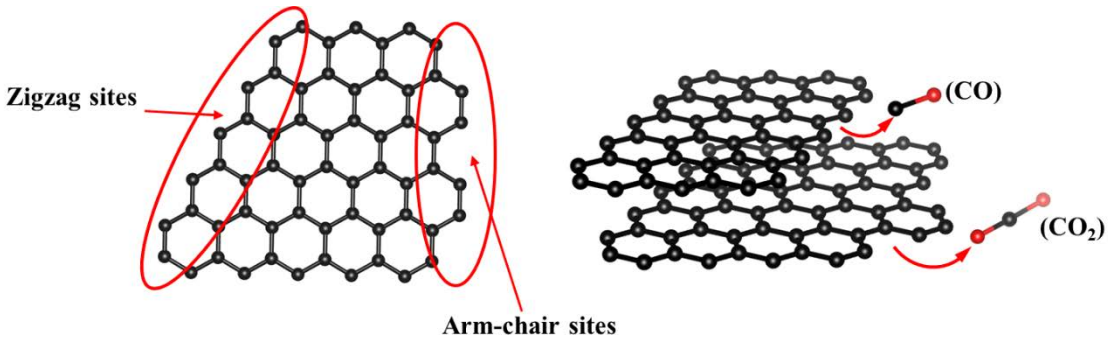

Figure 2.1 Active sites for oxidation to occur can be represented two dimensionally as zigzag and armchair sites. Desorption of reaction products occur as carbon monoxide and carbon dioxide.

Oxidation of nuclear graphite in air has been extensively studied [20-28] and can be expressed generically by the following reactions.

$$C + \frac{1}{2}O_2 \rightarrow CO \quad (2.1)$$

$$C + O_2 \rightarrow CO_2 \quad (2.2)$$

There are many other compounds, such as H_2O, which may oxidize graphite; but for this study molecular oxygen is the primary oxidizing reactant.

Oxidation of graphite may be categorized into three regimes: regime 1 or the chemical regime, regime 2 or the in-pore diffusion-controlled regime, and regime 3 or the sublimation regime [25]. Regime 1 is characterized by temperatures below 600°C and low oxidation rates [26,27]. Within regime 1, oxidation occurs slowly, and oxidizing gasses are allowed to penetrate deep within the graphite structure, resulting in uniform oxidation throughout the sample. Regime 2 is within the temperature range 600-900°C [26,27]. In regime 2, activation energy for oxidation may be reduced by as much as half [28]. Oxidation occurs closer to the graphite surface, although diffusion into the porous network is still occurring. Regime 3 occurs at temperatures above 900°C where carbon oxidation reactions will occur primarily on the surface [23]. While temperature may be a major factor in determining oxidation regime, other factors such as microstructure, sample size, geometry, oxidizing gasses and flow rate will influence the temperature boundaries between oxidation regimes [29]. Here, oxidation was conducted within the temperature range of 575-625°C, where oxidation is believed to be uniform and slow, allowing for more precise experimental control.

Oxidation experiments were conducted in a horizontal tube furnace with a 5 cm inner diameter and 122 cm long alumina process tube. A jet-polishing type apparatus constructed out of 304L stainless steel, in which oxygen is used as an etchant to perform oxidation, was fabricated for use within the tube furnace. The apparatus allows oxidizing gasses to be introduced to both sides of the specimen. Figure 2.2 (a) and (b) show a simple schematic of the oxidation system along with the fabricated apparatus. Figure 2.2

(c) shows how graphite specimens were supported by a machined washer and positioned between two Au TEM grids with a 1 mm hole to selectively oxidize the center of the specimen. Nuclear grade graphites were oxidized in a temperature range between 575-625°C with zero grade compressed air (20.9% O_2, 79.1% N_2) introduced at a flow rate of 5 standard liters per minute. The tube furnace atmosphere was purged with N_2 until the target oxidizing temperature was reached, and N_2 was re-introduced after desired oxidation times.

A Leica DM6000 optical microscope with MultiFocus capability was used to study the progression of oxidation and final perforation by monitoring the thickness profiles of these samples. Scanning electron microscopy studies on the oxidized samples were conducted with an FEI Teneo. Room-temperature bright-field and high resolution transmission electron microscopic (HRTEM) studies were performed using a JEOL-2100 HR TEM operated at 200kV.

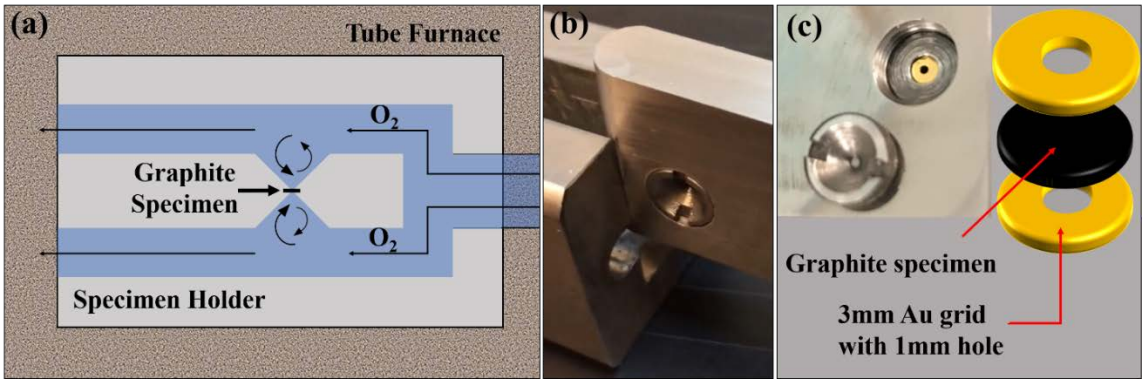

Figure 2.2 (a) Schematic of the oxidation system used to selectively oxidize graphite specimens. (b) Specimen holder constructed of 304L stainless steel. (c) Threaded plug removed to show washer used to support 3 mm graphite specimen which is positioned between two Au TEM aperture grids to selectively oxidize the center of graphite specimens.

2.3 Results and Discussion

TEM specimens of nuclear grade graphites prepared to electron transparency via oxidation have been shown to produce self-supporting 3 mm TEM specimens. Figures 2.3 (a) and (b) show optical micrographs of IG-110 before and after oxidation at 625°C for 30 minutes. The thickness profile recorded from one of the sides of the sample shown in Figs.3 (c) and (d) confirms the selective oxidation of the sample's center. The outer edge of the sample was not affected by the oxidation and thick enough to provide mechanical support to the specimen. Self-supporting TEM specimens which do not require the use of support grids are vital for high temperature in-situ TEM as well as neutron irradiation studies which will require heating of specimens to temperatures above 800°C. Common specimen grids such as Cu, Au, Ni and Mo, have been shown to be unstable at high temperatures in which sublimation and deposition of metal from grids occurs and in which subsequent interaction of the metal with the specimen may mislead interpretations of experimental results [30].

Ion milling imparts irradiation damage into TEM specimens. This damage includes defect production and surface layer amorphization [31,32]. Specifically, for NBG-18 and IG-110, this damage includes closure of Mrozowski cracks, lattice defects and amorphization. Figure 2.4 (a) and (b) show bright-field TEM images recorded from an NBG-18 sample prepared with conventional ion-milling techniques for comparison. Low-kV, low-angle ion-milling finishing was conducted on the specimen at 1kV and 2° for 20 minutes after perforation; however, this process does not completely remove the amorphous region or resulting microstructural defects. Amorphous carbon can be seen in Figure 2.4 (a) near the hole edge of the specimen, indicating that the graphite

microstructure has been damaged by the Ar^+ ions. The HRTEM imaging in Figure 2.4 (b) shows defects within the graphite lattice and amorphous carbon occurring, not only on the edge of the specimen, but in the bulk of the material as well.

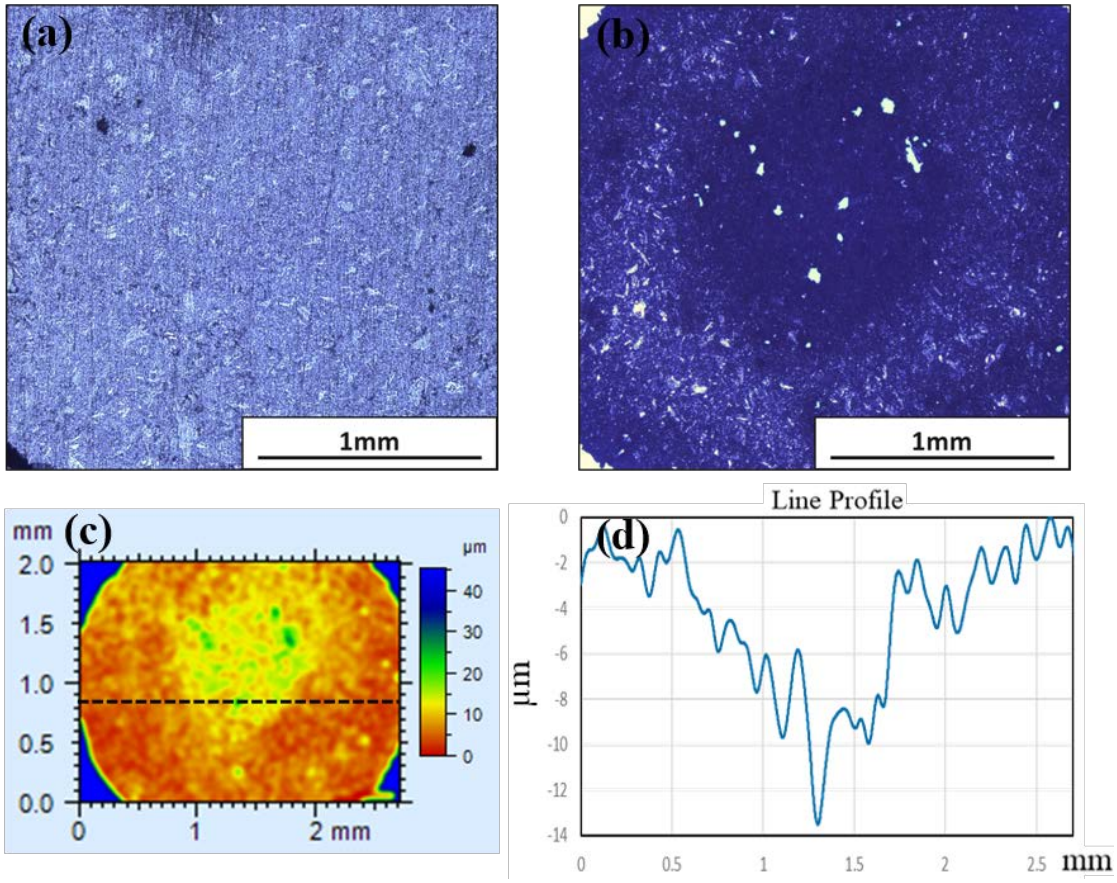

Figure 2.3 (a) & (b) show respectively the optical images of IG-110 sample before and after oxidation at 625°C for 30 min. (c) Optical z stacking depth map of oxidized NBG-18 specimen. (d) Line profile from depth map in (c) showing that the oxidation is preferential to the center of the discs, creating self-supporting TEM specimens.

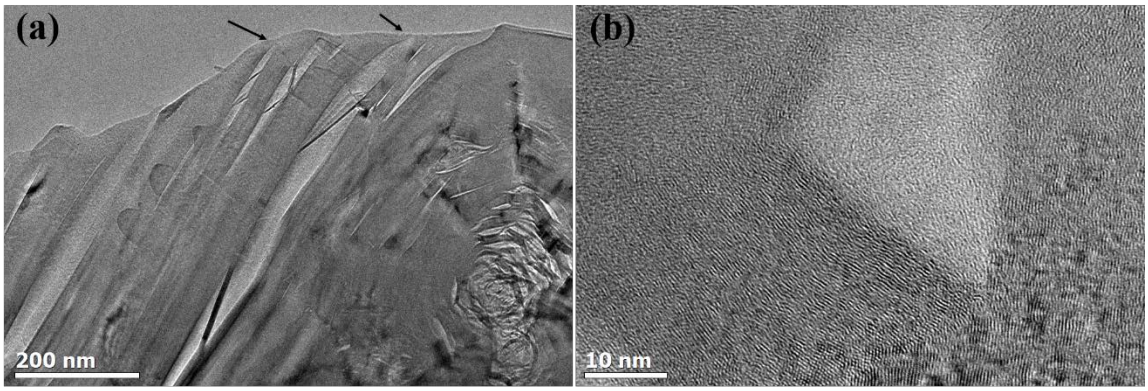

Figure 2.4 (a) Bright-field TEM micrograph of an NBG-18 specimen prepared using conventional ion-milling technique with the area of milling damage indicated with arrows, i.e., closure of Mrozowski cracks and the presence of amorphous carbon near hole edge. (b) HRTEM micrograph near QI particle seen in (a) showing defects which are indistinguishable from those created by ion-milling.

Specimens of NBG-18 were successfully oxidized to electron transparency in a temperature range of 575-625°C (Figure 2.5). NBG-18 oxidized at the given temperatures required approximately 30 minutes of oxidation to produce electron-transparent specimens; although experimental results varied, some specimens being over- or under-oxidized in 30 minutes. This variation is believed to be due to the large grain and pore structure found in NBG-18 [33,34]. Given the inhomogeneous nature of the microstructure, along with many microstructural features being larger than the area being oxidized, variance in experimental results can be expected. Variability in experimental results may also be attributed to the accuracy to which specimens can be mechanically thinned to 60 μm.

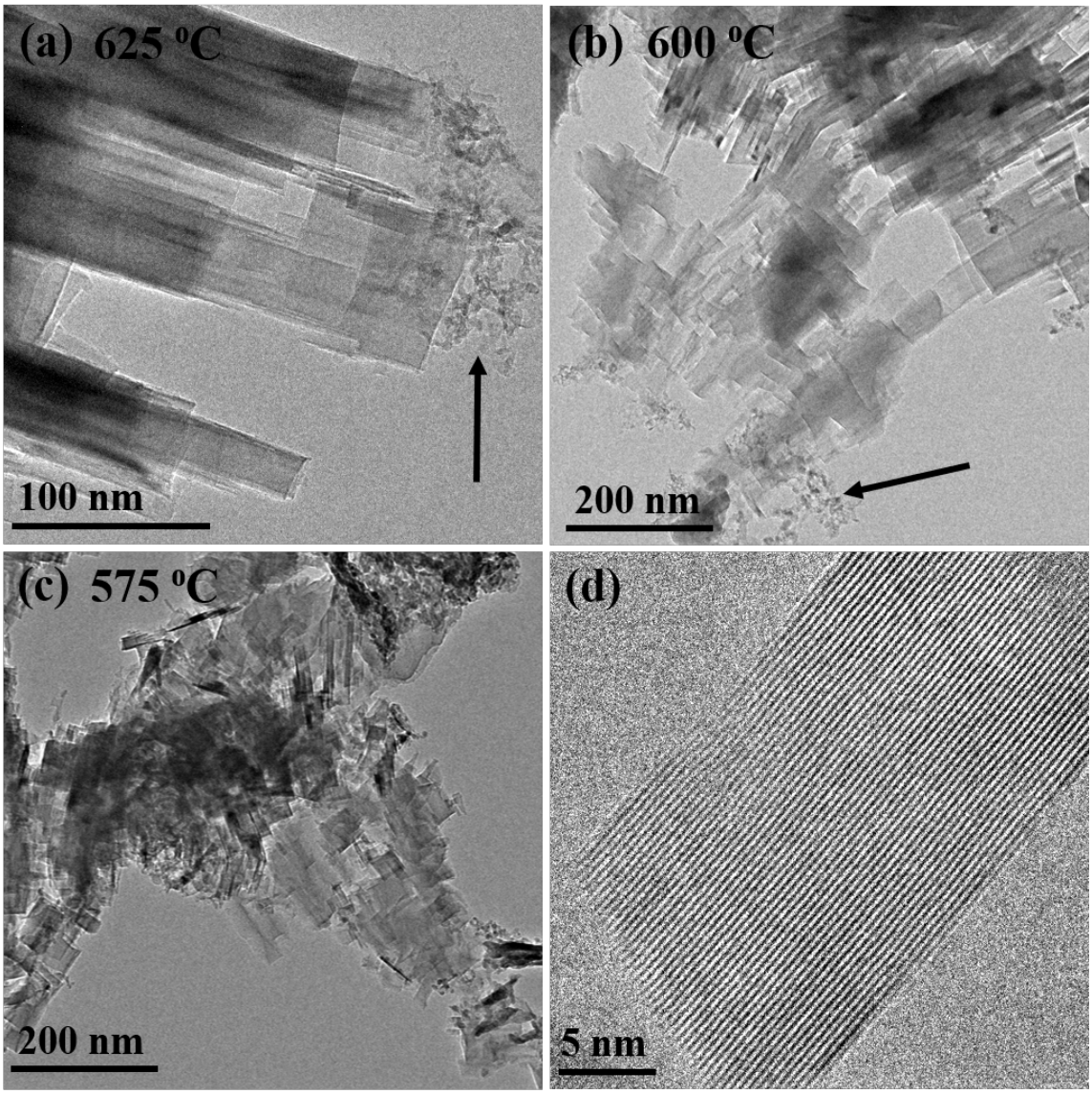

Figure 2.5 Bright-field TEM micrographs of NBG-18 nuclear graphite oxidized to electron transparency between the temperatures of 575-625°C. At temperatures of 625°C (a) and 600°C (b), areas of crystalline graphite are present, although amorphous carbon is observed in many areas, indicated by black arrows. Decreasing oxidation temperature leads to a decrease of amorphous material around leading basal plane edges. Oxidation temperature of 575°C (c) shows large areas of un-damaged basal plane edges ideal for lattice imaging (d).

TEM analysis of specimens shows the presence of crystalline graphite at oxidation temperatures of 575-625°C, as seen in Figure 2.5 (a-c), although accompanying the crystalline structure is the presence of amorphous carbon in many areas of specimens oxidized at 625°C and 600°C, as shown in Figures 2.5 (a) and (b). Experimental results

show the amount of amorphous carbon, as an artifact from oxidation, decreases with decreasing temperature. 575°C was chosen as the optimal condition for sample preparation. This temperature, as shown in Figures 2.5 (c) and (d), produced large areas of preserved crystallinity, produced minimal amorphous carbon surrounding graphite flakes and lattice, and was experimentally practical for oxidation times. The resulting single graphite flakes with no surrounding damage are ideal for graphite lattice imaging and further electron or neutron irradiation studies.

The appearance of amorphous carbon may be an indication of surface chemistry changing as oxidation temperature is increased. At the lower oxidation temperatures of regime 1, molecular oxygen is chemisorbed onto the basal plane of graphite in bridge positions over the C−C bonds, forming epoxy groups [35]. As the temperature of oxidation is increased, new oxygen functional groups, such as ethers, which have been shown to be more thermally stable, may be formed and remain on the surface at room temperature [36]. These remaining functional groups may explain the presence of amorphous carbon seen at higher oxidation temperatures, and is theorized to cause bending, distortion and unzipping of the graphite lattice [37].

Bright-field TEM images of IG-110 oxidized at 625-575°C are shown in Figures 2.6 (a-d). Experimental results show the same trends as that of NBG-18; a larger amount of amorphous carbon is seen at oxidation temperatures of 625°C and 600°C, shown in Figure 2.6 (a) and (b); whereas there is little to no amorphous carbon surrounding graphite crystals at 575°C, shown in Figure 2.6 (c) and (d). Oxidation experiments for IG-110 yielded consistent results for set oxidation times. Specimens achieved electron

transparency with 60 minutes of oxidation at 575°C and required 40 minutes of oxidation at temperatures of 600°C and 625°C.

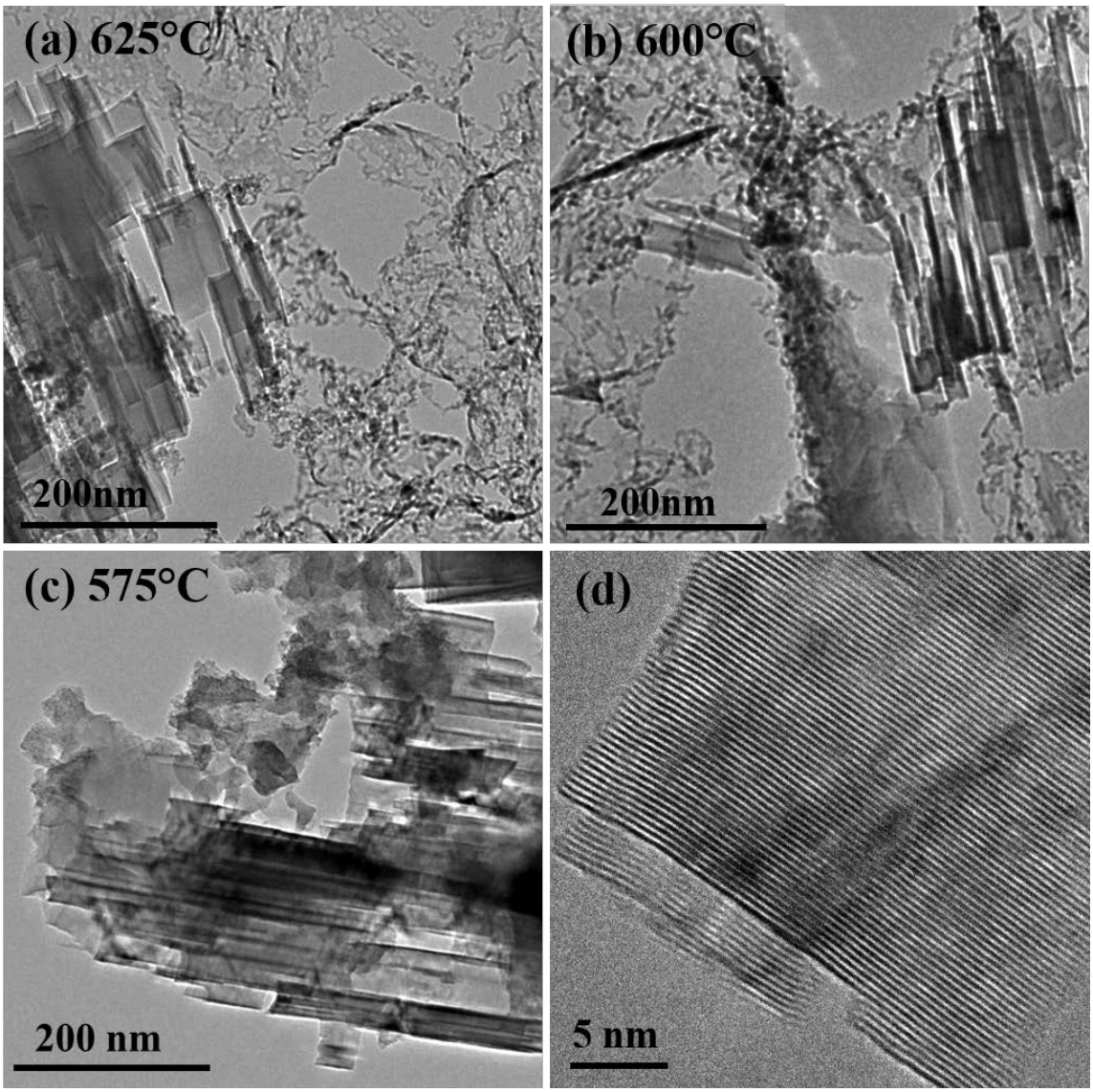

Figure 2.6 Bright-field TEM micrographs of IG-110 nuclear graphite oxidized to electron transparency at temperatures of (a) 625°C, (b) 600°C and (c) 575°C. The same behavior of decreasing amount of amorphous material as oxidation temperature decreases is observed. (d) HRTEM of IG-110 oxidized at 575°C showing un-damaged graphite lattice.

Oxidative specimen preparation was also shown to be successful with HOPG; however, due to the orientation of HOPG's basal plane edges, the amount of active

surface area for oxidation to occur is drastically reduced with respect to IG-110. Confirmation that oxidation primarily occurs on the leading basal plane edges can be seen in the secondary-electron SEM image in Figure 2.7 (a) by the presence of distinct steps in the basal plane layers. Electron transparency was achieved with 3 hours of oxidation at 575°C. Large areas of preserved crystallinity are indicated throughout the specimen by the presence of moiré fringes continuing to the edge of the specimen as seen in Figure 2.7 (b). HOPG specimens are crucial for the analysis of irradiation-induced defects such as basal plane dislocations via imaging along the c-axis.

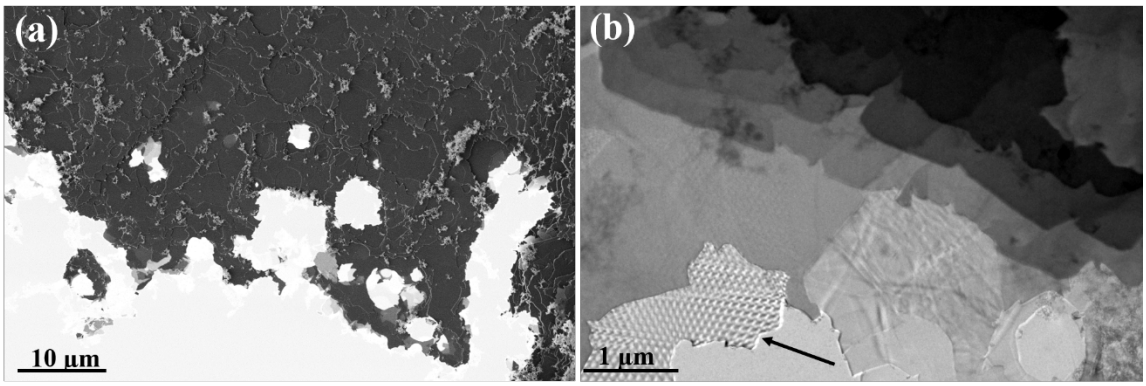

Figure 2.7 (a) Secondary Electron SEM image of oxidized HOPG specimen. (b) Bright field TEM image of oxidized HOPG specimen with moiré fringes indicated with black arrow.

TEM specimens of graphite prepared via oxidation consist of thin crystals which are ideal for HRTEM lattice imaging because they contain no damaged surface layers; however, as with all TEM specimens, care must be taken when extrapolating bulk mechanical behavior from essentially two-dimensional specimens in plane stress conditions. Observations in such specimens may not be directly comparable to macroscopic changes of bulk material. The data collected on the specimens examined in

this study can be used as a baseline for both in-situ electron-irradiation and neutron-irradiation studies.

2.4 Conclusions

A new oxidation-based TEM specimen preparation has been developed and shown to produce self-supporting electron transparent specimens of nuclear graphite grades NBG-18 and IG-110 as well as HOPG. Nuclear graphite specimens oxidized at 575^{o}C showed defect free lattice images. Oxidation times varied depending on the grade and starting thickness. These specimens are imperative as an irradiation free baseline for microstructural defect analysis of graphites exposed to electron and neutron irradiation studies. This technique also eliminates the need for expensive techniques such as focused ion beam to prepare nuclear graphite TEM specimens.

2.5 References

[1] Allen, T.R., Sridharan, K., Tan, L., Windes, W.E., Cole, J.I., Crawford, D.C., and Was, G.S. Materials Challenges for Generation IV Nuclear Energy Systems, Nucl. Technol. 162 (2008) 342–357.

[2] F. Banhart, Irradiation effects in carbon nanostructures, Reports Prog. Phys. 62 (1999) 1181–1221.

[3] R.E. Nightingale, Nuclear Graphite, Academic press, New York (1962).

[4] J. H.W. Simmons, Radiation Damage in Graphite, Pergamon Press, Oxford, (1965).

[5] Kelly, BT, Brocklehurst, JE, and Gittus, JH. Irradiation damage in graphite. Graphite Structures for Nuclear Reactors, Conference organised by the Nuclear Energy Group of the Institution of Mechanical Engineers, 7th - 9th March. (1972) 17-28.

[6] C. Karthik, J. Kane, D.P. Butt, W.E. Windes, R. Ubic, Neutron irradiation induced microstructural changes in NBG-18 and IG-110 nuclear graphites, Carbon 86 (2015) 124–131.

[7] C. Karthik, J. Kane, D.P. Butt, W.E. Windes, R. Ubic, In situ transmission electron microscopy of electron-beam induced damage process in nuclear grade graphite, J. Nucl. Mater. 412 (2011) 321–326.

[8] T. Tanabe, S. Muto, K. Niwase, on the Mechanism of Dimensional Change of Neutron-Irradiated Graphite, Appl. Phys. Lett. 61 (1992) 1638–1640.

[9] M. Takeuchi, S. Muto, T. Tanabe, S. Arai, T. Kuroyanagi, Damage process in electron-irradiated graphite studied by transmission electron microscopy. II. Analysis of extended energy-loss fine structure of highly oriented pyrolytic graphite, Philos. Mag. A Phys. Condens. Matter, Struct. Defects Mech. Prop. 76 (1997) 691–700.

[10] K. Niwase, Formation of dislocation dipoles in irradiated graphite, Mater. Sci. Eng. A. 400–401 (2005) 101–104.

[11] S. Muto, T. Tanabe, Fragmentation of graphite crystals by electron irradiation at elevated temperatures, J. Electron Microsc. 48 (1999) 519–523.

[12] S. Muto, S. Horiuchi, T. Tanabe, Local structural order in electron-irradiated graphite studied by high-resolution high-voltage electron microscopy, J. Electron Microsc. 48 (1999) 767–776.

[13] A. Asthana, Y. Matsui, M. Yasuda, K. Kimoto, T. Iwata, K.I. Ohshima, Investigations on the structural disordering of neutron-irradiated highly oriented pyrolytic graphite by X-ray diffraction and electron microscopy, J. Appl. Crystallogr. 38 (2005) 361–367.

[14] A. Chuvilin, U. Kaiser, E. Bichoutskaia, N.A. Besley, A.N. Khlobystov, Direct transformation of graphene to fullerene, Nat. Chem. 2 (2010) 450–453.

[15] J.A. Hinks, A.N. Jones, A. Theodosiou, J.A. van den Berg, S.E. Donnelly, Transmission Electron Microscopy Study of Graphite under in situ Ion Irradiation, J. Phys. Conf. Ser. 371 (2012) 12046.

[16] S.C. Tsai, E.W. Huang, J.J. Kai, F.R. Chen, Microstructural evolution of nuclear grade graphite induced by ion irradiation at high temperature environment, J. Nucl. Mater. 434 (2013) 17–23.

[17] H.M. Freeman, B.E. Mironov, W. Windes, M.M. Alnairi, A.J. Scott, A.V.K. Westwood, R.M.D. Brydson, Micro to nanostructural observations in neutron irradiated nuclear graphites PCEA and PCIB, J. Nucl. Mater. 491 (2017) 221–231.

[18] K.Y. Wen, T.J. Marrow, B.J. Marsden, The microstructure of nuclear graphite binders, Carbon 46 (2008) 62–71.

[19] C. Karthik, J. Kane, D.P. Butt, W.E. Windes, R. Ubic, Microstructural characterization of next generation nuclear graphites, Microsc. Microanal. 18 (2012) 272–278.

[20] Yavorsky, IA, and Malanov, MD. On the reactivity of basal and prismatic faces of pyrographite crystallites. Carbon 7 (1969) 287-291.

[21] Hippo, EJ, Murdie, N, and Hyjazie, A. The role of active sites in the inhibition of gas carbon reactions. Carbon 27 (1989) 689-695.

[22] Abrahamson, J. The surface energies of graphite. Carbon 11 (1973) 337-362.

[23] J.J. Kane, C. Karthik, R. Ubic, W.E. Windes, D.P. Butt, An oxygen transfer model for high purity graphite oxidation, Carbon 59 (2013) 49–64.

[24] W.H. Huang, S.C. Tsai, C.W. Yang, J.J. Kai, The relationship between microstructure and oxidation effects of selected IG- and NBG-grade nuclear graphites, J. Nucl. Mater. 454 (2014) 149–158.

[25] J Walker, P.L., J Rusinko, Frank, LG Austin, Gas Reactions of Carbon, Advan. Catal. 11 (1959) 133-221.

[26] International Atomic Energy Agency, Irradiation Damage in Graphite Due to Fast Neutrons in Fission and Fusion Systems, IAEA-TECDOC-1154, Vienna, 2000.

[27] W. Choi, B. Kim, E. Kim, S. Chi, S. Park, Oxidation behavior of IG and NBG nuclear graphites, Nucl. Eng. Des. 241 (2011) 82–87.

[28] X. Luo, X. Yu, S. Yu, Oxidation performance of graphite material in reactors, Front. Energy Power Eng. China (2008) 471–474.

[29] J.J. Kane, C.I. Contescu, R.E. Smith, G. Strydom, W.E. Windes, Understanding the reaction of nuclear graphite with molecular oxygen: Kinetics, transport, and structural evolution, J. Nucl. Mater. 493 (2017) 343–367.

[30] Z. Zhang, D. Su, Behaviour of TEM metal grids during in-situ heating experiments, Ultramicroscopy. 109 (2009) 766–774.

[31] L.A. Giannuzzi, F.A. Stevie, A review of focused ion beam milling techniques for TEM specimen preparation, Micron. 30 (1999) 197–204.

[32] H.H. Jin, C. Shin, J. Kwon, Fabrication of a TEM sample of ion-irradiated material using focused ion beam microprocessing and low-energy Ar ion milling, J. Electron Microsc. 59 (2010) 463–468.

[33] J. Kane, C. Karthik, D.P. Butt, W.E. Windes, R. Ubic, Microstructural characterization and pore structure analysis of nuclear graphite, J. Nucl. Mater. 415 (2011) 189–197.

[34] S.P. Jing, C. Zhang, J. Pu, H.Y. Jiang, H.H. Xia, F. Wang, X. Wang, J.Q. Wang, C. Jin, 3D microstructures of nuclear graphite: IG-110, NBG-18 and NG-CT-10, Nucl. Sci. Tech. 27 (2016) 1–8.

[35] J.L. Li, K.N. Kudin, M.J. McAllister, R.K. Prud'homme, I.A. Aksay, R. Car, Oxygen-driven unzipping of graphitic materials, Phys. Rev. Lett. 96 (2006) 5–8.

[36] R. Larciprete, P. Lacovig, S. Gardonio, A. Baraldi, S. Lizzit, Atomic Oxygen on Graphite : Chemical Characterization and Thermal Reduction J. Phys. Chem. C 116 (2012) 9900–9908.

[37] T. Sun, S. Fabris, Mechanisms for oxidative unzipping and cutting of graphene, Nano Lett. 12 (2012) 17–21.

CHAPTER THREE: FORMATION OF CARBON NANOSTRUCTURES IN NUCLEAR GRAPHITE UNDER HIGH-TEMPERATURE IN SITU ELECTRON-IRRADIATION*

This chapter is published by Elsevier in *Carbon* and should be referenced appropriately.

Reference:

S. Johns, T. Poulsen, J.J. Kane, W.E. Windes, R. Ubic, C. Karthik, Formation of carbon nanostructures in nuclear graphite under high-temperature in situ electron-irradiation, Carbon N. Y. 143 (2019) 908–914.

*This chapter includes modifications the originally published version.

FORMATION OF CARBON NANOSTRUCTURES IN NUCLEAR GRAPHITE UNDER HIGH-TEMPERATURE IN SITU ELECTRON-IRRADIATION

Steve Johns[1]

Tyler Poulsen[1]

Joshua J. Kane[2]

William E. Windes[2]

Rick Ubic[1]

Chinnathambi Karthik[1]

Accepted for publication in:

Carbon

November, 2018

[1] *Micron School of Materials Science and Engineering, Boise State University, Boise, ID 83725, USA*

[2] *Idaho National Laboratory, 2525 Fremont Ave, Idaho Falls, ID 83402, USA*

Abstract

Defect evolution in nuclear graphite has been studied in real time using high-temperature in situ transmission electron microscopy. In situ electron-irradiation was conducted at 800°C on a 200 kV transmission electron microscope with a dose rate, given in terms of displacements per atom per second, of approximately 1.46×10^{-3} dpa/s. Defect domains consisting of ordered arrangements of pentagons, hexagons, and heptagons exist intrinsically in nuclear graphite and in addition are readily produced via electron-irradiation; however, at elevated temperatures these defect domains undergo atomic rearrangements resulting in the formation of carbon nanostructures via curling and closure of the basal planes. The formation of fullerenes and other structures due to thermal annealing or high-temperature electron-irradiation has been observed in disordered regions of the microstructure and interstitially between basal planes. These defect structures result in localized swelling and expansion of crystallites along the c axis; thus, it is proposed as one of the many atomic mechanisms involved in the dimensional change of nuclear graphite subjected to high-temperature irradiation.

3.1 Introduction

Nuclear graphite is commonly used as a moderating material as well as a key structural component in nuclear reactor designs. It is also a candidate material for the future Generation IV reactors such as the very high temperature nuclear reactor (VHTR), which may operate at up to 1000°C [1]. While in reactors, irradiation damage is accumulated in graphite over time from a fluence of fast neutrons. During irradiation, significant structural changes to the crystalline structure of graphite occurs, leading to plastic deformation. Irradiation-induced microstructural changes can play an important

role in adversely affecting the mechanical properties (and hence performance) of nuclear graphites; however, a clear consensus on the various atomic mechanisms responsible for irradiation-induced microstructural evolution has not yet emerged, which yields uncertainty in accurately predicting component in-service lifetimes. In part, this uncertainty is due to the difficulty in monitoring the dynamic response of graphite during irradiation at the atomic level.

While in situ monitoring of the atomic level response of graphite in nuclear reactors remains impossible; in situ transmission electron microscopy (TEM) offers a way to monitor the dynamic atomic response of graphite during irradiation-induced defect production, in which electrons are used as a substitute for neutrons. While electron-irradiation does provide a method to overcome difficulties in monitoring the atomic level response of graphite, considerations must be taken as the dose rate for electron-irradiation (10^{-4} - 10^{-3} dpa/s) is far greater than that of typical neutron-irradiation (10^{-7} dpa/s) [1]. Electron-irradiation is generally observed experimentally to primarily cause point defects; however, theory proposed by Oen [2] suggests that secondary cascade collisions have only a small contribution at high electron accelerating voltages; whereas cascade damage can be significant under irradiation by neutrons given their larger mass. In any event, the mobility and annealing rate of defects are Arrhenius in nature [3]; therefore, as the operating temperature of many nuclear reactors is above 450°C, as will be that of the VHTR, cascade damage is partially annealed out between individual cascade events, giving a net effect of isolated point-defect damage [4]. In addition, given a low density of collision cascades due to the wide spacing of graphite's basal planes [4], high-temperature neutron-irradiation may arguably be comparable to

high dose-rate electron-irradiation [5,6].

On the atomic scale, radiation displacement of carbon atoms causes contraction in the a/b direction (i.e., parallel to the basal planes) and expansion in the c- direction (i.e., perpendicular to the basal planes) [7-10]. The formation of interstitial loops between basal planes is generally believed to result in c-axis expansion due to the formation of additional basal planes and a-axis contraction from displacement of atoms within the basal planes [8]; however, alternative explanations for dimensional change in nuclear graphite are given by recent theoretical models of basal plane defects, such as five- and seven-member rings [11,12], the buckling of basal planes, and the so called "ruck and tuck" of basal planes [13]. The buckling and distortion in sp^2 bonded materials is known to occur in the presence of defect domains consisting of ordered arrangements of pentagons, hexagons, and heptagons, in which the atomic arrangement departs from the typical honeycomb structure [14]. Specific defects include the so called Stone-Wales defect and the Haeckelite allotrope of carbon [15]. These basal plane defects are commonly modeled two-dimensionally within graphene ribbons (isolated graphene strips). Density functional theory (DFT) and molecular dynamics (MD) studies provide a means for further analysis of the stability, scalability, and other key physical properties of materials with these defect structures. Stable basal plane defects cause strain with respect to unstressed graphene and have been proposed to result in out-of-plane "blistering" of approximately 2 Å [12]. Furthermore, MD studies have shown that graphene ribbons of a critical size (rectangular ribbons of 56 atoms or more), along with the presence of five-member rings and high temperature (~525-925°C), will curl and edges will meet resulting in closure and the formation of open-ended hollow structures (i.e., nanotubes) [16]. MD

studies have also shown graphene-to-fullerene transformations under simulated electron-irradiation [17].

Many in situ electron-irradiation studies which analyze the c-axis expansion of crystallites, amorphization, fragmentation of basal planes, tortuous nanotexture and line-defect formation of graphite have been conducted [3,6,18-21]. Koike's [18] room temperature electron-irradiation TEM studies showed 300% expansion along the c axis in a crystallite of highly oriented pyrolytic graphite (HOPG). The proposed mechanism for the extraordinary swelling along the c axis was given by fragmentation of basal planes due to small interstitial clusters. Room-temperature electron-irradiation studies on graphitized carbon fibers by Muto and Tanabe [19] additionally showed swelling along the c axis; however, experimental results showed homogenous swelling of the lattice spacing contradicting the proposed expansion due to fragmentation. It should also be noted that experimental results from Refs. [18] and [19] did not provide evidence of stable interstitial or vacancy dislocation loops, and their existence at room temperature remains controversial. Other experimentally deduced mechanisms proposed for irradiation-induced structural changes in nuclear graphite at room temperature include the formation of new basal planes via dislocation climb [6]; however, electron-irradiation studies conducted at elevated temperatures remains scant [3,20,21]. Of the few studies conducted, that of Muto and Tanabe [20] showed that above temperatures of approximately 125°C the mechanisms controlling irradiation damage change at a critical dose inferred from electron diffraction patterns. At temperatures below 125°C, an increase in lattice spacing was observed; however, at temperatures above approximately 400°C lattice spacings remained unchanged, indicating that during irradiation the

graphite structure was not altered locally. As such, there remains no clear consensus to the atomic mechanisms that contribute to dimensional changes seen in nuclear graphite. While there remains a dearth of experimental studies of graphite at elevated temperatures, there have been many studies of the alterations within disordered carbonaceous species irradiated with energetic electrons, in which the formation of fullerenes, nanotubes and carbon onions have been observed [9,22-24]; however, in-situ TEM experiments of these phenomena occurring within nuclear graphites under irradiation at elevated temperatures have not yet been conducted.

Almost all graphitic precursors, such as soot particles, or any disordered graphitic species have been shown to transform to fullerene phases when subjected to sufficient irradiation with an electron beam [25]. Nuclear graphites have a complex microstructure composed of filler, binder, quinoline insoluble (QI) particles, micropores, turbostratic graphite phase, and lenticular cracks nanometers to several hundreds of nanometers in length known as Mrozowski cracks [26,27]. Mrozowski cracks form between basal planes due to weak Van der Waals bonding and volumetric shrinkage during cooling from graphitization temperatures. Given the complexity of this microstructure, a high density of various defects exists; therefore, studies conducted on areas of the microstructure with well aligned crystallites, such as filler particles, in which lattice fringes are imaged perpendicular to the c axis, may not be an accurate depiction of the bulk material. Furthermore, one might expect the presence of under-coordinated carbon atoms in poorly graphitized areas of the microstructure including phase boundaries, crystallite boundaries, and within many microstructural features such as QI particles and Mrozowski cracks. Distortions in the graphitic structure may be expected when any non-

six-sided rings are present. In addition, given defect production due to high temperature and irradiation, non-equilibrium conditions are maintained while graphite is in nuclear reactors, which may stabilize fullerene phases and other carbon nanostructures. In this work, high-temperature in situ electron-irradiation studies have been conducted on nuclear graphite IG-110. Experimental results show the morphology and ordering of carbon nanostructures not only in disordered areas of the microstructure, but interstitially between basal planes as well. The formation of these nanostructures is proposed as one of the many mechanisms resulting in the dimensional changes seen in high-temperature irradiated nuclear graphite.

3.2 Experimental

3.2.1 Sample Preparation and Microscopy

IG-110 nuclear graphite (Toyo Tanso Co., Kagawa, Japan) is a petroleum-coke-based, fine-grained, iso-molded nuclear graphite chosen because it is a common reference fine-grained graphite. Bulk samples of IG-110 were cut into approximately 0.5 mm thick slabs using a low-speed diamond wafering blade. Samples were further mechanically thinned to approximately 60 μm via grinding and polishing, then specimens 3 mm in diameter were cut using a rotary disc cutter (Model 360, Southbay, San Clemente, CA). Final thinning of specimens to electron-transparency was achieved by Ar^+ ion-milling using an ion polishing system (Model 691, Gatan, Pleasanton, CA). Low-voltage, low-angle ion-milling finishing was conducted on the specimens at 1 kV and 2° for 20 minutes after perforation to minimize ion-induced damage. In addition, electron-transparent specimens were also prepared via controlled oxidation in which the center of the 3 mm specimen discs were selectively oxidized. Experimental conditions for the

preparation of TEM specimens of nuclear graphite via controlled oxidation can be found elsewhere [28]. Oxidized TEM specimens are free of irradiation-induced artifacts from ion-milling; thus, they may be used as a baseline to confirm that any experimental observations at near no irradiation damage are not artifacts caused by ion-milling induced irradiation. Bright-field and high-resolution transmission electron microscopy (HRTEM) studies were performed using a JEOL-2100 HR TEM (JEOL Ltd., Tokyo, Japan) operated at 200 kV. In-situ heating experiments were conducted with a double-tilt heating holder (Model 652, Gatan, Pleasanton, CA) in which specimens were heated at a rate of 10°C/minute. It should be noted that any material imaged with a TEM will experience potentially damaging electron irradiation; however, care was taken to perform all beam alignments and focusing off regions of interest to reduce electron beam-induced damage; in addition, low exposure times (0.35s) were used while imaging. Hereafter, baseline images are labeled as having 'near-0 dpa'.

3.2.2 DPA calculations

To evaluate the dose of radiation damage experienced by a material, a commonly used parameter that characterizes the number of atoms displaced from their normal lattice sites as a result of energetic particle bombardment is the 'displacements per atom' (dpa). To determine the dose experienced by a material in a transmission electron microscope, the flux of electrons at operating conditions of the microscope must first be calculated. The flux is calculated with the total beam current, i_{tot}, the radius of the beam, r_0, and the magnification used, M. The following expression represents the total flux of electrons,

$$J = \frac{i_{tot}}{C \times \pi \left(\frac{r_0}{M}\right)^2} \tag{3.1}$$

where C is the fundamental charge ($1.60217662 \times 10^{-19}$ C). Evaluating the expression for a total current of 4.01×10^{-10} A, a beam radius of 18 mm, and a magnification of 600,000 gives a flux of 9×10^{23} electrons $m^{-2}s^{-1}$. The dose rate, given in dpa/s, is given by the product of the flux and the total cross section for atomic displacement, σ_{tot}.

$$\text{dpa/s} = J\sigma_{tot} \tag{3.2}$$

Solutions for the total cross section for atomic displacement have been provided by Oen [2] with the following two equations (3.3) and (3.4), assuming $E_D \leq T_m \leq 2E_D$ and $T_m > 2E_D$ respectively

$$\sigma_{tot}(E_i) = \frac{0.06515Z^2(E_i + 0.511)^2}{E_i^2(E_i + 1.022)^2}\left\{\int_{E_D/T_m}^{1} \frac{dx}{x^2} M(x,E)\right\} \tag{3.3}$$

$$\sigma_{tot}(E_i) = \frac{0.06515Z^2(E_i + 0.511)^2}{E_i^2(E_i + 1.022)^2}\left\{\int_{E_D/T_m}^{2E_D/T_m} \frac{dx}{x^2} M(x,E) + \int_{2E_D/T_m}^{1} \frac{T}{2E_D}\frac{dx}{x^2} M(x,E)\right\} \tag{3.4}$$

where E_i is the energy of the incident electron, E_D is the threshold energy for displacement of a given element of atomic number Z, and $x = T/T_m$, which is the ratio of the primary knock-on energy T and the maximum transferred energy T_m resulting from a head-on collision. The function $M(x,E)$ yields the ratio of the Mott and Rutherford cross sections, the solutions for which are given by Ref. [29]. Assumptions implicit in Eqs. 2 – 4 follow the Kinchin and Pease Model [30] which assumes only one atomic displacement will occur for primary knock-on energies in the range $E_D \leq T \leq 2E_D$, and

the number of atomic displacements for primary knock-on energies $T > 2E_D$ is given by the ratio $T/2E_D$. Reported values for E_D in graphite show a great variation in the literature [5,9,21,31] and range from 12-60 eV; however, Banhart [9] suggests an appropriate polycrystalline value between 15-20 eV. Assuming a value of 20 eV for E_D, and a 200 keV incident electron energy, the total displacement cross section for carbon is given in Ref. [2] as 16.25 barns. Evaluating Eq. (3.2) with the given values for electron flux and the total displacement cross section yields an approximated dose rate of 1.46×10^{-3} dpa/s.

3.3 Results and Discussion

Figure 3.1 shows bright-field TEM micrographs of nuclear graphite IG-110 prepared by conventional ion-milling technique. Figure 3.1 (a) shows a boundary region near the termination of a filler particle. Boundary regions between phases in nuclear graphite may extend several hundred nanometers and are composed of Mrozowski cracks, pores, misaligned basal planes and randomly oriented crystals. Figure 3.1 (b) shows QI particles that are often found in the binder phase of nuclear graphites. The micrographs shown in Figure 3.1 depict representative areas of the microstructure in which there is no long-range order to crystals, basal planes are misaligned, and disordered graphitic phases exist on the microscopic scale.

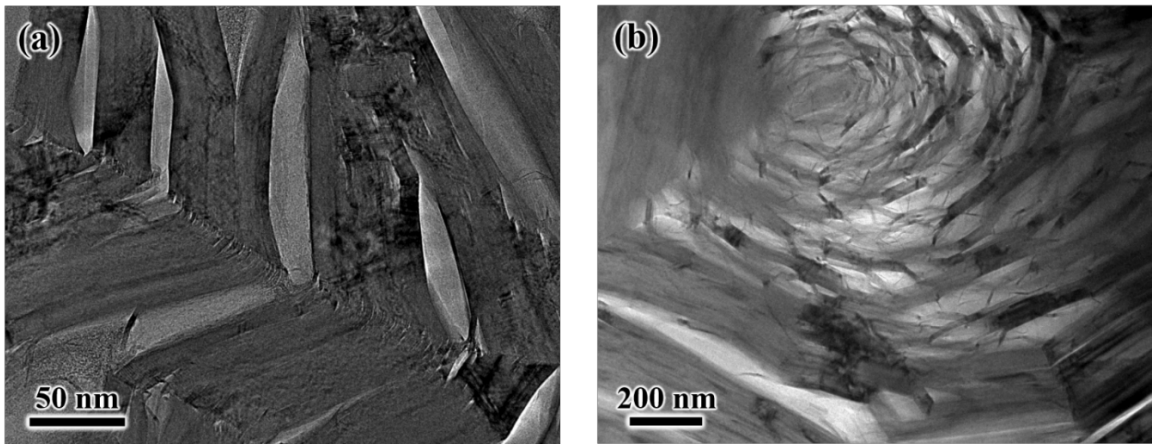

Figure 3.1 Bright-field TEM micrographs showing the complex microstructure of IG-110 in (a) a region in the phase boundary between a filler particle and the binder phase and (b) QI particles found in the binder phase.

Figure 3.2 (a) and (b) show a specimen of IG-110 prepared via oxidation and imaged at room temperature with very little electron beam exposure and therefore approximately 0 dpa. Although this technique has been shown to produce isolated artifact-free crystals of nuclear graphite [28], basal plane edges which contain under-coordinated carbon atoms are exposed (*i.e.*, while such specimens are artifact-free, they are not defect-free), whereas Figure 3.2 (c) and (d) show specimens of IG-110 prepared via ion-milling. The micrographs of IG-110 in Figure 3.2 were all taken near 0 dpa. Figure 3.2 (a) was taken at room temperature while Figure 3.2 (b-d) were taken at 800°C. While basal plane edges are left largely unaltered at room temperature, curling and closure of basal plane edges is observed as loops in oxidized specimens with localized swelling indicated, Figure 3.2 (b), and in ion-milled specimens as either hollow nanotube-like structures within Mrozowski cracks, Figure 3.2 (c) or interstitially as a line defects, Figure 3.2 (d). These results show experimentally that the curling and closure of basal planes is not a result of irradiation but of thermal annealing only. Furthermore,

given Figure 3.2 (b), the curling and closure of basal planes cannot be explained as simply an artifact introduced by ion milling.

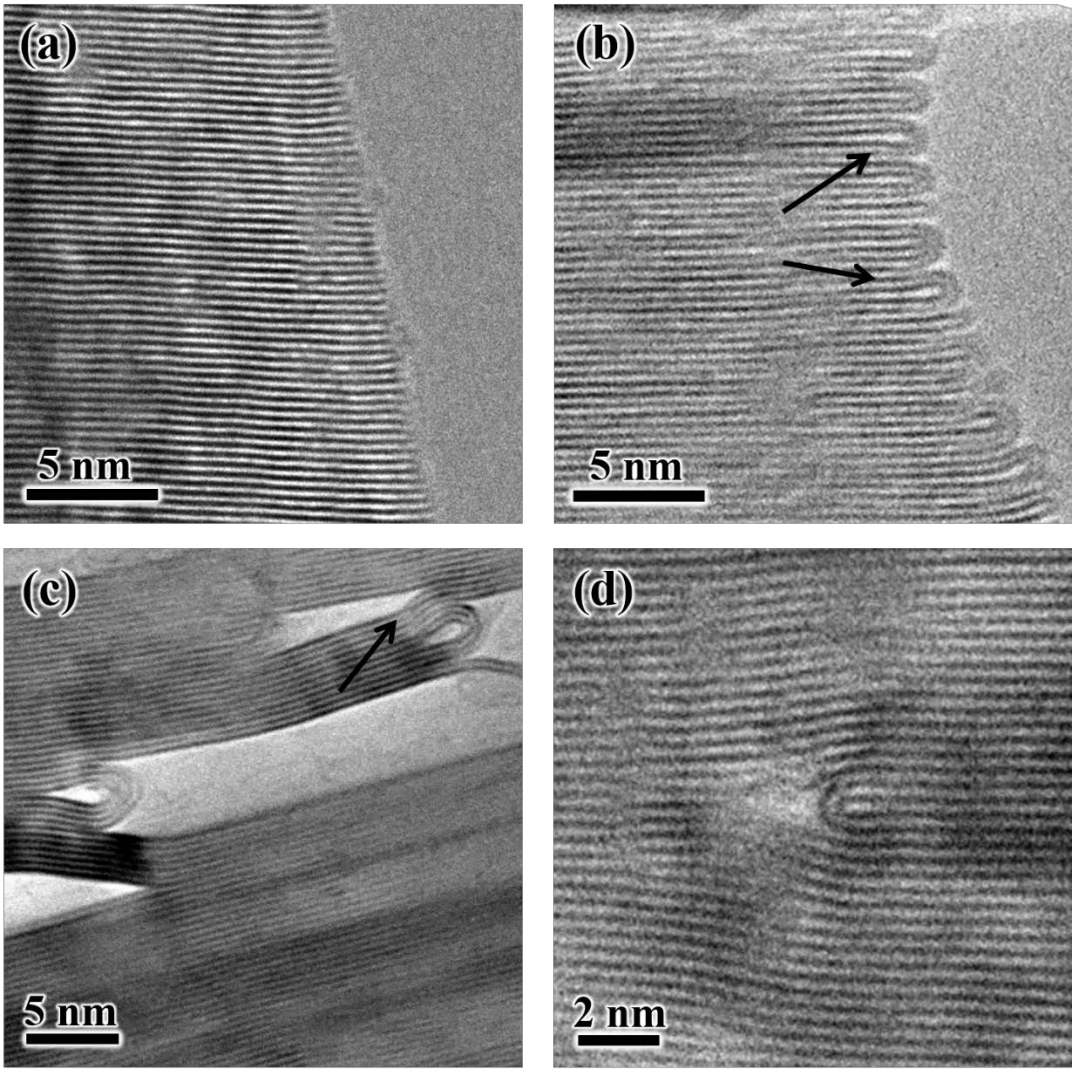

Figure 3.2 HRTEM images of IG-110 imaged at ~0 dpa. (a) TEM specimen prepared via oxidation of IG-110 imaged at room temperature showing no curling or closure of basal planes. (b) Oxidation-prepared TEM specimen showing curling of basal planes and localized swelling at the edge of a crystallite imaged at 800°C. (c) Ion-milled TEM specimen imaged at 800°C showing curling and localized swelling of basal planes in disordered region of the microstructure. (d) Curling of incomplete basal planes around a prismatic dislocation in ion-milled IG-110 imaged at 800°C.

Figure 3.3 shows the effect of electron-irradiation at 800°C on IG-110 prepared via oxidation. The oxidized specimen of IG-110 irradiated to 1.75 dpa depicted in Figure

3.3 (a) shows that under-coordinated carbon atoms near the edges of crystals will transform into carbon onions upon continued irradiation. Carbon onions are a non-equilibrium structure consisting of concentric shells of fullerenes which self-assemble under irradiation. Formation of concentric-shelled fullerene phases due to electron-irradiation from graphitic or amorphous carbon precursors was first observed by Ugarte [22] and may be expected to form in any highly disordered phase of carbon irradiated at high temperatures; however, their evolution and existence in disordered phases of nuclear graphite has not previously been reported. The present experimental results shown in Figure 3.3 (a) show that the formation of carbon onions will occur in nuclear graphite where basal plane edges and under-coordinated atoms are exposed. As carbon onions form in un-constrained areas near voids or pores, their contribution to dimensional and property changes observed in nuclear graphite remains an open question; however, other distortions to the graphite lattice may occur. The oxidized specimen of IG-110 irradiated to approximately 1.44 dpa depicted in Figure 3.3 (b-d) illustrates several mechanisms of basal plane distortion, including Figure 3.3 (b) the curling and closure of a basal plane interstitially forcing adjacent planes apart, Figure 3.3 (c) the rucking of basal planes, and Figure 3.3 (d) the separation of basal planes creating voids. It is clear from this image that many different mechanisms are responsible for observed dimension changes in nuclear graphite at elevated temperatures. The difficulties in acquiring quality micrographs (*i.e.*, snapshots) from in situ heating studies should be noted. Significant mechanical drift in all axial directions may occur during in situ analysis and increases with temperature.

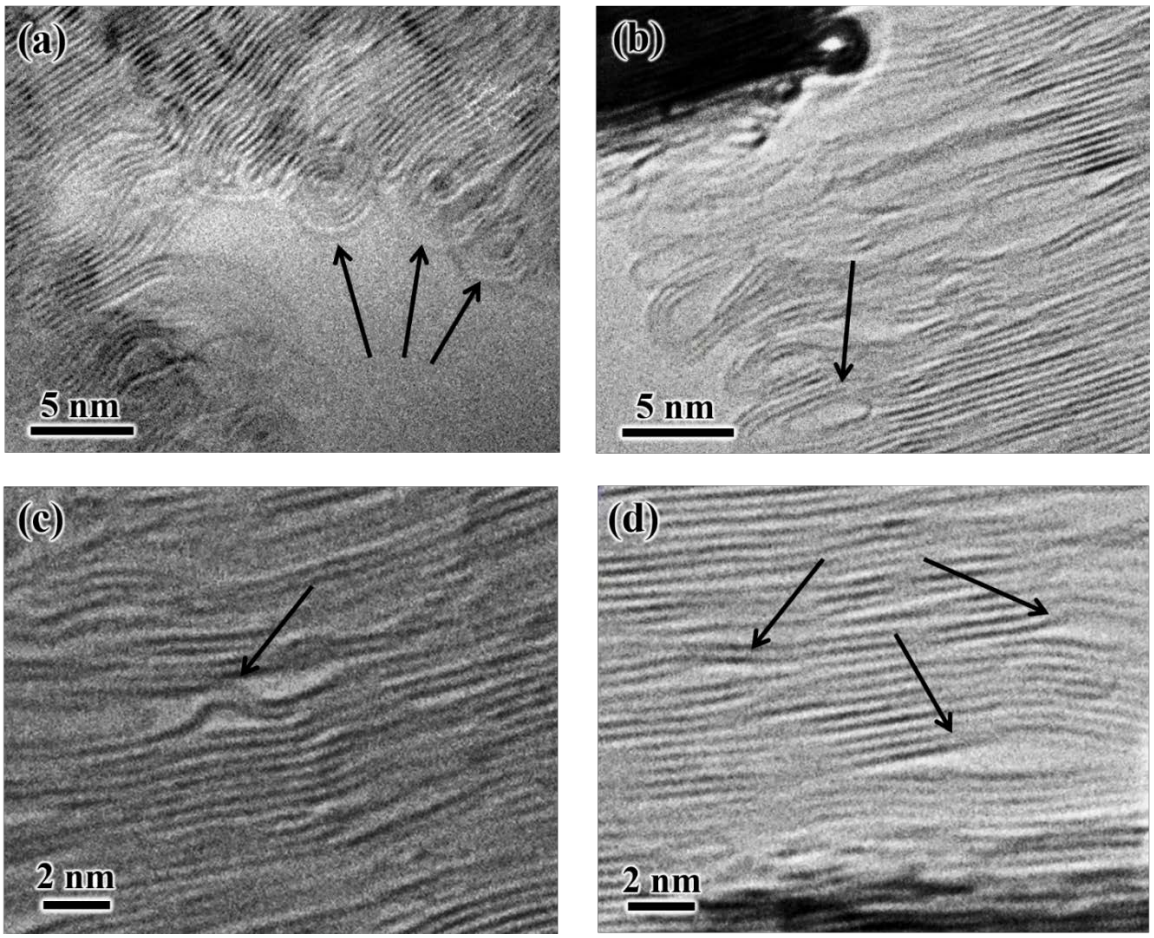

Figure 3.3 HRTEM micrographs of IG-110 prepared via oxidation imaged at 800°C. (a) Specimen irradiated to 1.75 dpa where the formation of carbon onions is indicated. (b-d) Specimen irradiated to ~1.44 dpa where significant distortion of the basal planes is observed. Area (b) shows the curling and closure of a basal plane interstitially, (c) shows the rucking of basal planes, and in (d) basal plane separation and voids are visible.

Figure 3.4 (a-f) shows an in situ electron-irradiation study of IG-110 prepared via ion-milling conducted at 800°C from approximately 0 to 1.77 dpa. Figure 3.4 (a) shows the initial state of a crystallite within the center of a QI particle, with the initial crystallite size measured along the *c* axis labeled. As the structure accumulates irradiation damage, displaced atoms appear to form small aggregate defects, which distort basal planes and are observed as blurred strain fields, indicated in Figure 3.4 (b). With continued electron-irradiation, nucleation and growth of a larger defect structure is observed in Figure 3.4 (c-

e). Figure 3.4 (f) shows a nanotube-like defect interstitially formed, resulting in significant expansion in the c direction, with the width of the indicated crystallite increasing from 3.71 nm to 5.61 nm which is an increase of approximately 51%. In addition, the clear contrast of the observed defect in Figure 3.4 (f) suggests that the defect must be stable and extend through the majority of the specimen's thickness [19] (approximately 115 nm measured via electron energy loss spectroscopy with the log-ratio method [32]). An in situ video showing the formation of the carbon onions is provided as Video 1 from which the snap shot shown in Fig. 3(a) was taken (found in the online version of this article). Supplementary video related to this article can be found at: doi.org/10.1016/j.carbon.2018.11.077.

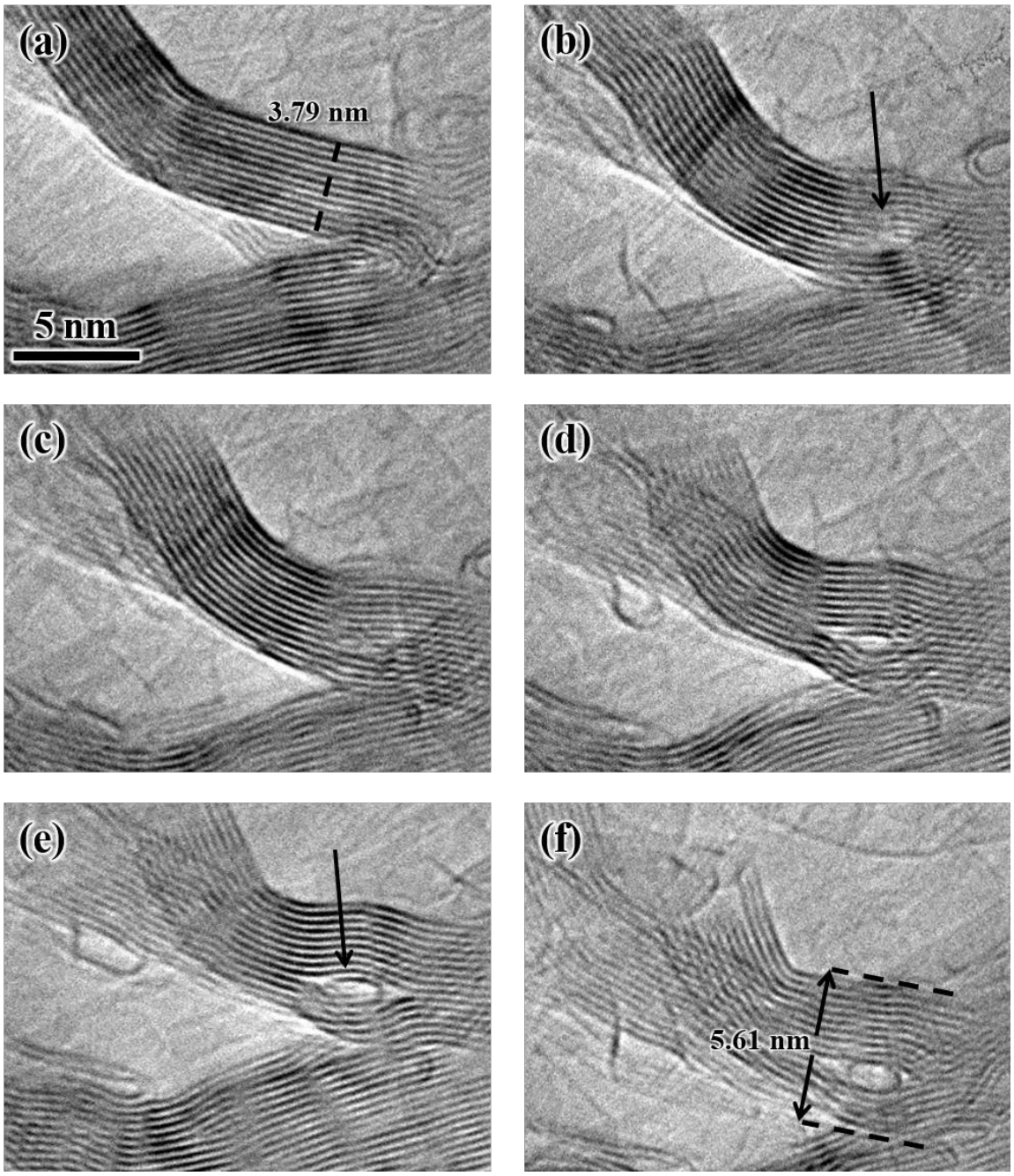

Figure 3.4 HRTEM micrographs within a QI particle at 800°C. (a) Initial micrograph at ~0 dpa with initial size of the crystallite along the c axis labeled. (b) After 0.90 dpa where the indicated strain field suggests the presence of defects. (c) After 1.01 dpa where accumulation of defects is apparent within the structure. (d) 1.29 dpa & (e) 1.47 dpa show the curling and closure of interstitially displaced carbon atoms into a nanotube-like defect that remains stable under continued electron-irradiation, as shown in (f) after 1.77 dpa with final crystallite size along the c axis labeled.

A possible interpretation of the evolution of the hollow nanotube-like defect seen in Figure 3.4 (f) could be interlayer bonding occurring between basal planes. While exposed to electron-irradiation, displacement of carbon atoms from equilibrium postitions occurs, resulting in interstitial and vacancy defect species. It is generally believed that, in the case of single-bonded interstials, binding sites are created in the adjacent interlayer regions due to interuption of π bonding within basal planes [33], which may result in the formation of small aggregrates (4±2 atoms) of cross-linking interstitials. Interlayer bonding may also occur from divacancy species, such as the so called $V_2^1\beta\beta$ and $V_2^2\beta\beta$ interlayer divacancies (in the notation of Ref. [34]); however, only the later has been proposed to result in nucleation of extended interlayer defects [35] and is depicted in Figure 3.5 The notation V_2 denotes a vacancy species in which two atoms surrounding each vacancy are able to form bonds within the plane where two under-cordinated atoms are situated directly above one another (α site), as indicated by the red square in Figure 3. 5. In the case of a $V_2^2\beta\beta$ divacancy, the superscript 2 denotes the vacancies occur at second nearest interplane neighbour positions, and β denoting a vacant lattice site position below a ring center in the adjacent layer. This divacancy results in twofold coordinated carbon atoms which allow bonding interactions between basal planes similar to a spiro interstitial (ground state carbon atom interstitial consisting of four bonds, two bonds with each adjacent basal plane) [8]. It is proposed that the $V_2^2\beta\beta$ interlayer divacancy will remain immobile at temperatures below 1000°C and may therefore result in further interlayer bonding from under-coordinated atoms [35]. After a $V_2^2\beta\beta$ defect is formed, nucleation of an extended interlayer defect, such as the so called "V_7-V_7 interlayer defect" (in the notation of Ref. [34]) where four interlayer bonds occur as a

result of two vacancy lines in adjacent layers consisting of seven vacancies in both α and β sites along the zig-zag direction. This interlayer defect has been both simulated and found experimentally with room-temperature HRTEM studies [6,35]. It is proposed that further growth of an extended interlayer defect species may occur, and as irradiation continues, bonds in under-coordinated carbon atoms linking the basal planes are broken via atomic displacements resulting in an interstitial "ribbon of graphene" with undercoordinated carbon atoms on the edges of the ribbon. The resulting ribbon curls and closure occurs forming the nanotube-like structure (Figure 3.4 (f)). Further molecular dynamics studies could provide confirmation of the stability of these defect structures and a possible formation mechanism.

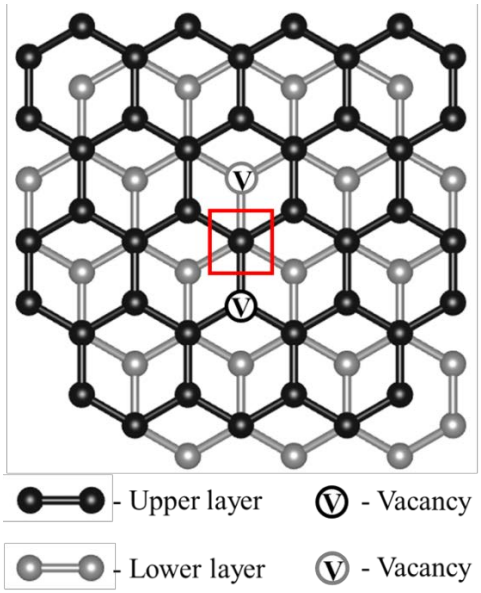

Figure 3.5 Schematic of a $V_2^2\beta\beta$ interlayer divacancy, where the square highlights two under-coordinated atoms that may form an interlayer bond. A color version of this figure can be found online.

The mechanisms responsible for the dimension change observed in nuclear graphite while subjected to irradiation is believed to be a function of temperature. Room temperature electron-irradiation studies have proposed several mechanisms to explain the

resulting dimensional change in nuclear graphite [6,18,19]. However, larger and stable defect structures have not been observed at ambient temperatures. At elevated temperatures it is generally believed that the mobility of interstitial and vacancy defects increases resulting in atomic rearrangement of atoms and/or agglomeration of point defects [8]. The curling and closure of basal planes due solely to thermal annealing, as seen in Figure 3.2, has been found to occur at lower temperature (750°C, see supplementary data); however, the formation of stable fullerene defects via electron-irradiation was not achievable below 750°C in practical experimental times. The formation of the stable defect structure shown in Figure 3.4 (f) exemplifies the difference in the response of electron-irradiation conducted at room temperature compared to electron-irradiation at elevated temperatures. Furthermore, the experimental results of this study demonstrate that there is no single mechanism responsible for the dimensional change in nuclear graphite; thus, it is believed that many temperature-dependent mechanisms are responsible for dimensional change in nuclear graphite.

3.4 Conclusions

The formation of carbon nanostructures via curling and closure of basal planes in graphitic networks is favorable not only with increased temperature but also in the presence of under-coordinated carbon atoms and defect species. This work shows experimental evidence that under electron-irradiation conducted at 800°C, nuclear graphite will form nanostructures not only in disorded phases of carbon, but interstitially between basal planes. The given experimental results show that the formation of carbon nanostructure defects due to thermal annealing or high-temperature electron-irraditation results in localized swelling and c-axis expansion in nuclear graphite; thus, it is an

additional atomic mechanism for the observed dimensional changes in nuclear graphite subjected to high-temperature irradiation.

3.5 Supplementary Data

Supplementary data associated with this article can be found, in the online version, at doi.org/10.1016/j.carbon.2018.11.077.

3.6 References

[1] T.R. Allen, K. Sridharan, L. Tan, W.E. Windes, J.I. Cole, D.C. Crawford, G.S. Was, Materials Challenges for Generation IV Nuclear Energy Systems, Nucl. Technol. 162 (2008) 342–357, doi:10.13182/NT08-A3961.

[2] O.S. Oen, Cross Sections for Atomic Displacenewis in Solids By Fast Electrons, Distribution. (1955).

[3] H.M. Freeman, A.J. Scott, R.M.D. Brydson, Thermal annealing of nuclear graphite during in-situ electron irradiation, Carbon N. Y. 115 (2017) 659–664, doi:10.1016/j.carbon.2017.01.057.

[4] J.H.W. Simmons, Radiation Damage in Graphite, in: J. V. Dunworth (Ed.), 1st Edition, Pergamon, 1965.

[5] D.F. Pedraza, J. Koike, Dimensional changes in grade H-451 nuclear graphite due to electron irradiation, Carbon N. Y. 32 (1994) 727–734, doi:10.1016/0008-6223(94)90095-7.

[6] C. Karthik, J. Kane, D.P. Butt, W.E. Windes, R. Ubic, In situ transmission electron microscopy of electron-beam induced damage process in nuclear grade graphite, J. Nucl. Mater. 412 (2011) 321–326, doi:10.1016/j.jnucmat.2011.03.024.

[7] R.E. Nightingale, Nuclear Graphite, Academic Press, (1962).

[8] R.H. Telling, M.I. Heggie, Radiation defects in graphite, Philos. Mag. 87 (2007) 4797-4846, doi:10.1080/14786430701210023.

[9] F. Banhart, Irradiation effects in carbon nanostructures, Reports Prog. Phys. 62 (1999) 1181–1221, doi:10.1088/0034-4885/62/8/201.

[10] J.E. Brocklehurst, B.T. Kelly, The dimensional changes of highly-oriented pyrolytic graphite irradiated with fast neutrons at 430°C and 600°C, Carbon N. Y. 31 (1993) 179–183, doi:10.1016/0008-6223(93)90170-F.

[11] F. Banhart, J. Kotakoski, A. V Krasheninnikov, Structural Defects in Graphene, ACS Nano. 5 (2011) 26–41, doi:10.1021/nn102598m.

[12] M.T. Lusk, L.D. Carr, Nanoengineering defect structures on graphene, Phys. Rev. Lett. 100 (2008) 1–4. doi:10.1103/PhysRevLett.100.175503.

[13] M.I. Heggie, I. Suarez-Martinez, C. Davidson, G. Haffenden, Buckle, ruck and tuck: A proposed new model for the response of graphite to neutron irradiation, J. Nucl. Mater. 413 (2011) 150–155, doi:10.1016/j.jnucmat.2011.04.015.

[14] J. Gruber, A.C. Lang, J. Griggs, M.L. Taheri, G.J. Tucker, M.W. Barsoum, Evidence for Bulk Ripplocations in Layered Solids, Sci. Rep. 6 (2016) 1–8, doi:10.1038/srep33451.

[15] H. Terrones, M. Terrones, E. Hernández, N. Grobert, J.C. Charlier, P.M. Ajayan, New metallic allotropes of planar and tubular carbon, Phys. Rev. Lett. 84 (2000) 1716–1719, doi:10.1103/PhysRevLett.84.1716.

[16] D.H. Robertson, D.W. Brenner, C.T. White, On the way to fullerenes: Molecular dynamics study of the curling and closure of graphitic ribbons, J. Phys. Chem. 96 (1992) 6133–6135, doi:10.1021/j100194a011.

[17] S.T. Skowron, I. V. Lebedeva, A.M. Popov, E. Bichoutskaia, Approaches to modelling irradiation-induced processes in transmission electron microscopy, Nanoscale. 5 (2013) 6677–6692, doi:10.1039/c3nr02130k.

[18] J. Koike, D.F. Pedraza, Dimensional changes in highly oriented pyrolytic graphite due to electron-irradiation, J. Mater. Res. 9 (1994) 1899–1907, doi:10.1557/JMR.1994.1899.

[19] S. Muto, T. Tanabe, Damage process in electron-irradiated graphite studied by transmission electron microscopy. I. high-resolution observation of highly graphitized carbon fibre, Philos. Mag. A 76 (1997) 679–690, doi:10.1080/01418619708214029.

[20] S. Muto, T. Tanabe, Fragmentation of graphite crystals by electron-irradiation at elevated temperatures, J. Electron Microsc. (Tokyo). 48 (1999) 519–523, doi:10.1093/oxfordjournals.jmicro.a023710.

[21] K. Nakai, C. Kinoshita, A. Matsunaga, A study of amorphization and microstructural evolution of graphite under electron or ion irradiation, Ultramicroscopy. 39 (1991) 361–368, doi:10.1016/0304-3991(91)90216-S.

[22] D. Ugarte, Curling and closure of graphitic networks under electron-beam irradiation, Nature. 359 (1992) 707–709, doi:10.1038/359707a0.

[23] A. V. Krasheninnikov, K. Nordlund, Ion and electron irradiation-induced effects in nanostructured materials, J. Appl. Phys. 107 (2010), doi:10.1063/1.3318261.

[24] A.P. Burden, J.L. Hutchison, Real-time observation of fullerene generation in a modified electron microscope, J. Cryst. Growth. 158 (1996) 185–188, doi:10.1016/0022-0248(95)00547-1.

[25] F. Banhart, Structural transformations in carbon nanoparticles induced by electron irradiation, Phys. Solid State. 44 (2002) 399–404, doi:10.1134/1.1462655.

[26] K.Y. Wen, T.J. Marrow, B.J. Marsden, The microstructure of nuclear graphite binders, Carbon N. Y. 46 (2008) 62–71, doi:10.1016/j.carbon.2007.10.025.

[27] C. Karthik, J. Kane, D.P. Butt, W.E. Windes, R. Ubic, Microstructural characterization of next generation nuclear graphites, Microsc. Microanal. 18 (2012) 272–278, doi:Doi 10.1017/S1431927611012360.

[28] S. Johns, W. Shin, J.J. Kane, W.E. Windes, R. Ubic, C. Karthik, A new oxidation based technique for artifact free TEM specimen preparation of nuclear graphite, J. Nucl. Mater. 505 (2018) 62–68, doi:10.1016/j.jnucmat.2018.03.058.

[29] Zeitler Elmar, Olsen Haakon, Elastic Scattering of Electrons and Positrons by Screened Nuclei , Zeitschrift Für Naturforsch. A . 21 (1966) 13-21, doi:10.1515/zna-1966-0901.

[30] G.H. Kinchin, R.S. Pease, The Displacement of Atoms in Solids by Radiation, Reports Prog. Phys. 18 (1955) 1.

[31] M.W. Lucas, E.W.J. Mitchell, The threshold curve for the displacement of atoms in graphite: Experiments on the resistivity changes produced in single crystals by fast electron irradiation at 15°K, Carbon N. Y. 1 (1964) 345–352, doi:10.1016/0008-6223(64)90290-8.

[32] T. Malis, S.C. Cheng, R.F. Egerton, EELS log-ratio technique for specimen-thickness measurement in the TEM, J. Electron Microsc. Tech. 8 (1988) 193–200. doi:10.1002/jemt.1060080206.

[33] M.I. Heggie, Interstitial string model for defective graphites, Carbon N. Y. 30 (1992) 71–74, doi:10.1016/0008-6223(92)90108-9.

[34] R.H. Telling, C.P. Ewels, A.A. El-Barbary, M.I. Heggie, Wigner defects bridge the graphite gap, Nat. Mater. 2 (2003) 333–337, doi:10.1038/nmat876.

[35] T. Trevethan, P. Dyulgerova, C.D. Latham, M.I. Heggie, C.R. Seabourne, A.J. Scott, P.R. Briddon, M.J. Rayson, Extended interplanar linking in graphite formed from vacancy aggregates, Phys. Rev. Lett. 111 (2013) 1–5, doi:10.1103/PhysRevLett.111.095501.

CHAPTER FOUR: EXPERIMENTAL EVIDENCE FOR ‘BUCKLE, RUCK AND TUCK’ IN NEUTRON IRRADIATED GRAPHITE*

This chapter is published by Elsevier in *Carbon* and should be referenced appropriately.

Reference:

S. Johns, L. He, J.J. Kane, W.E. Windes, R. Ubic, C. Karthik, Experimental evidence for ‘buckle ruck and tuck’ in neutron irradiated graphite, Carbon N. Y. 159 (2019) 119 - 121.

*This chapter includes modifications the originally published version.

EXPERIMENTAL EVIDENCE FOR 'BUCKLE, RUCK AND TUCK' IN NEUTRON IRRADIATED GRAPHITE

Steve Johns[1]

Lingfeng He[2]

Joshua J. Kane[2]

William E. Windes[2]

Rick Ubic[1]

Chinnathambi Karthik[1]

Accepted for publication in:

Carbon

December, 2019

[1] *Micron School of Materials Science and Engineering, Boise State University, Boise, ID 83725, USA*

[2] *Idaho National Laboratory, 2525 Fremont Ave, Idaho Falls, ID 83402, USA*

Abstract

The current mainstream theory for radiation-induced dimensional change of nuclear graphite is based on the notion that interstitially displaced carbon atoms will coalesce into dislocation loops (i.e., additional basal planes). This standard atomic-displacement model has been challenged by theories based on first principle calculations. The so-called 'ruck and tuck' of basal planes has been proposed as an alternative mechanism to explain the observed *c*-axis expansion under irradiation; however, no such defects have been observed experimentally so far. In this study, the first experimental evidence for the presence of a 'ruck and tuck' defect in high-temperature neutron-irradiated nuclear graphite is presented.

4.1 Introduction

Graphite has historically been used as a moderator material in nuclear reactor designs and is now a candidate core material for the future envisioned Generation IV very high-temperature reactors (VHTRs) and the molten salt-cooled reactors (MSRs) [1]. Despite the fact radiation damage in nuclear graphite has been the subject of scientific investigation for over 70 years, irradiation-induced defect evolution remains poorly understood. On the atomic scale, displacing radiation invokes Frankel pair formation; where vacancies arise within the basal planes leading to contraction on the *a*-*b* plane, while interstitially displaced atoms result in expansion in the *c* direction. The standard model assumes that interstitially displaced carbon atoms will coalesce into additional basal planes resulting in swelling of crystallites in the *c* direction; however, the standard model inadequately explains many property changes observed in irradiated nuclear graphite, including the actual dimensional change and Wigner energy release [2]. Wigner

energy release is reasoned by the standard model to arise from point defect aggregation or annihilation; however, cryogenic irradiations show Wigner energy release at temperatures which cannot overcome the 1.3 eV activation energy for the migration of interstitials [2-4]. In addition, the amount of dimensional change which would arise from the formation of an additional basal plane is reported to be less than a half that of the measured change [5]. Furthermore, transmission electron microscopy (TEM) analysis of nuclear graphite damaged by particle radiation provides little or no evidence of the growth of additional basal planes from the aggregation of interstitial atoms [6-8]. To address these inadequacies of the standard model, Heggie *et. al.* proposed the 'buckle, ruck and tuck' model [2]. Using first principle calculations, they suggested that two sets of four basal edge dislocations (as a result of radiation damage) will pile up and glide past each other on nearby basal planes resulting in the so-called 'ruck and tuck' defect contributing to significant *c* axis expansion; however, the 'ruck and tuck' defect has not been widely accepted as a plausible defect mechanism as it has never been observed experimentally via TEM analysis. On the other hand, studies on ripplocations by Barsoum *et. al.* report a spontaneous nucleation of the 'ruck and tuck' defect during their molecular dynamic studies of graphite and argued its existence is likely plausible [9,10].

4.2 Experimental

In this study, neutron irradiated nuclear graphite was supplied by Idaho National Laboratory as part of the advanced graphite creep capsule (AGC-3) experiments. Nuclear graphite IG-110 was neutron-irradiated at 817°C to a dose of 3.56 displacements per atom (dpa). For a detailed description of irradiation conditions, we refer the reader to Ref. [11] (sample ID: EA3609). Bulk irradiated samples were mechanically thinned with 1200

grit SiC paper to approximately 60 μm. Final thinning to electron transparency was achieved by Ar^+ ion-milling followed by low-voltage, low-angle ion-milling finishing at 1 kV and 2° for 20 minutes using a Gatan PIPS II 695. High resolution transmission electron microscopy (HRTEM) studies were performed using a JEOL-2100 HR TEM operated at 100 kV.

4.3 Results and Discussion

Figure 4.1 shows HRTEM micrographs of IG-110 neutron-irradiated to a dose of 3.56 dpa at 817°C. Figure 4.1 (a) shows two lattice defects (marked by arrows) which result in swelling along the *c* axis. Figure 4.1 (b) shows the upper defect, as shown in (a), at higher magnification where a 'ruck and tuck' defect is clearly visible resulting in significant expansion along the *c* axis of the crystallite. For comparison, the inset image shows a representation of the originally proposed defect structure in which there is observed a remarkable similarity. These results are the first experimental evidence for the 'ruck and tuck' defect as proposed by Heggie *et. al.* [2]. Figure 4.1 (c) and (d) show similar defect structures observed from other parts of the sample and evidence that the 'ruck and tuck' defect, or folding of basal planes, is a plausible irradiation-induced defect structure occurring in high-temperature neutron-irradiated nuclear graphite.

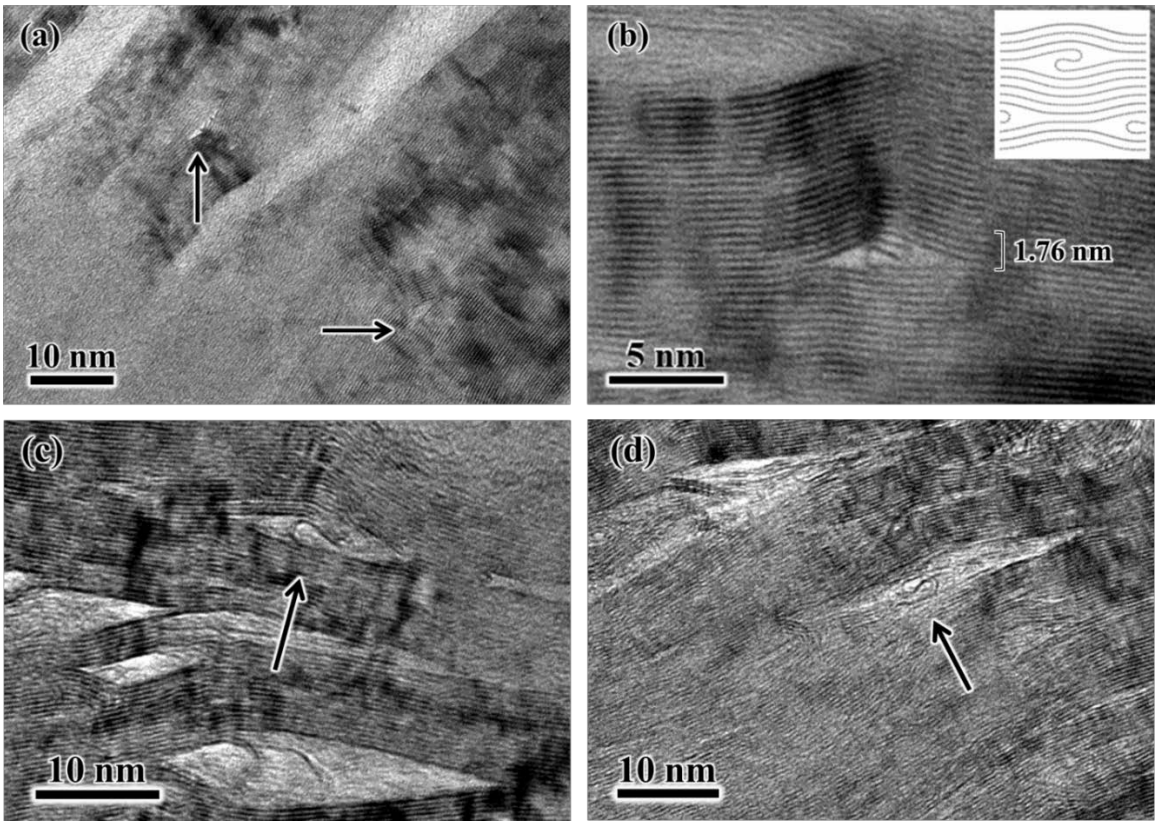

Figure 4.1 HRTEM micrograph of IG-110 neutron-irradiated to a dose of 3.56 dpa at 817°C. (a) shows two indicated defects resulting in c axis expansion. (b) shows the upper defect as indicated in (a) at higher magnification. The inset in (b) shows the proposed 'ruck and tuck' defect by M.I. Heggie et al. [2] reprinted with permission from Elsevier. (c) and (d) show similar defect structures which exhibit the folding of basal planes.

The 'ruck and tuck' defect shown in Figure 4.1 (b) is composed of three graphite basal planes, one which is folded interstitially and two adjacent. The displacement along the *c* axis between the two adjacent basal planes is 1.76 nm. When comparing this value to the measured spacing of three basal planes of well-ordered graphite (0.68 nm as measured from Fig. 1 (b)) the resulting expansion along the *c*-axis is 159%. This value is well above the theoretical value for the formation of a single additional basal plane (50%). Heggie *et. al.* suggested if considering the 'perfect' case, the dimensions of a 'ruck and tuck' defect may be approximated via adoption of the chiral indexing of carbon nanotubes, (*j, k*) [2]. The diameter of a nanotube is given by the following relationship,

$$D = \frac{a}{\pi}\sqrt{j^2 + jk + k^2} \tag{4.1}$$

where *a* is the lattice constant. DFT simulations showed the 'ruck and tuck' defect was composed of partial nanotubes zig-zag in nature (i.e., *k*=0) and the appropriate indexing included (7, 0) [2]. Evaluating equation (4.1) for *a* = 0.246 nm and a chiral index of (7, 0), gives an approximated diameter of 0.55 nm for each partial nanotube. It follows that the theoretical displacement of the basal planes adjacent to the defect is given by two nanotube diameters and two interplanar spacings of 0.34 nm. The approximated theoretical displacement is 1.8 nm along the *c* axis which is in exceptional agreement of our experimental results (1.76 nm).

The defects shown in Fig. 4.1 are a result of high-temperature irradiation and do not exist intrinsically within unirradiated nuclear graphites [12,13]. Heggie *et. al.* suggested that the ruck and tuck mechanism would only become favorable at irradiation temperatures above 250°C [2]. The Buckle, ruck and tuck model proposed that basal dislocations are pinned by interlayer defects (such as spiro-interstitials) at temperatures below 250°C, at temperatures greater than 250°C pinning defects mostly disappear and basal dislocations are free to interact and pile up, with the possible consequence of ruck and tuck [2]. However, our previously reported high-temperature electron-irradiation studies of nuclear graphite IG-110 show no evidence of the formation of carbon nanostructures or fullerene-like defects below temperatures of 750°C [8]. In addition, previously reported studies conducted on IG-110 neutron-irradiated at 674°C to nearly twice the dose of this study (6.7 dpa), showed no evidence of such defects [7]; therefore, temperature is believed to be a significant factor when considering the formation of such

defects and could explain why these defects have not been previously observed in lower-temperature irradiation studies.

4.4 Conclusions

The HRTEM micrographs presented here are the first experimental evidence showing the existence of the ‘ruck and tuck’ defect. The defect structures previously proposed, and experimentally verified here, will give valuable insight to unresolved quantitative anomalies of the standard model of graphite expansion and may improve the understanding of current empirical and theoretical models of irradiation-induced property changes in nuclear graphite. Furthermore, the adoption of a new model for irradiation-induced defect production could potentially directly influence the design of next-generation nuclear reactors and both the operation and decommissioning of current graphite-moderated reactors.

4.5 References

[1] B.J. Marsden, A.N. Jones, G.N. Hall, M. Treifi, P.M. Mummery, Graphite as a core material for Generation IV nuclear reactors, in: P. Yvon (Ed.), Struct. Mater. Gener. IV Nucl. React., Woodhead Publishing, 2017: pp. 495–532.

[2] M.I. Heggie, I. Suarez-Martinez, C. Davidson, G. Haffenden, Buckle, ruck and tuck: A proposed new model for the response of graphite to neutron irradiation, J. Nucl. Mater. 413 (2011) 150–155. doi:10.1016/j.jnucmat.2011.04.015.

[3] L. Bochirol, E. Bonjour, Irradiation of graphite at low temperature by neutrons and electrons. Measurement of stored energy and of variation in electrical resisitivity, Carbon N. Y. 6 (1966) 661–669. doi:10.1016/0008-6223(68)90010-9.

[4] C.P. Ewels, R.H. Telling, A.A. El-Barbary, M.I. Heggie, P.R. Briddon, Metastable Frenkel Pair Defect in Graphite: Source of Wigner Energy?, Phys. Rev. Lett. 91 (2003) 1–4. doi:10.1103/PhysRevLett.91.025505.

[5] W.N. Reynolds, P.A. Thrower, The nucleation of radiation damage in graphite, Philos. Mag. 12 (1965) 573–593.

[6] J.A. Hinks, S.J. Haigh, G. Greaves, F. Sweeney, C.T. Pan, R.J. Young, S.E. Donnelly, Dynamic microstructural evolution of graphite under displacing irradiation, Carbon N. Y. 68 (2014) 273–284. doi:10.1016/j.carbon.2013.11.002.

[7] C. Karthik, J. Kane, D.P. Butt, W.E. Windes, R. Ubic, Neutron irradiation induced microstructural changes in NBG-18 and IG-110 nuclear graphites, Carbon N. Y. 86 (2015) 124–131. doi:10.1016/j.carbon.2015.01.036.

[8] S. Johns, T. Poulsen, J.J. Kane, W.E. Windes, R. Ubic, C. Karthik, Formation of carbon nanostructures in nuclear graphite under high-temperature in situ electron-irradiation, Carbon N. Y. 143 (2019) 908–914. doi:10.1016/j.carbon.2018.11.077.

[9] J. Gruber, A.C. Lang, J. Griggs, M.L. Taheri, G.J. Tucker, M.W. Barsoum, Evidence for Bulk Ripplocations in Layered Solids, Sci. Rep. 6 (2016). doi:10.1038/srep33451.

[10] M.W. Barsoum, G.J. Tucker, Deformation of layered solids: Ripplocations no basal dislocations, Scr. Mater. 139 (2017) 166–172. doi:10.1016/j.scriptamat.2017.04.002.

[11] W.E. Windes, D.T. Rohrbaugh, W.D. Swank, D.L. Cottle, AGC-3 Specimen Post-Irradiation Examination Data Package Report, Idaho National Laboratory, 2017. INL/EXT-17-43823.

[12] C. Karthik, J. Kane, D.P. Butt, W.E. Windes, R. Ubic, Microstructural characterization of next generation nuclear graphites, Microsc. Microanal. 18 (2012) 272–278. doi: 10.1017/S1431927611012360.

[13] G. Zheng, P. Xu, K. Sridharan, T. Allen, Characterization of structural defects in nuclear graphite IG-110 and NBG-18, J. Nucl. Mater. 446 (2014) 193–199. doi:10.1016/j.jnucmat.2013.12.013.

CHAPTER FIVE: FULLERENE-LIKE DEFECTS IN HIGH-TEMPERATURE NEUTRON-IRRADIATED NUCLEAR GRAPHITE*

This chapter is published by Elsevier in *Carbon* and should be referenced appropriately.

Reference:

S. Johns, L. He, k. Bustillo, W.E. Windes, R. Ubic, C. Karthik, Fulleren-like defects in high-temperature neutron-irradiated nuclear graphite, Carbon N. Y. 166 (2019) 113-122.

*This chapter includes modifications from the originally published version.

FULLERENE-LIKE DEFECTS IN HIGH-TEMPERATURE NEUTRON-IRRADIATED NUCLEAR GRAPHITE

Steve Johns[1]

Lingfeng He[2]

Karen Bustillo[3]

William E. Windes[2]

Rick Ubic[1]

Chinnathambi Karthik[1]

Accepted for publication in:

Carbon

May, 2020

[1] Micron School of Materials Science and Engineering, Boise State University, Boise, ID 83725, USA

[2] Idaho National Laboratory, 2525 Fremont Ave, Idaho Falls, ID 83402, USA

[3] National Center for Electron Microscopy, Molecular Foundry, Lawrence Berkeley National Laboratory, Berkeley, CA, 94720, USA

Abstract

Irradiation-induced defect evolution in graphite is particularly important for its application in graphite-moderated nuclear reactors. The evolution of defects directly influences macroscopically observed property changes in irradiated nuclear graphite which, in turn, can govern the lifetime of graphite components. This article reports novel defect structures and the irradiation response of microstructural features occurring in high-temperature irradiated nuclear graphite IG-110. High resolution transmission electron microscopy (HRTEM) was used to characterize specimens neutron-irradiated at a high temperature (≥ 800°C) at doses of 1.73 and 3.56 atomic displacements per atom (dpa). Concentric shelled and fullerene-like defects were found to result in swelling along the *c*-axis and contraction along the *a*/*b*-axis of crystallites. Furthermore, such defects are shown to occur within, and partially fill, Mrozowski cracks prior to turnaround dose. In addition, in situ TEM under similar irradiation conditions was used to capture the real-time dynamic evolution of defects, providing unambiguous analysis of the evolution of the graphite structures during irradiation. Results suggest the mainstream theory for radiation damage in nuclear graphite (which assumes additional basal plane formation as the sole reason) to be an incorrect interpretation of defect evolution contributing to irradiation-induced property changes at higher temperatures.

5.1 Introduction

Graphite has historically been used as a key material in many nuclear reactor designs dating back to the very first reactor to achieve criticality in 1942 (Chicago Pile 1). Since that time, graphite has remained a candidate material for nuclear reactors as it is relatively inexpensive, easily machined into complex geometries, and has suitable

physical/chemical properties. In addition, graphite is envisioned to be used in the Generation IV reactor concepts such as the molten salt reactors (MSRs) and very high temperature reactors (VHTRs) [1]. Given the current and historical use of graphite in nuclear reactors, irradiation-induced defect evolution remains an active field of research; however, atomic mechanisms governing irradiation-induced property changes in nuclear graphite remains poorly understood.

On the atomic scale, irradiation-induced displacement of carbon atoms will cause contraction along the *a* and *b* directions and expansion along *c*. The historically proposed theory for the evolution of interstitially displaced carbon atoms assumes displaced atoms will migrate and coalesce resulting in additional basal plane formation (Figure 5.1). This atomic displacement model stems from early TEM analyses conducted on irradiated natural graphite. Thrower et al. [2] showed the presence of large dislocation loops in neutron-irradiated natural graphite; however, sample preparation included high-temperature annealing (>1600°C). Indeed, precipitation of point defects into dislocation loops was often aided in early studies. Amelinckx et al. [3] reported observations of dislocation loops in irradiated natural graphite; however, interstitial dislocation loops were only observed after quenching in the damage caused by electron-irradiation conducted at 2700-3000°C, and subsequently annealing at 1200°C. Ex-situ results post-annealing are arguably ambiguous and may not be a valid interpretation of the actual defect evolution which occurs during operation of nuclear reactors. More recent TEM studies on nuclear graphite subjected to energetic particle bombardment (electrons, ions, and neutrons) provides little or no evidence to support the historical atomic-displacement model [4-12]. Additionally, computational modelling studies give evidence for

alternative theories for defect evolution (e.g. “ruck and tuck” and “ripplocations”) [13-15].

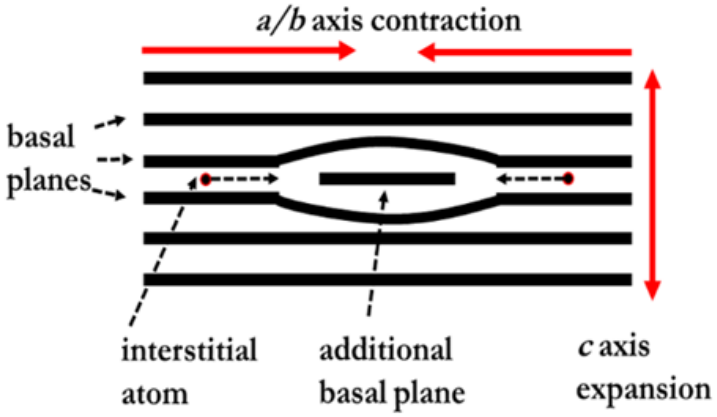

Figure 5.1 Schematic showing the initially proposed atomic displacement model for dimensional change in nuclear graphite where interstitially displaced atoms cause a/b-axis contraction and coalesce to form additional basal planes (c-axis expansion).

Irradiation-induced defect evolution is a fundamental response that in turn directly influences the many property changes of nuclear graphite subjected to displacing irradiation. The macroscopic dimensional change observed in irradiated nuclear graphite is one such property change of importance. In large part, dimensional change provides valuable insight to the lifetime and maintenance of graphite components used in nuclear reactors. The amount of dimensional change may vary amongst each grade of nuclear graphite due to processing techniques and the resulting microstructure [16-18]; however, in general the dimensional change is often modeled empirically by quadratic functions as depicted in Figure 5.2 [19,20]. Initially, there is a high rate of shrinkage during the onset of irradiation, but with prolonged irradiation the rate of shrinkage slows and eventually the graphite starts to expand (“turnaround”). Swelling of the graphite continues until eventually the component returns to its pre-irradiation dimensions (“crossover”). As

shown in Figure 5.2, the phenomenon of turnaround is a strong function of temperature; where under high-temperature irradiation turnaround occurs at a relatively low fluence of fast neutrons [18,21]. The mainstream theory for dimensional change in irradiated nuclear graphite holds that porosity and microcracks (Mrozowski cracks) initially accommodate irradiation-induced swelling along the *c*-axis and thus result in a net decrease in dimensional change due to contraction along the *a/b*-axis. Mrozowski cracks are lenticular cracks, nanometers to several hundred nanometers in length, which form during cooling from graphitization temperatures [22]. The formation of such cracks is due to weak Van der Waals bonding between planes and large differences in the coefficients of thermal expansion (CTE) between the *a* and *c* axes of crystallites. As a result, Mrozowski cracks have lengths on the *a/b* plane and widths along the *c* axis of crystallites (thus accommodating *c*-axis expansion). When the accommodating porosity is largely reduced as a result of irradiation-induced expansion of crystallites, turnaround is soon reached. Continued irradiation and swelling of crystallites along the *c*-axis leads to internal stresses causing new cracks to form and runaway dimensional change [18,23].

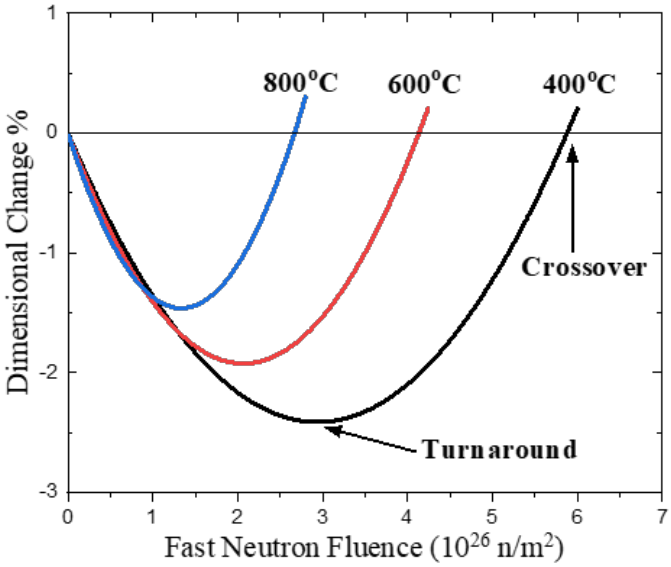

Figure 5.2 Empirically based curves for dimensional change in neutron-irradiated IG-110 at various temperatures [20].

The curves shown in Figure 5.2 are reproduced from empirical models extrapolated from irradiation data of nuclear graphite IG-110 [19,20]. The basis for such empirical models stems from the seminal work of Kelly et al, [24,25] which showed that bulk dimensional change of highly oriented pyrolytic graphite (HOPG) could be expressed as a function of crystallite dimensional change in directions of the *c* and *a* axes. In the case of polycrystalline graphites, the empirical model includes an additional term to account for dimensional change due to porosity [26,27]. The model can be summarized by the following equation as a function of fast neutron fluence [19]:

$$G_x(\gamma) = A_x G_c(\gamma) + (1 - A_x) G_a(\gamma) + F_x(\gamma) \tag{5.1}$$

where,

x: Direction (not specific)

γ: Fast neutron fluence (10^{26} n/m^2, E>0.1 MeV)

$G_x(\gamma)$: Fractional dimensional change of bulk graphite

A_x: Structural factor

$G_c(\gamma)$: Fractional dimensional change of *c*-axis direction in a graphite grain

$G_a(\gamma)$: Fractional dimensional change of *a*-axis direction in a graphite grain

$F_x(\gamma)$: Fractional dimensional change from pores

The variables $G_c(\gamma)$ and $G_a(\gamma)$ are derived from test data for HOPG subjected to fluences of fast neutrons [25]. The dimensional change of HOPG as a function of fast neutron fluence is shown to be linear along the *c* and *a* axes at irradiation temperatures greater than 250°C; therefore, $G_c(\gamma)$ and $G_a(\gamma)$ can be modeled by linear functions. Porosity is believed to decrease prior to the turnaround fluence, due to *c*-axis expansion, then increase beyond turnaround when internal stresses generate new porosity. Thus, $F_x(\gamma)$ may not be described by a linear function and may be quadratic [19]. The resulting percent dimensional change is given in literature by the following [19,20]:

$$\text{Dimensional change} = a_1\gamma^2 + a_2\gamma \tag{5.2}$$

where a_1 and a_2 are temperature-dependent empirical constants.

While empirical models do show reasonable agreement with irradiation data, an atomic mechanism responsible for early turnaround behavior remains to be adequately explained in literature. Considering the model of additional basal plane formation; it is uncertain how such large dimensional changes during high-temperature irradiation can be observed at relatively low fluences which arguably cannot generate enough interstitials or vacancies to add enough additional basal planes to account for the *c*-axis expansion of crystallites, nor enough vacancies for contraction along the *a/b* axes. Indeed, the actual measured dimensional change exceeds that which would be expected from additional basal plane formation [13,28,29]. The temperature-dependent turnaround behavior in

irradiated nuclear graphite has in part been attributed to closure of the accommodating Mrozowski cracks due to an increase in CTE [23]. In situ annealing via TEM does provide experimental evidence that Mrozowski cracks will decrease in dimension due solely to thermal annealing; however, not generally to the extent of closure [30]. In addition, the linear coefficient of thermal expansion along *c* shows little change within the temperature range 600-800°C [31]; thus, additional mechanisms must be contributing to early turnaround behavior in high-temperature irradiated nuclear graphite. This anomaly leads to the conclusion that a more practical explanation for the temperature-dependent dimensional change behavior must lie in the nature of the defects themselves.

The effect of high-temperature electron-irradiation conducted on IG-110 recently [12] showed interstitially formed carbon nanostructures resulting in *c*-axis expansion of crystallites; however, defect structures in that work evolved in a relatively unconstrained TEM foil, leaving open the question of whether such defects would also be observed in bulk neutron-irradiated nuclear graphite. In this work, the effect of high-temperature neutron-irradiation on nuclear graphite IG-110 is presented. New defect structures, which occur interstitially and within disordered regions of the microstructure, have been observed; and the irradiation-induced response of microstructural features subjected to high-temperature neutron-irradiation are reported. In addition, with the use of electron-irradiation as a surrogate for fast neutron-irradiation, the dynamic evolution of such defect structures is discussed.

5.2 Experimental

IG-110 nuclear graphite (Toyo Tanso Co., Kagawa, Japan) is a petroleum-coke-based, fine-grained, iso-molded nuclear graphite. Neutron-irradiated IG-110 was supplied

by Idaho National Laboratory as part of the advanced graphite creep capsule (AGC-3) experiments. Two IG-110 neutron-irradiated samples were characterized; the first irradiated at 813°C to 1.73 dpa (sample ID: EA3611) and the second irradiated at 817°C to a dose of 3.56 dpa (sample ID: EA3609). For a detailed description of irradiation conditions, the reader is referred to Ref. [32]. These samples are considered to be irradiated to a relatively low dose as the approximate turnaround dose at 800°C is 11 dpa [19,20]. The dose is often reported either as a fluence of fast neutrons or dpa, the units are interchangeable and may be converted by the multiplier 8.23×10^{-26} dpa/n/m^2 [33]. The dose and irradiating temperature were chosen with consideration of the operating regimes of the future envisioned Gen IV reactors (up to 1000°C [34]) and are similar to the dose and temperature used in previously reported in situ electron-irradiation studies [12] which showed the formation of carbon nanostructures (~2 dpa at 800°C). Bulk irradiated samples were mechanically thinned with 1200 grit SiC paper to approximately 60 μm then cut into 3mm discs using a Gatan TEM specimen disc punch. Final thinning to electron transparency was achieved by Ar^+ ion-milling followed by low-voltage, low-angle ion-milling finishing at 1 kV and 2° for 20 minutes using a Gatan PIPS II 695.

Room-temperature HRTEM studies were performed using a JEOL-2100 TEM operated at 100 kV. This operating voltage is below the reported threshold value for an incident electron to overcome the displacement energy (30 eV) in graphite [35]; in addition, care was taken to capture micrographs from regions of interest without allowing prolonged exposure to the electron beam. In situ electron-irradiation was conducted on as-prepared unirradiated specimens of IG-110 at the National Center for Electron Microscopy using an image aberration-corrected FEI ThemIS 60-300 STEM/TEM

operated at 200 kV and equipped with a double-tilt heating holder (Model 652, Gatan, Pleasanton, CA). The dose rate during electron-irradiation is calculated by the product of flux of electrons and the cross section for atomic displacement; further discussion on the calculation of dose rate during electron-irradiation may be found elsewhere [12,36]. The dose rate during electron-irradiation was approximately 2.5×10^{-3} dpa/s; total doses did not exceed 2.5 dpa and, for clarity, the dose for electron-irradiation tests are reported in seconds of electron beam exposure. While the flux of electron-irradiation far exceeds that of neutron-irradiation (10^{-3} dpa/s compared to 10^{-7} dpa/s [34]), electron-irradiation is primarily observed to cause point-defect damage whereas irradiation with neutrons will cause cascade damage owing to their heavier mass. In any event, during high-temperature neutron-irradiation, cascade damage partially anneals between individual cascade events, giving an approximated net effect of isolated point-defect damage [37].

5.3 Results and Discussion

Figure 5.3 shows HRTEM micrographs of high-temperature neutron-irradiated IG-110 in disordered regions of the microstructure where accommodating porosity on the microscopic scale is abundant. Figure 5.3 (a) and (b) show IG-110 neutron-irradiated at 813°C to 1.73 dpa where the indicated defects are shown to be domains of non-planar basal planes (i.e., fullerene-like defects). Classifying these defects as “fullerene-like” is not to imply strictly the traditional definition of a closed structure such as a Buckminsterfullerene or the open-ended cylindrical carbon nanotube; as many hybrid structures are possible, “fullerene-like” is used to include many nanoallotropes of carbon as suggested by Cataldo [38]. Figure 5.3 (c) and (d) show IG-110 neutron-irradiated at 817°C to 3.56 dpa in which fullerene-like defects were similarly observed in disordered

regions of the microstructure. Figure 5.3 (c) shows the presence of fullerene-like defects occurring within a Mrozowski crack. Figure 5.3 (d) shows additional evidence of fullerene-like defects present within the accommodating porosity. The defects shown in Figure 5.3 provide an insight to the macroscopic theory for dimensional change. As already mentioned, closure of the accommodating porosity has generally been believed to occur from *c*-axis expansion of crystallites due to interstitial defect species; however, shown in Figure 5.3 is evidence that defects are forming *within* the accommodating porosity at a relatively low dose which may impede further irradiation induced *c*-axis expansion induced by prolonged irradiation. Figure 5.3 (d) additionally shows the presence of a 'ruck and tuck' defect resulting in localized *c*-axis expansion. The authors have recently reported the first experimental evidence of such defects [39]; however, the additional observation of this defect here is worth noting and adds validity to the so-called 'buckle, ruck and tuck' model proposed by Heggie et al. [13].

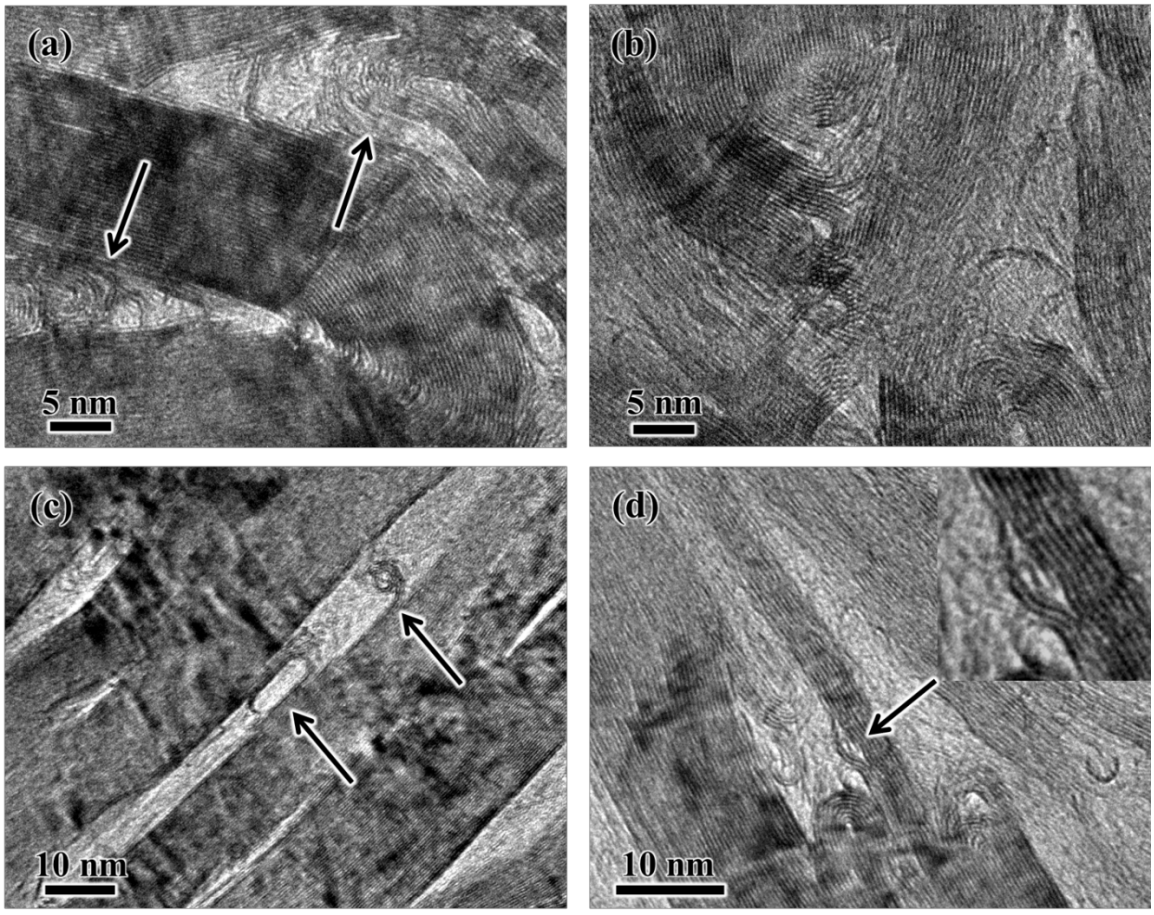

Figure 5.3 HRTEM images of high-temperature neutron-irradiated IG-110. (a) and (b) show the presence of fullerene-like defects occuring within disordered regions of the microstructure (813°C to 1.73 dpa). (c) and (d) show further evidence of fullerene-like defects occuring within the accommodating porosity in a sample irradiated at 817°C to 3.56 dpa; within a Mrozowski crack in (c) and additionally a 'ruck and tuck' defect in (d).

The defect structures shown in Figure 5.3 (and throughout this manuscript) were not observed in areas of the microstructure where there is a high degree of long-range order (such as filler particles). Fullerene-like defects were found to occur in areas of the microstructure in which accommodating porosity is abundant (Figure 5.5 (a)). While both neutron-irradiated specimens showed the presence of such defects, the *apparent* concentration of defects was greater in the higher-dose specimen (817°C to 3.56 dpa). The authors acknowledge that definitive conclusions of defect concentration may not be

solely conducted via TEM analysis due to the complex and inhomogeneous nature of nuclear graphite's microstructure and the sample analysis being confined to an electron-transparent area of a TEM specimen; nevertheless, the observations of fullerene-like defects were noted to be far more frequent in the higher dose specimen.

Figure 5.4 shows HRTEM micrographs of IG-110 neutron-irradiated at 817°C to 3.56 dpa where fullerene-like defects are occurring interstitially causing *c*-axis expansion of crystallites. Figure 5.4 (a) shows a fullerene-like defect resulting in significant amount of swelling in the *c* direction which results in closure near the top portion of the neighboring Mrozowski crack. Figure 5.4 (b-d) show larger fullerene-like structures (~5 nm in diameter) consisting of several concentric shells of basal planes. The defects shown in Figure 5.4 (b-d) all result in significant expansion of crystallites along the *c*-axis. Furthermore, the defects in Figure 5.4 (b-d) result in the appearance of new nanocracks via delamination of basal planes. The current macroscopic theory for dimension change suggests that the generation of new porosity will occur *after* porosity can no longer accommodate additional *c*-axis expansion of crystallites [18,23]; however, Figure 5.4 (b-d) clearly show evidence of new crack formation as a result of the evolution of fullerene-like defects.

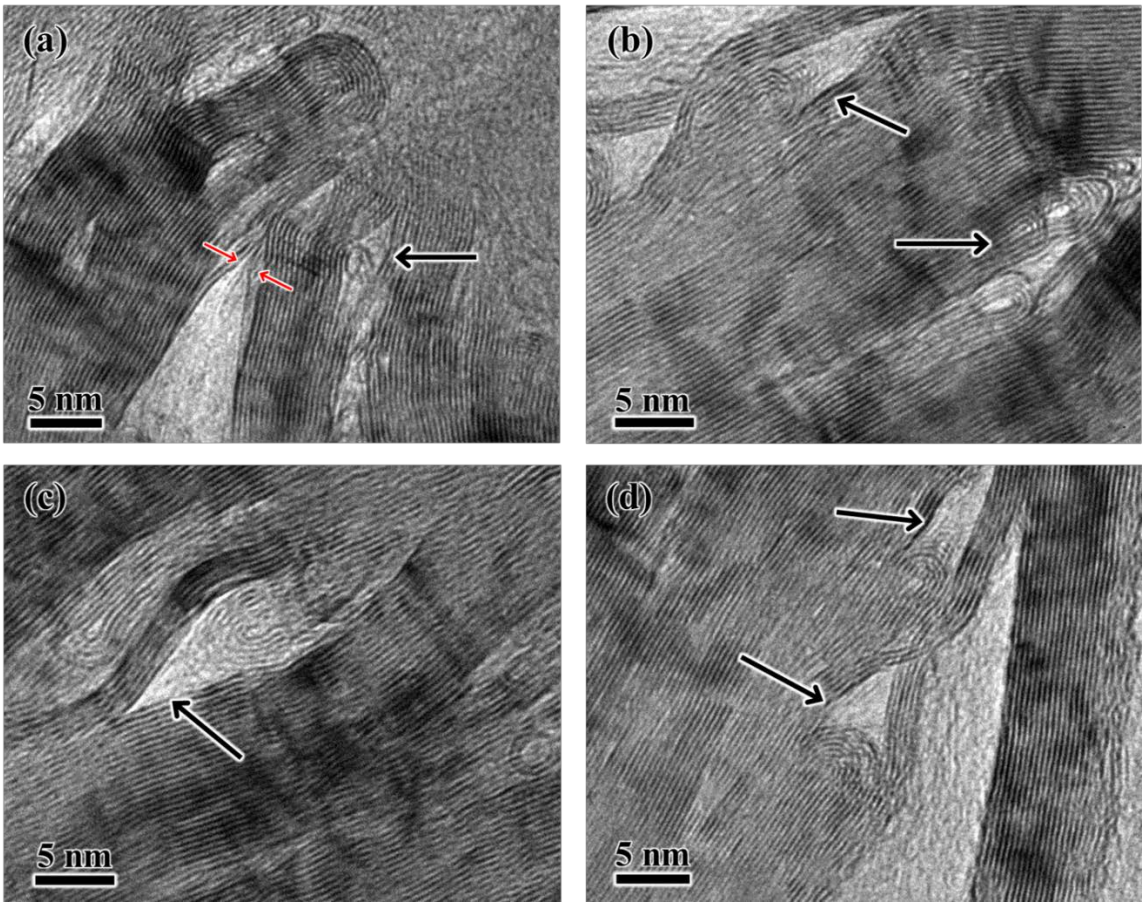

Figure 5.4 HRTEM micrographs of IG-110 neutron-irradiated at 817°C to 3.56 dpa showing fullerene-like defects occurring interstitially resulting in c-axis expansion. In (a), the indicated defect results in closure of a portion of a Mrozowski crack (red arrows). (b) shows a cluster of fullerene-like defects occurring interstitially and an additionally the formation of a new crack as indicated. (c) shows an interstitial fullerene-like defect approximately 5 nm in diameter which results in delamination of basal planes as indicated. (d) shows fullerene-like defects occurring in relatively unconstrained areas of the microstructure resulting in closure and generation of new cracks.

Figure 5.5 (a) shows a bright-field TEM micrograph of un-irradiated as-prepared nuclear graphite IG-110 in a disordered region of the microstructure in which several Mrozowski cracks are present. Figure 5.5 (b) shows a micrograph of a Mrozowski crack in as-prepared nuclear graphite IG-110. The crack shows phase contrast, indicating that, rather than being void of material, the crack contains disordered carbon (as do the cracks in the micrographs shown in Figures 5.3 & 5.4). Neighboring the Mrozowski crack is

ordered graphite, as confirmed by the well defined (00*l*) (*l* = 2n) reflections. Within the Mrozowski crack, the fast Fourier transform (FFT) shows significant diffuse scattering, consistent with a largely disordered graphitic phase. The authors acknowlege that there remains debate in the literature about whether Mrozowski cracks are void or contain material [40]; however, these results indicate the presence of disordered material within the cracks as suggested in other studies [10,30,41]. Of the cited literature, Freeman et. al. [41] confirmed the presence of material within Mrozowski cracks via electron energy loss spectroscopy (EELS). In addition, Wen et al. [30] prepared specimens via microtomy which eliminates the possibility of amorphous carbon being redeposited via ion-milling during specimen preparation. It is conjectured that the presence of this disordered carbon within in the microstructure of nuclear graphite is significant. Well observed in the literature is a self-organization phenomenom of disordered carbonaceous species into fullerene-like structures when subjected to irradation [12,42-45]. This phenomenon may explain why the formation of such fullerene-like defects occur in these areas of the microstructure aside from the crystallites being locally unconstrained due to accomodating porosity.

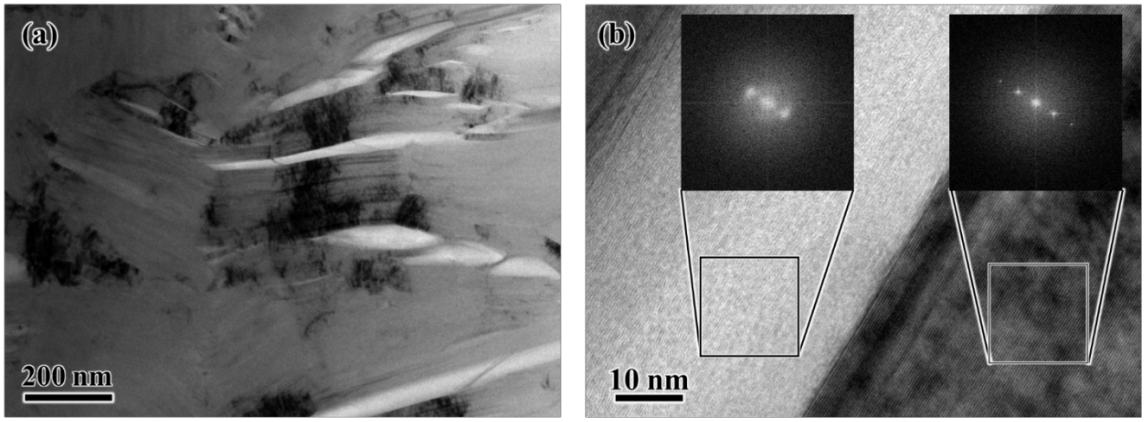

Figure 5.5 (a) Bright-field TEM micrograph of Mrozowski cracks in un-irradiated nuclear graphite IG-110. (b) HRTEM micrograph of a Mrozowski crack showing disordered graphitic phase present within the Mrozowski crack. The insets in (b) are FFTs of the indicated areas.

Figure 5.6 shows HRTEM micrographs of IG-110 neutron-irradiated at 817°C to 3.56 dpa in which a disordered graphitic phase is abundant. Figure 5.6 (a) shows a circular defect structure consisting of concentric basal planes. Figure 5.6 (b) shows an additional concentric shelled defect found in a disordered region of the microstructure. A possible interpretation of the defects shown in Figure 5.6 is that they are cross-sections through carbon onions. A carbon onion is a non-equilibrium defect structure which can form from the self-organization of disordered graphitic phase upon irradiation. Carbon onions can reportedly occur in a wide range of diameters ranging from a two-shell configuration of approximately 1.4 nm diameter to onions consisting of hundreds of shells with diameters up to microns [44]; however, this phenomenon has not been previously reported to occur in high-temperature neutron-irradiated nuclear graphite. The authors acknowledge that it is not possible to empirically establish the spherical nature of these defects from two-dimensional TEM micrographs; however, given the strong evidence of the formation of such defects via energetic particle bombardment [12,42-45], there is a strong *a priori* argument that the defect structures depicted in Figure 5.6 are

indeed evidence of carbon onions having formed upon high-temperature neutron-irradiation. Furthermore, a possible interpretation of the defect indicated in Figure 5.6 (a) is a nautilus-type structure which has previously been proposed as a precursor to larger onion-like structures such as the defect indicated in Figure 5.6 (b) [46]. A possible consequence of the formation of carbon onions is a reduction in the coherent length of crystallites along the *a/b* axes. The formation of such structures from irradiated basal planes would suggest a new mechanism for contraction of crystallites along the *a*-axis; however, confirming *a*-axis contraction from ex situ analysis is ambiguous, as the initial state of the crystallite and the evolution of the defect is not known.

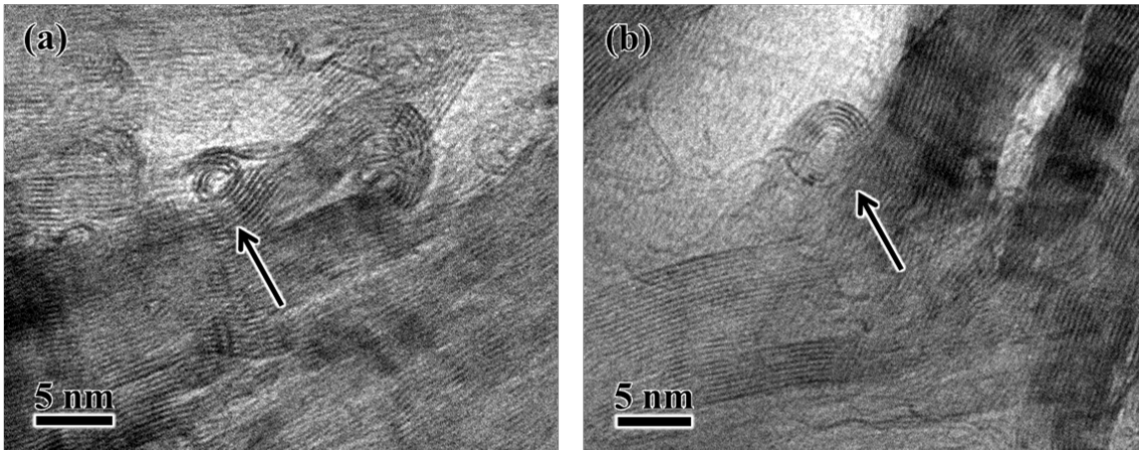

Figure 5.6 HRTEM micrographs of neutron-irradiated IG-110 (3.56 dpa at 817°C). Shown in (a) is a circular concentric shelled fullerene-like defect. Shown in (b) is an additional concentric shelled defect approximately 5 nm in diameter occurring within disordered regions of the microstructure.

To further investigate the defects shown in Figure 5.6, in situ TEM was utilized to capture the initial state of crystallites and dynamic evolution of irradiation-induced defects. While in situ TEM analysis with fast neutrons remains impossible, an appropriate surrogate is argued in literature to be high-flux electron-irradiation [7,12]. Figure 5.7 shows HRTEM micrographs taken from an in situ video recording of IG-110 electron-

irradiated (200keV, 2.5×10^{-3} dpa/s) at 800°C. Figure 5.7 (a) shows a crystallite at the start of the experiment, with minimal electron-irradiation. In this instance, the closure and rearrangement of basal planes on the edge of the crystallite is due solely to thermal annealing as has been previously reported by the authors [12]. Figure 5.7 (b) shows the same crystallite after 160s of electron-irradiation, where two caged fullerenes are indicated by the left arrow. With prolonged electron-irradiation, these structures are observed to recombine into the crystallite and result in growth along the *c*-axis of the crystallite via formation of defective basal planes on the surface, indicated by the left arrow in Figure 5.7 (c). The basal planes indicated by the right arrow in Figure 5.7 (b), are shown to contract along the *a* axis of the crystallite and evolve into concentric shells as shown by Figure 5.7 (c-f). Additionally, Figure 5.7 (c-f) shows the evolution and growth of defective basal planes into a concentric shelled defect with pronounced curvature. Figure 5.7 shows experimental evidence that concentric shelled onion-like defects can form from relatively well-ordered graphitic phase via irradiation-induced defect production. It is well observed in literature that the presence of non-six-member carbon rings (basal plane dislocations) will result in out-of-plane distortion and buckling of basal planes [13,47,48]; the defect structures shown in Figure 5.7 are believed to be formed via the interaction of such basal plane defects produced by irradiation. The results shown in Figure 5.7 give experimental evidence that the formation of fullerene-like defects is a dominant defect evolution mechanism in high-temperature irradiated nuclear graphite. Furthermore, Figure 5.7 shows the dynamic evolution of such structures in which basal planes contract along the *a/b* axes, resulting in swelling along the *c* axis.

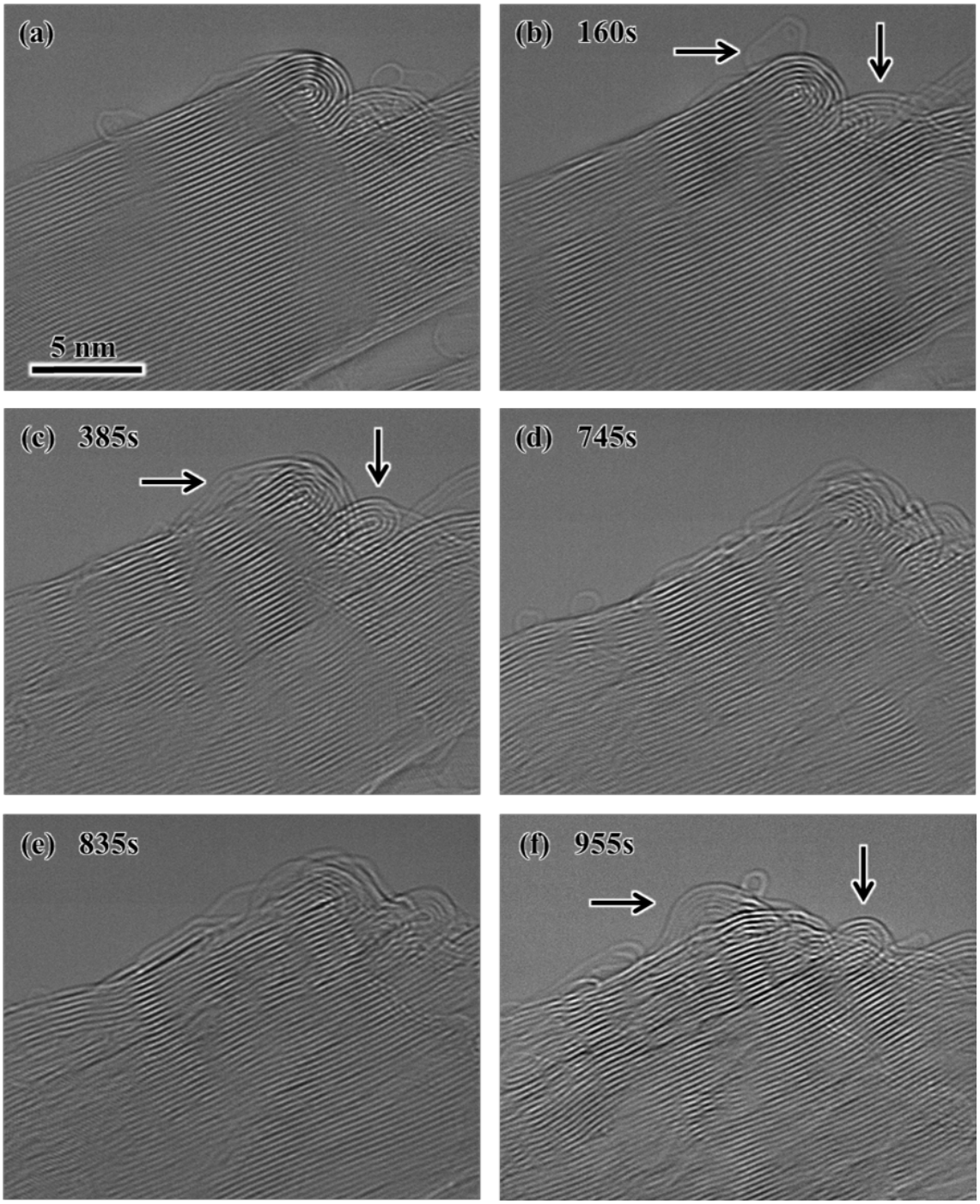

Figure 5.7 HRTEM micrographs taken from in-situ electron-irradiation conducted at 800°C. (a) shows a crystallite of IG-110 with minimal electron-irradiation in which the curling of exposed basal plane edges is due solely to thermal annealing. (b-f) shows the same crystallite in (a) after continued electron beam exposure, where the evolution of defective basal planes results in the concentric shelled defect indicated by the left arrow in (f). Additionally, the basal planes indicated by the right arrow in (b) are observed to undergo a-axis contraction via the formation of a fullerene-like structure (b-f).

Figure 5.8 (a) shows ca. 50 nm diameter circular structures found in IG-110 neutron-irradiated at 817°C to 3.56 dpa. Figure 5.8 (b) shows a HRTEM micrograph of (a) where basal planes are resolved in the structure and exhibit a concentric arrangement. Such defects have not been observed in un-irradiated nuclear graphites and are believed to be formed via neutron-irradiation [16,17]. Nuclear graphites have intrinsic circular microstructural features known as quinoline insoluble (QI) particles. QI particles are poorly graphitized rosette-like structures that form due to aromatic molecules present within the binder material during manufacturing. QI particles act as templates which promote graphitization of the surrounding binder, forming a wide, porous rosette-like arrangement of crystallites which is retained for up to several hundreds of nanometers (as shown in Figure 5.9 (a)). When subjected to sufficient neutron-irradiation, QI particles will become fully dense, resulting in the generation of new cracks [10,49]. Contescu et al. [49] observed structures similar to those shown in Figure 5.8 in nuclear graphite G347A neutron-irradiated past turnaround (29.8 dpa at 450°C) and reasoned the dense concentric shelled defects were indeed the evolution of QI particles subjected to high-dose neutron-irradiation; however, the defects they observed (as well as those in Figure 5.8) cannot be the evolution of irradiated QI particles as both the length scale and surrounding microstructures are inconsistent with those of QI particles [17]. Thus, the concentric shelled fullerene-like structures shown in Figure 5.8 are believed to be irradiation-induced defects.

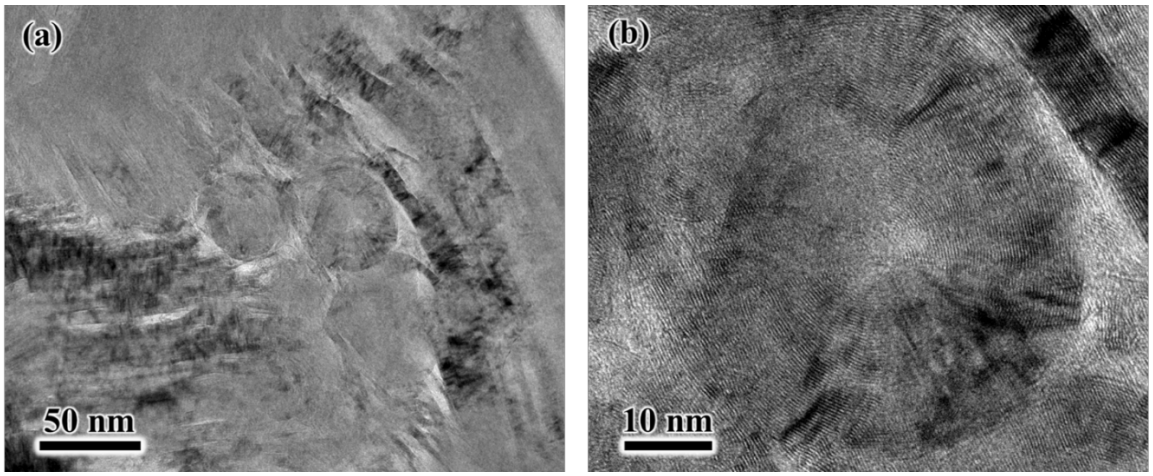

Figure 5.8 (a) Bright-field TEM micrograph of neutron-irradiated IG-110 (3.56 dpa at 817°C) showing circular graphitic structures. (b) HRTEM micrograph of the feature shown in (a) in which basal planes are observed to have a concentric arrangement.

Figure 5.9 shows a bright-field TEM image of QI particles in as-prepared IG-110 (a) and in high-temperature neutron-irradiated IG-110 (b-d). Shown in Figure 5.9 (a), QI particles exhibit a porous rosette-like arrangement of crystallites up to several hundred nanometers wide. In contrast, the defects shown in Figure 5.8 (a) have diameters of less than 50 nm and are formed between crystallites of different orientation, which is inconsistent with the QI particles shown in Figure 5.9 (a) and reported in Ref [17]. Figure 5.9 (b) shows a QI particle in IG-110 neutron-irradiated at 813°C to 1.73 dpa where much of the porous structure is retained and only a slight densification of the rosette-like structure is observed. Figure 5.9 (c) shows a QI particle irradiated to a higher dose (3.56 dpa at 817°C) where densification is clearly apparent in comparison to Figure 5.9 (a) and (b); however, full densification is not observed. As a result of the densified microstructure, cracking between neighboring crystallites occurs (indicated by the arrows). Cracking of the surrounding microstructure around QI particles as a result of irradiation has previously been reported; however, the irradiating dose was nearly twice

that of this study [10]. Figure 5.9 (d) shows several partially densified QI particles in neutron-irradiated IG-110 (3.56 dpa at 817°C) where there is a significant amount of additional porosity arising from densification of the QI.

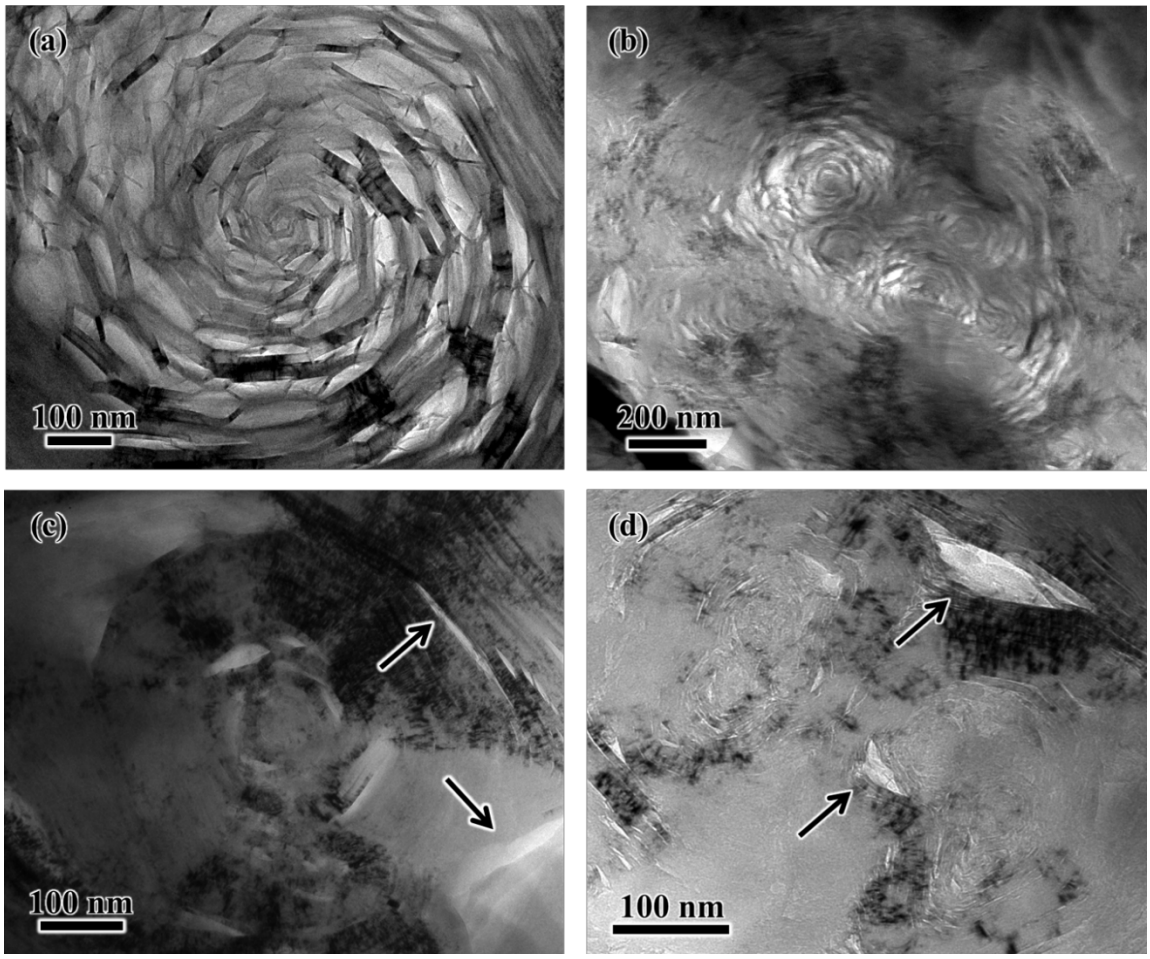

Figure 5.9 Bright-field TEM micrographs of a QI particle in as-prepared nuclear graphite IG-110 (a), and in neutron-irradiated IG-110 (b-d). With neutron-irradiation at 813°C to 1.73 dpa, slight densification is observed; however, much of the porous structure is retained (b). At higher dose neutron-irradiation (3.56 dpa at 817°C), densification of the QI particles is shown and additionally the formation of new cracks as indicated by arrows (c & d).

Aside from the observed macroscopic dimensional change as a result of irradiation damage, other property changes are directly affected by the evolution of defect structures within the graphite structure, such as the CTE. Figure 5.10 shows a comparison

of the empirical models for dimensional change and CTE change in IG-110 neutron-irradiated at 800°C [20]. The CTE rapidly increases at the onset of irradiation, then rapidly decreases until turnaround, after which it continues to linearly decrease more slowly. Initially, the bulk response of CTE change in nuclear graphite is buffered by the accommodating porosity. In general, the increase is believed to occur when *c*-axis expansion has caused closure in porosity. The decrease in CTE is reasoned to occur as a result of new porosity occurring from additional *c*-axis expansion and internal stresses causing the growth of new porosity [50]; however, this conclusion does not agree with the macroscopic theory for dimensional change. As noted in Figure 5.10, the decrease in CTE occurs *before* the turnaround fluence, and according to the present understanding, new porosity should not occur until *after* the turnaround fluence. The vertical reference line in Figure 5.10 shows the fluence used in this study, which is close to the fluence at which the empirical model predicts the initial decrease in CTE would occur. The results shown in Figure 5.4 show evidence of the formation of new microcracks occurring before the turnaround fluence which may explain the observed decrease in CTE at low fluence.

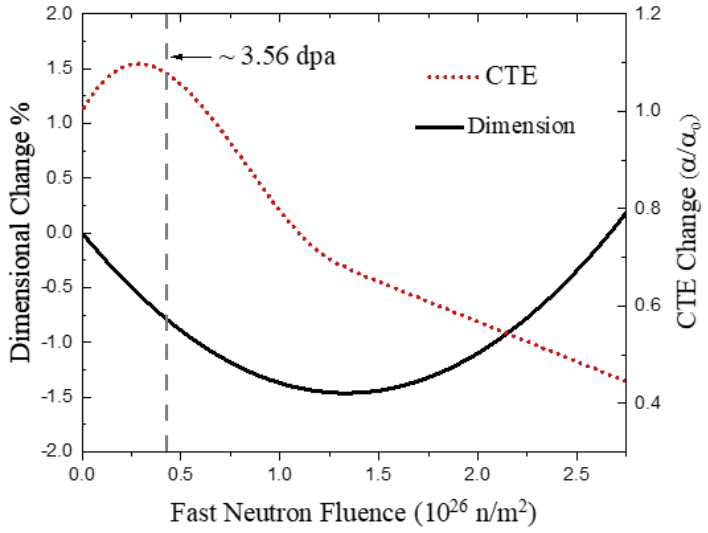

Figure 5.10 Empirical models for irradiation induced dimensional change (left axis) and CTE (right axis) in IG-110 (800°C). The vertical dashed line shows the fluence of this study.

5.4 Conclusions

TEM analysis of high-temperature neutron-irradiated graphite confirms the presence of fullerene-like defects occurring interstitially and within the Mrozowski cracks. These defects are found to occur in high concentrations in disordered regions of the microstructure and have not been previously observed in neutron-irradiated nuclear graphite [10,24-27,51,52]. The results reported here do not provide any evidence to support the previously proposed atomic displacement model as an appropriate interpretation of defect evolution in high-temperature irradiated nuclear graphite. To the contrary, these results suggest fullerene-like defects are a dominant mechanism contributing to dimensional change, the filling and closure of accommodating porosity, and in some instances the generation of new porosity prior to turnaround fluence. It is worth noting that these processes are observed to occur at a relatively low irradiation dose and at temperatures above 750°C [12]. Previously reported studies on graphite NBG-18 neutron-irradiated to nearly twice the dose used in this study (6.7 dpa at 678°C)

showed no evidence of such defects [10]. Given these results, the authors believe that such defects form via a thermally activated mechanism. As such, to improve the empirical relationships for dimensional change given in equation (1), an Arrhenius term may be an appropriate addition. These observations give a valuable insight into the observed property changes of neutron-irradiated nuclear graphite. In addition, the present results agree with previously reported high-temperature electron-irradiation studies which showed the formation of fullerene-like defects in-situ and give additional validity to the use of high-flux electron-irradiation as a useful approximation to that of neutron-irradiation. Future studies may include characterization of nuclear graphite neutron-irradiated at high-temperature (800°C and above) at and beyond the turnaround fluence. Additional characterization could include annealing experiments combined with differential scanning calorimetry, which may give insight into stored energy and activation energy regimes, and spectroscopic techniques (EELS and Raman) which may provide insight to defect concentration.

5.5 References

[1] B.J. Marsden, A.N. Jones, G.N. Hall, M. Treifi, P.M. Mummery, Graphite as a core material for Generation IV nuclear reactors, in: P. Yvon (Ed.), Struct. Mater. Gener. IV Nucl. React., Woodhead Publishing, 2017: pp. 495–532.

[2] P.A. Thrower, Interstitial and vacancy loops in graphite irradiated at high temperatures, Br. J. Appl. Phys. 15 (1964) 1153–1159. doi:10.1088/0508-3443/15/10/302.

[3] S. Amelinckx, P. Delavignette, Dislocation loops due to quenched-in point defects in graphite, Phys. Rev. B. (1960) 50.

[4] J. Koike, D.F. Pedraza, Dimensional changes in highly oriented pyrolytic graphite due to electron-irradiation, J. Mater. Res. 9 (1994) 1899–1907. doi:10.1557/JMR.1994.1899.

[5] S. Muto, T. Tanabe, Damage process in electron-irradiated graphite studied by transmission electron microscopy. I. high-resolution observation of highly graphitized carbon fibre, Philos. Mag. A Phys. Condens. Matter, Struct. Defects Mech. Prop. 76 (1997) 679–690. doi:10.1080/01418619708214029.

[6] S. Muto, T. Tanabe, Fragmentation of graphite crystals by electron irradiation at elevated temperatures, J. Electron Microsc. (Tokyo). 48 (1999) 519–523. doi:10.1093/oxfordjournals.jmicro.a023710.

[7] C. Karthik, J. Kane, D.P. Butt, W.E. Windes, R. Ubic, In situ transmission electron microscopy of electron-beam induced damage process in nuclear grade graphite, J. Nucl. Mater. 412 (2011) 321–326. doi:10.1016/j.jnucmat.2011.03.024.

[8] B.E. Mironov, H. Freeman, A.P. Brown, F.S. Hage, A.J. Scott, A.V.K. Westwood, J.-P. Da Costa, P. Weisbecker, R.M.D. Brydson, Electron irradiation of nuclear graphite studied by transmission electron microscopy and electron energy loss spectroscopy, Carbon N. Y. 83 (2014) 106–117. doi:10.1016/j.carbon.2014.11.019.

[9] J.A. Hinks, S.J. Haigh, G. Greaves, F. Sweeney, C.T. Pan, R.J. Young, S.E. Donnelly, Dynamic microstructural evolution of graphite under displacing irradiation, Carbon N. Y. 68 (2014) 273–284. doi:10.1016/j.carbon.2013.11.002.

[10] C. Karthik, J. Kane, D.P. Butt, W.E. Windes, R. Ubic, Neutron irradiation induced microstructural changes in NBG-18 and IG-110 nuclear graphites, Carbon N. Y. 86 (2015) 124–131. doi:10.1016/j.carbon.2015.01.036.

[11] H.M. Freeman, A.J. Scott, R.M.D. Brydson, Thermal annealing of nuclear graphite during in-situ electron irradiation, Carbon N. Y. 115 (2017) 659–664. doi:10.1016/j.carbon.2017.01.057.

[12] S. Johns, T. Poulsen, J.J. Kane, W.E. Windes, R. Ubic, C. Karthik, Formation of carbon nanostructures in nuclear graphite under high-temperature in situ electron-irradiation, Carbon N. Y. 143 (2019) 908–914. doi:10.1016/j.carbon.2018.11.077.

[13] M.I. Heggie, I. Suarez-Martinez, C. Davidson, G. Haffenden, Buckle, ruck and tuck: A proposed new model for the response of graphite to neutron irradiation, J. Nucl. Mater. 413 (2011) 150–155. doi:10.1016/j.jnucmat.2011.04.015.

[14] J. Gruber, A.C. Lang, J. Griggs, M.L. Taheri, G.J. Tucker, M.W. Barsoum, Evidence for Bulk Ripplocations in Layered Solids, Sci. Rep. 6 (2016). doi:10.1038/srep33451.

[15] M.W. Barsoum, G.J. Tucker, Deformation of layered solids: Ripplocations no basal dislocations, Scr. Mater. 139 (2017) 166–172. doi:10.1016/j.scriptamat.2017.04.002.

[16] K.Y. Wen, T.J. Marrow, B.J. Marsden, The microstructure of nuclear graphite binders, Carbon N. Y. 46 (2008) 62–71. doi:10.1016/j.carbon.2007.10.025.

[17] C. Karthik, J. Kane, D.P. Butt, W.E. Windes, R. Ubic, Microstructural characterization of next generation nuclear graphites, Microsc. Microanal. 18 (2012) 272–278. doi:Doi 10.1017/S1431927611012360.

[18] B.J. Marsden, M. Haverty, W. Bodel, G.N. Hall, A.N. Jones, P.M. Mummery, M. Treifi, Dimensional change, irradiation creep and thermal/mechanical property changes in nuclear graphite, 61 (2016) 155–182. doi:10.1080/09506608.2015.1136460.

[19] T. Shibata, E. Kunimoto, M. Eto, S. Shiozawa, K. Sawa, T. Oku, T. Maruyama, Interpolation and extrapolation method to analyze irradiation-induced dimensional change data of graphite for design of core components in very high temperature reactor (VHTR), J. Nucl. Sci. Technol. 47 (2010) 591–598. doi:10.1080/18811248.2010.9720956.

[20] S. Mohanty, S. Majumdar, M. Srinivasan, U.S.N.R. Commission, HTGR Graphite Core Component Stress Analysis Research Program – Task 1 Technical Letter Report, 2011.

[21] A.A. Campbell, Y. Katoh, Summary Report on Effects of Irradiation on Material IG-110 - Prepared for Toyo Tanso Co ., Ltd ., 2017.

[22] S. Mrozowski, Mechanical strength, thermal expansion and structure of cokes and carbons, Proc. 1st 2nd Conf. Carbon. (1954) 31. doi:papers://D9F9AA35-5CC8-482E-89C5-625C9FC6984D/Paper/p2585.

[23] G.B. Neighbour, Modelling of dimensional changes in irradiated nuclear graphites, J. Phys. D. Appl. Phys. 33 (2000) 2966–2972. doi:10.1088/0022-3727/33/22/315.

[24] B.T. Kelly, W.H. Martin, P.T. Nettley, Dimensional Changes in Pyrolytic Graphite under Fast-Neutron Irradiation, Philos. Trans. R. Soc. A Math. Phys. Eng. Sci. 260 (1966) 37–49.

[25] B.T. Kelly, J.E. Brocklehurst, High dose fast neutron irradiation of highly oriented pyrolytic graphite, Carbon N. Y. 9 (1971) 783–789.

[26] B.T. Kelly, W.H. Martin, P.T. Nettley, Dimensional Changes in Polycrystalline Graphites under Fast-Neutron Irradiation, Philos. Trans. R. Soc. A Math. Phys. Eng. Sci. 260 (1966) 51–71.

[27] J.E. Brocklehurst, B.T. Kelly, Analysis of the dimensional changes and structural changes in polycrsytalline graphite under fast neutron irradiation, Carbon N. Y. 31 (1993) 155–178.

[28] W.N. Reynolds, P.A. Thrower, The nucleation of radiation damage in graphite, Philos. Mag. 12 (1965) 573–593.

[29] R.H. Telling, M.I. Heggie, Radiation defects in graphite, 2007. doi:10.1080/14786430701210023.

[30] K. Wen, J. Marrow, B. Marsden, Microcracks in nuclear graphite and highly oriented pyrolytic graphite (HOPG), J. Nucl. Mater. 381 (2008) 199–203. doi:10.1016/j.jnucmat.2008.07.012.

[31] D.K.L. Tsang, B.J. Marsden, S.L. Fok, G. Hall, Graphite thermal expansion relationship for different temperature ranges, Carbon N. Y. 43 (2005) 2902–2906. doi:10.1016/j.carbon.2005.06.009.

[32] W.E. Windes, D.T. Rohrbaugh, W.D. Swank, D.L. Cottle, AGC-3 Specimen Post-Irradiation Examination Data Package Report, Idaho National Laboratory, 2017. INL/EXT-17-43823.

[33] G.L. Hawkes, J.W. Sterbentz, J.T. Maki, B.T. Pham, Thermal Predictions of the AGR-3/4 Experiment With Post Irradiation Examination Measured Time-Varying Gas Gaps, J. Nucl. Eng. Radiat. Sci. 3 (2017) 1–11. doi:10.1115/1.4037095.

[34] T.R. Allen, K. Sridharan, L. Tan, W.E. Windes, J.I. Cole, D.C. Crawford, G.S. Was, Materials Challenges for Generation IV Nuclear Energy Systems, Nucl. Technol. 162 (2008) 342–357. doi:10.13182/NT08-A3961.

[35] R.F. Egerton, P. Li, M. Malac, Radiation damage in the TEM and SEM, Micron. 35 (2004) 399–409. doi:10.1016/j.micron.2004.02.003.

[36] O.S. Oen, Cross Sections for Atomic Displacements in Solids By Fast Electrons, 1965.

[37] J.H.W. Simmons, Radiation Damage in Graphite, 1st Editio, Pergamon, 1965.

[38] F. Cataldo, The impact of a fullerene-like concept in carbon black science, Carbon N. Y. 40 (2002) 157–162. doi:10.1016/S0008-6223(01)00167-1.

[39] S. Johns, L. He, J.J. Kane, W.E. Windes, R. Ubic, C. Karthik, S. Johns, L. He, J.J. Kane, W.E. Windes, R. Ubic, C. Karthik, Experimental evidence for 'buckle, ruck and tuck' in neutron irradiated graphite, Carbon N. Y. (2019). doi:10.1016/j.carbon.2019.12.028.

[40] D. Liu, D. Cherns, Nano-cracks in a synthetic graphite composite for nuclear applications, Philos. Mag. 98 (2018) 1272–1283. doi:10.1080/14786435.2018.1433886.

[41] H.M. Freeman, A.N. Jones, M.B. Ward, F.S. Hage, N. Tzelepi, Q.M. Ramasse, A.J. Scott, R.M.D. Brydson, On the nature of cracks and voids in nuclear graphite, Carbon N. Y. 103 (2016) 45–55. doi:10.1016/j.carbon.2016.03.011.

[42] D. Ugarte, Curling and closure of graphitic networks under electron-beam irradiation, Nature. 359 (1992) 707–709. doi:10.1038/359707a0.

[43] F. Banhart, P.M. Ajayan, Carbon onions as nanoscopic pressure cells for diamond formation, Nature. 382 (1996) 433–435. doi:10.1038/382433a0.

[44] F. Banhart, Irradiation effects in carbon nanostructures, Reports Prog. Phys. 62 (1999) 1181–1221. doi:10.1088/0034-4885/62/8/201.

[45] F. Cataldo, On the Action of γ Radiation on Solid C 60 and C 70 Fullerenes: A Comparison with Graphite Irradiation, Fuller. Sci. Technol. 8 (2000) 577–593. doi:10.1080/10641220009351435.

[46] H.W. Kroto, K. McKay, The formation of quasi-icosahedral spiral shell carbon particles, Nature. 331 (1988) 328–331. doi:10.1038/331328a0.

[47] M.T. Lusk, L.D. Carr, Nanoengineering defect structures on graphene, Phys. Rev. Lett. 100 (2008) 1–4. doi:10.1103/PhysRevLett.100.175503.

[48] Y. Liu, B.I. Yakobson, Cones, pringles, and grain boundary landscapes in graphene topology, Nano Lett. 10 (2010) 2178–2183. doi:10.1021/nl100988r.

[49] C.I. Contescu, J.D. Arregui-Mena, A.A. Campbell, P.D. Edmondson, N.C. Gallego, K. Takizawa, Y. Katoh, Development of mesopores in superfine grain graphite neutron-irradiated at high fluence, Carbon N. Y. 141 (2019) 663–675. doi:10.1016/j.carbon.2018.08.039.

[50] G. Haag, Properties of ATR-2E Graphite and Property Changes due to Fast Neutron Irradiation, 2005. doi:0944-2952.

[51] L.L. Snead, T.D. Burchell, Y. Katoh, Swelling of nuclear graphite and high quality carbon fiber composite under very high irradiation temperature, J. Nucl. Mater. 381 (2008) 55–61. doi:10.1016/j.jnucmat.2008.07.033.

[52] S. Ishiyama, T.D. Burchell, J.P. Strizak, M. Eto, The effect of high fluence neutron irradiation on the properties of a fine-grained isotropic nuclear graphite, J. Nucl. Mater. 230 (1996) 1–7. doi:10.1016/0022-3115(96)00005-0.

CHAPTER SIX: CONCLUSIONS AND FUTURE WORK

6.1 Concluding Remarks

The irradiation-induced changes in the properties of nuclear graphite vary significantly amongst grades and are dependent upon the source of raw coke and processing technique. As many historical grades of nuclear graphite are now obsolete, new grades of graphite for application in Gen IV nuclear reactors must be qualified and characterized. The scope, size, cost and time of irradiation programs can be immense; however, these programs may be reduced by further understanding the relationship between irradiation-induced microstructural changes and properties. The work included in this dissertation focused on the characterization of high-temperature defect evolution in candidate nuclear graphite grades via innovative experimentation.

In Chapter Two, a novel oxidation-based TEM specimen-preparation technique was reported and optimized for nuclear graphite IG-110, NBG-18 and additionally HOPG. Thermal oxidation of nuclear graphite is preferential to the leading basal plane edges [1,2], therefore, HOPG sample preparation was modified to include dimple grinding until perforation. Oxidation time varied between each grade due to the inherent microstructural features of nuclear graphite being larger than the oxidized area ($\leq$ 1 mm) and the accuracy of initial mechanical thinning. An optimal temperature for oxidation in all grades was found to be 575°C. At higher temperatures (up to 625°C), the observed concentration of amorphous carbon increased. The increase in amorphous carbon is conjectured to be a result of the formation of new oxygen functional groups that remain

thermally stable on graphitic structures [3]. TEM specimens prepared via oxidation are shown to be free of irradiation-induced artifacts which can occur with traditional specimen-preparation techniques. Furthermore, oxidative TEM sample preparation of nuclear graphite provides an alternative to expensive techniques such as FIB.

Chapter Three demonstrates in situ TEM characterization of nuclear graphite undergoing electron-irradiation and heating. In situ heating was conducted on ion-milled specimens up to 800°C prior to irradiation damage (near zero dpa). The curling and closure of basal planes was observed as either hollow nanotube-like structures within Mrozowski cracks or interstitially as line defects. To ensure these observations were not artifacts produced via specimen preparation, annealing experiments were conducted on specimens prepared to electron transparency via oxidative techniques. Results showed leading basal-plane edges remained unreconstructed at room temperature and only after thermal annealing at 800°C (during which, the electron beam was off) were basal-plane edges found to reconstruct into small loops resulting in localized swelling; thus, domains of undercoordinated atoms in nuclear graphite show a fullerene-like transformation due solely to annealing. This phenomenon could explain the rapid increase in CTE during the onset of irradiation and additionally the delayed dimensional change (in some instances slight swelling) observed in low-dose irradiation studies (< 1 dpa) [4,5].

In situ heating and electron-irradiation showed the dynamic evolution of many fullerene-like defects not previously known to occur in high-temperature irradiated nuclear graphite, including carbon onions and interstitial nanotube-like defects, specifically in Figure 3.4, which resulted in ~51% expansion of a crystallite along the *c* axis. The formation of such defects is conjectured to be driven by the interaction of

vacancy species resulting in extended interatomic linking between adjacent basal planes [6]. It should be noted that the above-mentioned defect structures were not observed at temperatures below 750°C, thus, the formation of such defects is proposed to be a temperature-dependent mechanism. While Chapter Three shows novel defect mechanisms occurring during high-temperature irradiation, those defects evolved in an unconstrained TEM foil using electrons as surrogate particles, leaving the open question if such defects would also occur in actual high-temperature neutron-irradiation nuclear graphite.

Chapter Four shows fullerene-like defects occurring in ex-situ analysis of IG-110 neutron-irradiated at 817°C to a dose of 3.56 dpa. Specifically, results show the first direct experimental evidence of a 'ruck and tuck' defect [7]. The "buckle, ruck and tuck" model is an alternative theory for the response of graphite undergoing neutron irradiation and was proposed theoretically in 2011 by Prof. Malcolm Heggie et al. [7]; however, after many years without experimental evidence, the acceptance of this mechanism waned, and even Prof. Heggie began to doubt it. Sadly, Prof. Heggie did not live to see the evidence for his model, as he passed away on 17 January 2019.

Chapter Five further investigates the atomic defect structures and microstructural response of high-temperature neutron-irradiated nuclear graphite. TEM was used to characterize specimens neutron-irradiated at a high temperature (≥800 °C) at doses of 1.73 and 3.56 dpa. Areas of the microstructure where there is a high degree of long-range order, such as filler particles, did not show evidence of significant crystallite deformation driven by defect structures. In disordered regions of the microstructure (*e.g.*, binder, QI particles, and Mrozowski cracks), fullerene-like defects were found to be abundant and,

in some instances, cause displacement of basal planes in excess of 5 nm parallel to the *c* axis. Furthermore, direct evidence of such defects occurring within Mrozowski cracks is given and is a significant insight into both the nature of these cracks and irradiation-induced dimensional change.

The closure of Mrozowski cracks (onset of turnaround) is generally believed to occur from *c*-axis expansion. The early turnaround behavior during high-temperature irradiation is generally reasoned to occur due to an increase in CTE causing closure of small Mrozowski cracks prior to turnaround dose [8]. This theory lacks definitive microstructural evidence in literature, in fact, some results show Mrozowski cracks only slightly decrease in dimension due to thermal annealing and not to the extent of closure [9]. Chapter Five shows evidence of defects accumulating within the accommodating porosity (impeding further *c*-axis expansion) which provides an alternative explanation for early turnaround behavior in high-temperature irradiated nuclear graphite. In addition, the CTE begins to decrease at approximately *half* the turnaround dose and is reasoned to occur due to the closure of Mrozowski cracks and generation of new cracks due to internal stresses; however, this reasoning is contradicted by the consensus that closure of Mrozowski cracks occurs *at* turnaround. Thus, evidence of defects accumulating within the accommodating porosity provides valuable insight into these discrepancies.

Chapter Five additionally shows the formation of carbon onions due to neutron irradiation. Furthermore, it was suggested that larger concentric shelled defects (~50 nm in diameter) were not densified QI particles but the evolution of concentric shelled fullerene-like defects. As one cannot reasonably prove a formation mechanism solely by ex-situ analysis, high-temperature electron-irradiation was again used to provide

unambiguous results showing the dynamic evolution of concentric shelled defect structures. In addition, the high-temperature electron-irradiation studies presented in both Chapters Four and Five agree with results from actual high-temperature neutron irradiation and give additional validity to the use of high-flux electron irradiation as a useful approximation to that of neutron irradiation.

6.2 Future Work

6.2.1 Extend High-Temperature Neutron Irradiation of Candidate Nuclear Graphites

At present, many candidate graphite grades lack an adequate amount of irradiation data to develop even empirically based models of irradiation induced property change. Irradiation programs (such as the AGC) should continue efforts to validate next-generation nuclear graphites and specifically extend irradiation of candidate graphite grades to high temperature and doses at and beyond turnaround. Characterizing the nature of the accommodating porosity and Mrozowski cracks at turnaround dose is vital to understanding dimensional change in nuclear graphite. This includes comparing defect concentrations and structures in both unloaded and loaded specimens to further explore irradiation creep mechanisms. With modern advances in characterization techniques, such as aberration corrected TEM, atomic level defects may be identified with unprecedented clarity.

6.2.2 Extend TEM Characterization to In Situ Straining

Predicting the structural integrity of graphite components is largely dependent upon understanding the stress-strain relationship. Specifically, understanding how stress-induced damage is accommodated within the microstructure of nuclear graphite and the governing atomic mechanisms. In situ straining experiments generally are spatially

limited to the macro and mesoscale using optical or X-ray techniques [10–12]; however, to date there remains no in situ TEM straining experiments reported on nuclear graphite. In situ TEM straining can provide a means to monitor the evolution of stress-induced damage on the atomic scale. Furthermore, such experiments can also include in situ observations of irradiation damage (via electrons) of nuclear graphite under load which may provide novel insights towards atomic mechanisms related to irradiation creep.

6.2.3 Extend TEM Characterization to Spectroscopic Techniques

Quantitative analysis on irradiated nuclear graphite can be conducted via EELS. The low-loss region of the EELS spectrum includes information containing specimen thickness and relative density. The energy loss near edge structure (ELNES), which contains the ionization edges, and the extended energy loss fine structure (EXELFS), can be numerically analyzed to establish the relative amount of sp^2/sp^3 bonding. If the ELNES spectrum is normalized to a reference specimen, a percentage change in bonding character as a function of neutron dose could potentially be established.

6.2.4 Extend TEM Characterization to Electron Tomography

Mrozowski cracks hold a critical role in determining the nature of irradiation-induced dimensional change in nuclear graphite; however, a precise topological description of Mrozowski cracks has yet to be developed. This in part is due to the spatial resolution limit of most tomography characterization techniques. There have been significant advances in characterizing the porous structure of nuclear graphites using FIB-SEM tomography where the spatial resolution is approximately 150 nm [13]; however, 150 nm is nearing the upper limit of the width of Mrozowski cracks. In this work most Mrozowski cracks are observed to be 5-50 nm in width. Electron tomography

is a gradually maturing technique capable of reaching sub-nanometer resolution [14]. Electron tomography would provide novel insights towards a topological description of Mrozowski cracks and, in addition, may prove or disprove the presence of amorphous carbon within the Mrozowski cracks, which remains a subject of debate [15].

6.3 References

[1] I.A. Yavorsky, M.D. Malanov, On the reactivity of basal and prismatic faces of pyrographite crystallites, Carbon N. Y. 7 (1969) 287–291. doi:10.1016/0008-6223(69)90111-0.

[2] J.J. Kane, C. Karthik, R. Ubic, W.E. Windes, D.P. Butt, An oxygen transfer model for high purity graphite oxidation, Carbon N. Y. 59 (2013) 49–64. doi:10.1016/j.carbon.2013.02.053.

[3] R. Larciprete, P. Lacovig, S. Gardonio, A. Baraldi, S. Lizzit, Atomic Oxygen on Graphite: Chemical Characterization and Thermal Reduction, J. Phys. Chem. C. 116 (2012) 9900–9908. doi:10.1021/jp2098153.

[4] T.D. Burchell, L.L. Snead, The effect of neutron irradiation damage on the properties of grade NBG-10 graphite, J. Nucl. Mater. 371 (2007) 18–27. doi:10.1016/j.jnucmat.2007.05.021.

[5] B.J. Marsden, M. Haverty, W. Bodel, G.N. Hall, A.N. Jones, P.M. Mummery, M. Treifi, Dimensional change, irradiation creep and thermal/mechanical property changes in nuclear graphite, 61 (2016) 155–182. doi:10.1080/09506608.2015.1136460.

[6] T. Trevethan, P. Dyulgerova, C.D. Latham, M.I. Heggie, C.R. Seabourne, A.J. Scott, P.R. Briddon, M.J. Rayson, Extended interplanar linking in graphite formed from vacancy aggregates, Phys. Rev. Lett. 111 (2013) 1–5. doi:10.1103/PhysRevLett.111.095501.

[7] M.I. Heggie, I. Suarez-Martinez, C. Davidson, G. Haffenden, Buckle, ruck and tuck: A proposed new model for the response of graphite to neutron irradiation, J. Nucl. Mater. 413 (2011) 150–155. doi:10.1016/j.jnucmat.2011.04.015.

[8] G.B. Neighbour, Modelling of dimensional changes in irradiated nuclear graphites, J. Phys. D. Appl. Phys. 33 (2000) 2966–2972. doi:10.1088/0022-3727/33/22/315.

[9] K. Wen, J. Marrow, B. Marsden, Microcracks in nuclear graphite and highly oriented pyrolytic graphite (HOPG), J. Nucl. Mater. 381 (2008) 199–203. doi:10.1016/j.jnucmat.2008.07.012.

[10] M.R. Joyce, T.J. Marrow, P. Mummery, B.J. Marsden, Observation of microstructure deformation and damage in nuclear graphite, Eng. Fract. Mech. 75 (2008) 3633–3645. doi:10.1016/j.engfracmech.2007.11.003.

[11] M. Mostafavi, T.J. Marrow, Quantitative in situ study of short crack propagation in polygranular graphite by digital image correlation, Fatigue Fract. Eng. Mater. Struct. 35 (2012) 695–707. doi:10.1111/j.1460-2695.2012.01648.x.

[12] D. Liu, T. Zillhardt, P. Earp, S. Kabra, T. Connolley, T. James Marrow, In situ measurement of elastic and total strains during ambient and high temperature deformation of a polygranular graphite, Carbon N. Y. 163 (2020) 308–323. doi:10.1016/j.carbon.2020.03.020.

[13] J.D. Arregui-Mena, P.D. Edmondson, A.A. Campbell, Y. Katoh, Site specific, high-resolution characterisation of porosity in graphite using FIB-SEM tomography, J. Nucl. Mater. 511 (2018) 164–173. doi:10.1016/j.jnucmat.2018.08.047.

[14] P. Ercius, O. Alaidi, M.J. Rames, G. Ren, Electron Tomography: A Three-Dimensional Analytic Tool for Hard and Soft Materials Research, Adv. Mater. 27 (2015) 5638–5663. doi:10.1002/adma.201501015.

[15] D. Liu, D. Cherns, Nano-cracks in a synthetic graphite composite for nuclear applications, Philos. Mag. 98 (2018) 1272–1283. doi:10.1080/14786435.2018.1433886.